MATERIAL CHARACTERIZATION OF OPEN-CELL FOAMS BY FINITE ELEMENT BASED MICROMECHANICS METHODS

By

PRASANNA THIYAGASUNDARAM

A DISSERTATION PRESENTED TO THE GRADUATE SCHOOL
OF THE UNIVERSITY OF FLORIDA IN PARTIAL FULFILLMENT
OF THE REQUIREMENTS FOR THE DEGREE OF
DOCTOR OF PHILOSOPHY

UNIVERSITY OF FLORIDA

2010

To my mother, my father, my sister and my brother-in-law

ACKNOWLEDGMENTS

I want to extend my deepest heartfelt gratitude to my advisor Dr. Bhavani V. Sankar for his tutelage, support, and encouragement he has given me in these 4 years. I would remain ever indebted to him for all the opportunities he has given me in doing research, in tutoring undergraduate students, in writing technical journal articles, and also in giving technical talks at conferences. I would like to thank my co-advisor Dr. Nagaraj K. Arakere who has been immensely helpful in guiding me in this research work. I would also want to thank Dr. Youping Chen and Dr. Reynaldo Roque for serving on my PhD committee and for their very useful feedback on the contents of this thesis. Finally, I would like to acknowledge my family – especially my mother – for being there with me all the time giving me the support I have needed in both good and bad times.

TABLE OF CONTENTS

page

LIST OF TABLES

LIST OF FIGURES

LIST OF ABBREVIATIONS

$[C]$	Stiffness matrix of the foam
A	Cross sectional area of the strut
a_1	Length of representative volume element
a_2	Width of representative volume element
a_3	Height of representative volume element
b	Dimension of the top, bottom squares of the elongated tetrakaidecahedron unit cell
d	Length of the side of the equilateral triangle cross section
E_i	Young's modulus in the i direction
E_s	Elastic modulus of the strut material
f_{ij}	Force in the direction j for displacement is applied in the direction i
G_{ij}	Shear modulus of foam
I_x, I_y	Moment of inertia in X and Y directions
J	Torsion constant
K_I	Mode I stress intensity factor
K_{IC}	Mode I fracture toughness of the foam
K_{II}	Mode II stress intensity factor
K_{IIC}	Mode II fracture toughness of the foam
L	Dimension of the long edges of the elongated tetrakaidecahedron unit cell
l	Length of each strut in the tetrakaidecahedron
$p_1, p_2, q_1, q_2, s_1, s_2$	Parameters obtained from the compliance matrix of the foam
r	Distance from the crack tip to the boundary node
r	Radius of the 3-cusp hypocycloid cross section

u_i	Displacement in the *i* direction
V	Volume of representative volume element
Δu_i	Difference in translational displacement along axis i
$\Delta\theta_i$	Difference in rotational displacement along axis i
ε_0	Applied macro-strain
$\varepsilon_1, \varepsilon_2, \varepsilon_3$	Strain components in the principal *X, Y,Z* directions
v_{ij}	Poisson's ratio
v_s	Poisson ratio of the strut material
ρ_s	Density of the strut material
σ	Applied macro stress
σ_*	Failure strength of the constituent strut material
σ_i	Principal stress in the strut
σ_{tip}	Maximum stress ahead of the crack tip
ω_{xy}	Rotational displacement

Abstract of Dissertation Presented to the Graduate School
of the University of Florida in Partial Fulfillment of the
Requirements for the Degree of Doctor of Philosophy

MATERIAL CHARACTERISATION OF OPEN-CELL FOAMS BY FINITE ELEMENT BASED MICROMECHANICS METHODS

By

Prasanna Thiyagasundaram

August 2010

Chair: Bhavani V. Sankar
CoChair: Nagaraj K. Arakere
Major: Mechanical Engineering

Finite element based micromechanics methods have been used for predicting elastic properties, failure strengths, mode-I, mode-II and mixed mode fracture toughness of open-cell foams. In predicting the orthotropic elastic properties, foams with both equisided and Kelvin-elongated tetrakaidecahedron unit cells are studied. Periodic Boundary Conditions (PBCs) exploiting the special repeating microstructural geometry for these materials have been derived and have been applied on the micromechanical model to calculate the elastic properties. It is shown that the results for the elastic constants from these finite element based models agree well with the available analytical models. Further studies such as effect of a varying strut cross-section over a uniform strut cross-section on the elastic properties are also done in the same context.

Next, the procedures used for predicting the above elastic properties are extended to predict multi-axial failure strengths of these low density open cell foams with a microstructure made out of tetrakaidecahedral unit cells. Again, foams with both equisided tetrakaidecahedron and Kelvin-elongated tetrakaidecahedron as unit cells are studied. Failure strengths in different material directions are computed using direct

Micromechanics based Methods (DMM). Further, the effect of a varying strut cross section over a uniform strut cross section on failure strengths is also presented. Bi-axial failure envelopes for foams with equisided tetrakaidecahedron unit cells are shown to take the shape of a regular hexagon in the hydrostatic plane. The tri-axial failure envelope for foams made out of equisided tetrakaidecahedron unit cells is shown to have a shape of a double hexagonal pyramid. The bi-axial and tri-axial failure envelopes of foams with elongated tetrakaidecahedron unit cells are also plotted and the effect of anisotropy in foams with these unit cells on the failure envelopes is also discussed.

Next, global-local models are developed to predict fracture toughness of open cell foams. An approach of imposing displacements on the K-field boundary of the micromechanical model for finding the maximum tensile stress at the crack tip is used for predicting the fracture toughness of the foam. A convergence study is conducted by testing different model sizes to show that the calculated value of fracture toughness is an acceptable material property.

CHAPTER 1
INTRODUCTION

Background

All materials around us today can be broadly classified into metals, ceramics, polymers, natural materials and foams (Ashby, 2008). Among these materials (Figure 1-1), natural materials and foams are together called as cellular solids. A cellular solid is defined as one made up of an interconnected network of solid struts or plates which form the edges and faces of its cells (Gibson and Ashby, 1997). The cellular solid structures in the form of a two-dimensional array of polygons which pack to fill a plane area are called ‘honeycombs’. If the cells are polyhedral and they pack in three dimensions to fill space, they are called ‘foams’. If the solid of which the foam is made is contained in the cell edges only (as shown in Figure 1-2), is called ‘open-cell’ foam.

Historically foams have been in existence for a long time. In a study about the history of materials, (Ashby, 2008) there is a mention of naturally occurring foams such as bones and wood starting from 10000BC. One perspective that has triggered the need for understanding such materials has been the need for newer lighter materials that suit special applications such as in aircraft, space craft structures. Ashby states that (Ashby, 2008) the post 2nd world war period has been the starting point for fabrication of artificial cellular materials such as artificial polymers and silicon. These materials were widely used in the aircrafts that were made after the world war.

Another perspective that has been of keen interest to mathematicians and scientists has been to understand the geometry of these naturally occurring materials. In an elaborate treatise on the structure and properties of cellular solids (Gibson and Ashby, 1997), this is discussed, starting with Robert Hooke’s pursuit in understanding

the nearly perfect hexagonal cells of the material – cork (Figure 1-2a). There is a mention about Euclid (3rd century BC) and Pliny (AD 77) who studied the regularity in the geometry of the cells of materials such as the bee's honeycomb.

In the same work (Gibson and Ashby, 1997), there is also a mention about mathematicians Plateau (1873) and Lord Kelvin (1887) making significant contribution to the geometry of three-dimensional cellular solids through their pursuit for identifying efficient ways of partitioning 3 dimensional spaces. Plateau in his treatise on solid geometry identifies a rhombic dodecahedron (12-faced, garnet shaped figure – Figure 1-2) as a shape to partition space into a regular array of cells. However, Lord Kelvin identifies that a rhombic dodecahedron would not be the most efficient way to fill up space and that a tetrakaidecahedron (a 14 faceted figure) (Figure 1-3) would be the shape that best minimizes the surface area per unit volume and hence would be nature's most preferred shape to fill up space. Thus, tetrakaidecahedron has remained the most efficient geometry for the shape of unit cell for foams till recently when scientists (Weaire and Phelan, 1997) have come up with an even more efficient shape - an irregular pentagonal dodecahedron – to have a 0.3% lesser surface area to volume ratio than the tetrakaidecahedron. However tetrakaidecahedron is still the unit cell shape used by most researchers who study cellular materials.

Polyurethane foams were discovered by Otto Bayer and his research group at I.G.Farben industries in Germany in the late 1930s. However, it was not until the end of the Second World War that polyurethene foams became commercially available. Today the manufacturing processes of polyurethane foams are well developed. Polymer foams can be divided into either thermoplastics or thermosets, which are further divided into

rigid or flexible foams. The thermoplastics can usually be broken down and recycled, while thermosets are harder to recycle because they are usually heavily crosslinked.

Principle of Foaming

In order to understand the need to characterize foams, it is compulsory to have an understanding of the fundamentals of foaming process.

Polymer foams are made up of a solid and gas phase mixed together to form a foam. This generally happens by combining the two phases too fast for the system to respond in a smooth fashion. The resulting foam has a polymer matrix with either air bubbles or air tunnels incorporated in it, which is a closed-cell or an open-cell structure. Closed-cell foams are generally more rigid, while open-cell foams are usually flexible. The gas that is used in the foam is termed a blowing agent, and is either chemical or physical. Chemical blowing agents are chemicals that take part in a reaction or decompose, giving off chemicals in the process. Physical blowing agents are gases that do not react chemically in the foaming process and are therefore inert to the polymer forming the matrix.

Figure 1-4 shows a typical chemical system used for foam fabrication. Resin shown in the figure is the solid phase. In this process the foams are created as a colloidal suspension of a gas in a liquid created by an agitation process. The gas (carbon dioxide in the case of polyurethane foams) is created by a chemical reaction between a highly reactive isocyanate (resin) and a blowing agent such as Hydro Chloro Fluoro Carbon (HCFC). The liquid in the polyurethane foam is a combination of a polyol (compounds with multiple hydroxyl group) & surfactants (which act as emulsifiers in creating a colloidal suspension). The reaction that takes place during the formation of the foam is a three step process. First, a HCFC molecule reacts with an isocyanate

group to form a carbamic acid. Next, Carbamic acids which are unstable, decompose forming carbon dioxide and an amine. Finally, the amine reacts with more isocyanate to give a substituted urea. This urea is not very soluble in the reaction mixture and tends to form separate "hard segment" phases consisting mostly of polyurea. Since the polymerization reaction is exothermic, the blowing agents (HCFC) volatilize into a gas during the reaction process. They fill and expand the cellular polymer matrix (consisting of polyol and surfactants), creating a foam.

Thus, through bubble nucleation and expansion, foam cells are created. As mentioned earlier, the unit cells that are created from this kind of process would always want to optimize and minimize the surface area per unit volume and pack to fill space (Kelvin, 1887). Because of this, the repeating microstructural geometry of the foams is a tetrakaidecahedron (Figure 1-3).

Relative Density

Foams are versatile materials and are used in a variety of applications due to the unique combination of material properties they exhibit. The most important feature of these cellular solids is its relative density, ρ^*/ρ_s that is the density of the cellular material, ρ^*, divided by that of the solid from which the cell walls are made, ρ_s. An illustration for calculating foam's relative density assuming it to be made out of repeating cubical unit cells (Choi and Sankar, 2005) has been shown below.

Assuming the foam to be made out of struts of length *c* and square cross sections of dimension *h,* the density of this foam with mass m and volume V of the unit cell can be obtained as:

$$\frac{\rho^*}{\rho_s} = \frac{\frac{m}{V}}{\rho_s} = \frac{\frac{\rho_s\left(3h^2c - 2h^3\right)}{c^3}}{\rho_s} = \frac{\left(3h^2c - 2h^3\right)}{c^3} = 3\left(\frac{h}{c}\right)^2 - 2\left(\frac{h}{c}\right)^3 \quad (1\text{-}1)$$

With proper manufacturing control, this relative density can be controlled and either high density foams (used as structural load bearing members) or low density foams (used as simple cushioning or packaging materials) can be fabricated (Yamsaengsung, W., Sombatsompop, N., 2009). Varying relative densities would mean foams with varying material properties. Elaborate studies (Yamsaengsung et al, 2008, Demir et al, 2008, Thomas N et al, 1997) have been conducted to study how to manipulate the manufacturing parameters to yield various relative densities. For example Figure 1-6a and Figure 1-6b show the variation of relative density of Ethylene-Propylene-Diene-Monomer (EPDM) foams with varying amounts of chemical blowing agents. It is clear that as the blowing agent content, which is expressed in phr (parts per hundred of the resin) is increased, the porosity of the resulting foam goes up.

Hence it is evident that if the relative density of the foam can be related to its material property, the manufacturing parameter needed to obtain a particular kind of foam with the required stiffness can be calculated. This forms the fundamental basis for the need for analytical models. And hence, all the available literature on analytical models of foams relate the elastic property, failure strength, and fracture toughness of the foam with its relative density.

Need for Material Characterization - Special applications of Foams

Foams have been shown to have a great potential as core materials in sandwich construction for heat exchangers in military and commercial aerospace structures. This is especially because foams offer special advantages over other materials such as good thermal resistance, durability, low density, good impact damage tolerance and cost

effectiveness. A special application of foams in aerospace is as a core material for sandwich construction in Thermal Protection Systems (TPS) of space vehicles. Foams that are used in the currently existing thermal protection systems (TPS) (Oscar et al, 2007) cannot bear the thermo-mechanical loads as they are designed just for very low thermal conductivity and much attention has not been paid to their mechanical load bearing capacity. To overcome this, NASA has started the study of novel TPS concepts such as Integral Thermal Protection Systems (ITPS) in which the load-bearing function and thermal insulation are combined into a single structure (Figure 1-7). This new concept (Oscar et al, 2007, Lee et al, 2007) can be achieved by using foams as core of the sandwich structures since foams can be tailored for optimum performance. So there is a need to accurately characterize foams to be used for these applications.

The urgency in understanding foams has also increased after the Space Shuttle Columbia disaster in February 2003 which happened primarily due to foam shredding and debris formation (Weiser and Nemeth, 2004, Arakere et al 2008), that happened from the external fuel tank insulation of the space shuttle. In this report, Weiser and Nemeth study the different materials that go into the fabrication of the 2 major kinds of foams that are used in the external tanks designated as BX 265 and NCFI 24-124, and analyze the possible causes for void formation, porosity, cracks, cell elongation, delamination etc., that occur due to problems during fabrication process. From all literature addressing issues that relate to shredding of foams, lack of predictive tools for strengths, and fracture toughness of foams has been identified as one of the missing links in the design of structures containing foams. Hence, especially for aerospace

applications, there exists an urgent need for methodologies for fundamental material characterization of foams.

Need for Analytical Models for Material Characterization

Usually, experimental methods are used to determine the elastic properties of materials. Usual methods include uniaxial tension tests or compression tests, biaxial tests etc. These methods are well established and have been used for determining material properties for most materials for a long time.

There is a lot of literature available on data obtained from these standard tests on foams. To quote a few significant ones, Gong et al (Gong et al, 2005) in their experimental work discuss about the uniaxial compressive response of polyurethane open-cell foams (Figure 1-8). As is seen in the figure, there is a nearly linear elastic regime first, followed by an extensive load plateau which is again followed by a second branch of stiff response. In another work, Ridha et al illustrate the deformation of rigid polyurethane foams subjected to tension. They obtain results similar to the response obtained by Gong et al. They go on further to study the microstructure of these foams and illustrate that the shape of the unit cells clearly resemble a elongated tetrakaidecahedron and also by observing the microstructure characteristics detect that bending of the struts that define the cell structure is the primary mechanism that governs deformation and fracture. Additionally, both the studies above illustrate the anisotropic characteristics of these foams. In another elaborate study, Sullivan et al (Sullivan et al, 2008) in their experiments on BX265 and NCFI 24-124 (polyurethane foams used in external fuel tanks insulation) come up with the trends for the stress-strain curves as shown in Figure 1-9. As shown in the figure the anisotropy of the foam structure is evident, as the stiffness in the ‘rise direction’ is higher than the stiffness in

the ‘perpendicular to rise’ direction. The details of the same would be explained elaborately in the coming chapters.

Micromechanics Based Methods

Broadly, micromechanics is defined as the analysis of a heterogeneous material comprised of multiple phases based on the analysis of its individual constituent phases. Foams are heterogeneous materials consisting of two phases the solid phase and voids or porous phase in them (Figure 1-10). The available literature on micromechanics pertaining to the current problem can be divided into two broad sections as analytical formulation based micromechanics methods (where closed-form solutions for the properties are obtained) and finite element based micromechanics methods.

Micromechanics based methods have been utilized effectively for deriving analytical models for elastic properties assuming the unit cell to be made out of relatively simple geometries such as a cube or a hexagon. To illustrate a few, Gibson and Ashby (Gibson and Ashby, 1997) in their book on cellular materials derive analytical models using micromechanics based methods for foams made out of staggered cubical unit cells:

$$E^* = C \times E_s \times \left(\frac{\rho^*}{\rho_s} \right)^2 \tag{1-2}$$

Where, E^* is the Young’s modulus of the foam material, C is the constant of proportionality close to unity and $\left(\frac{\rho^*}{\rho_s} \right)$ is the relative density, E_s is the Young’s modulus of the solid material.

The same cubical unit cell assuming the struts as beams (Figure 1-5) has also been formulated by Choi and Sankar, (Choi and Sankar, 2005) using finite element

based methods and have been shown to match well with the analytical models of Gibson. The results obtained by them are as follows:

$$\left(\frac{E_s}{E^*}\right)=\left(\frac{c}{h}\right)^2 \tag{1-3}$$

Where, E^* is the Young's modulus of the foam material, $\left(\frac{\rho^*}{\rho_s}\right)$ is the relative density, c is the side of the cube and h is the side of the square cross-section. Again the properties vary as the square of the relative density.

Difficulties in the Existing Methods for Material Characterization

Even though experiments (as mentioned above) can be performed to determine the material characteristics, there are difficulties with performing experiments on these materials especially because:

a) Foams are anisotropic and so characterizing them through experimental methods would require testing a multiple experimental specimens.

b) Usually, depending upon the application, foam with an appropriate density can be fabricated. So, if we have to experimentally determine the variation of these stiffness properties with relative density, then again multiple specimens with different relative densities have to be prepared and have to be tested which would again be a rather time consuming process.

c) Due to these two reasons, analytical models have an obvious advantage over experimental material characterization. But analytical models with closed-form solutions for the elastic properties have their own deficiencies:

d) Deriving analytical models for relatively simple unit cell geometries like a cube or hexagon is easy. However if the unit cell geometries are complicated like an elongated tetrakaidecahedron – which is the typical unit cell geometry for open cell foams, deriving analytical models is a rather cumbersome process.

e) Results obtained from existing analytical models have innate deficiencies in them because of various assumptions that are made in the derivation.

Hence the current research focuses on using alternative approaches such as finite element (FE) based methods to characterize foams. Details about the specific

advantages these methods have over existing body of work on material characterization of foams would be evident as the chapters are perused.

Dissertation Outline

The outline of the dissertation is as follows. Chapter 2 presents Finite Element based Micromechanics methods to predict homogenized elastic properties of foams made out of tetrakaidecahedral unit cells. There is an elaborate section for literature review of the available analytical models for calculating elastic properties of cellular materials. However emphasis would be placed on the analytical models that pertain to the current problem which have been used specifically to get a comparison of the results obtained from FE based methods. In addition to this, special aspects such as variation in the calculated properties due to change in the strut cross-sectional area has also been mentioned. Also details pertaining to inadequacies in the existing analytical models that can be addressed very well using the FE based methods have been mentioned.

Chapter 3 presents Finite Element based Micromechanics methods to predict failure strengths of foams and their corresponding failure envelopes. Emphasis would be placed in using Direct Micromechanics based Methods (DMM) for obtaining the failure strengths. Methods for extending the micromechanics based methods for calculating the elastic properties is illustrated. Different aspects of the 2D and 3D failure envelopes obtained have been explained in detail.

Chapter 4 presents micromechanics based methods to predict fracture toughness of cellular materials made out of tetrakaidecahedral unit cells. Detailed literature review of the currently available analytical models for predicting fracture toughness of cellular materials has been provided. Also details of setting up a micromechanical model, and

details of calculating stresses at the struts close to crack tip have been provided. Detailed analysis of the convergence study for the calculated fracture toughness has been provided. Influence of rotation boundary conditions on the convergence of fracture toughness is also addressed.

Chapter 5 is a summary of all the important results and conclusions of the current work. Following the conclusion section, a future work section has also been provided to help using the knowledge gained from the current work to future investigation.

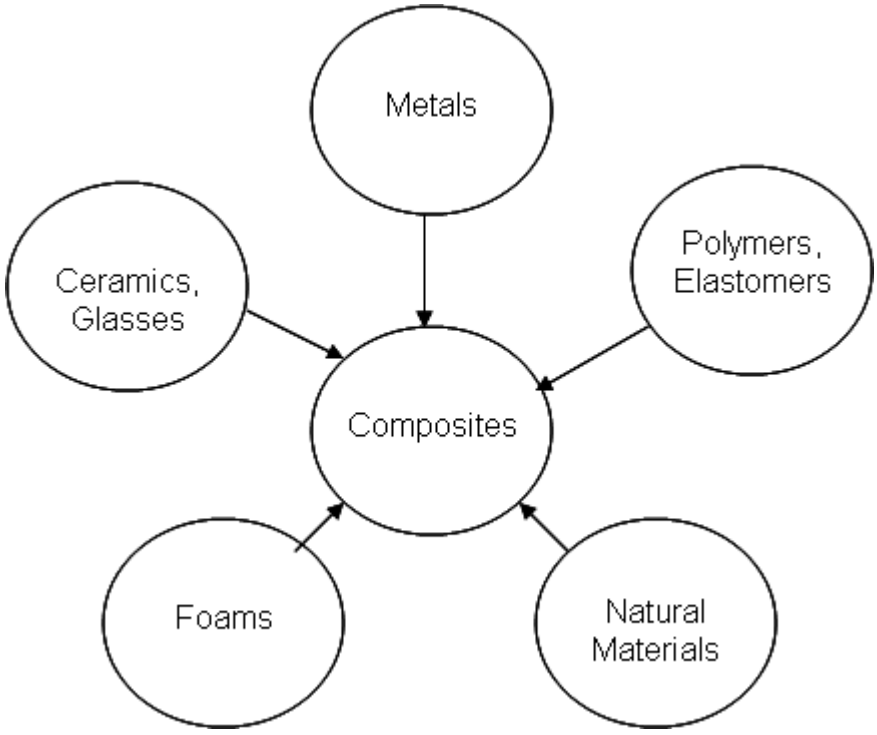

Figure 1-1. Classifying materials.

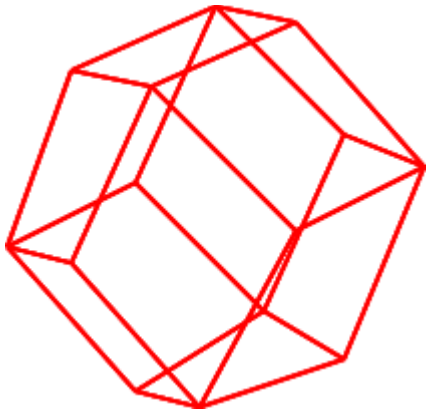

Figure 1-2. Geometry of cellular solids-Rhombic Dodecahedron used by Pleateau in 1873.

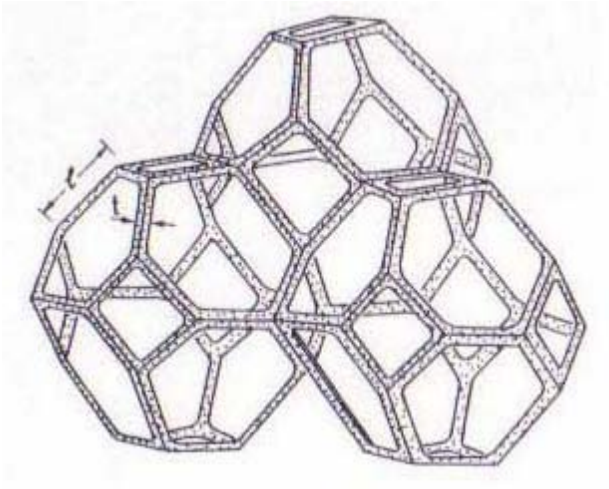

Figure 1-3. Tetrakaidecahedron

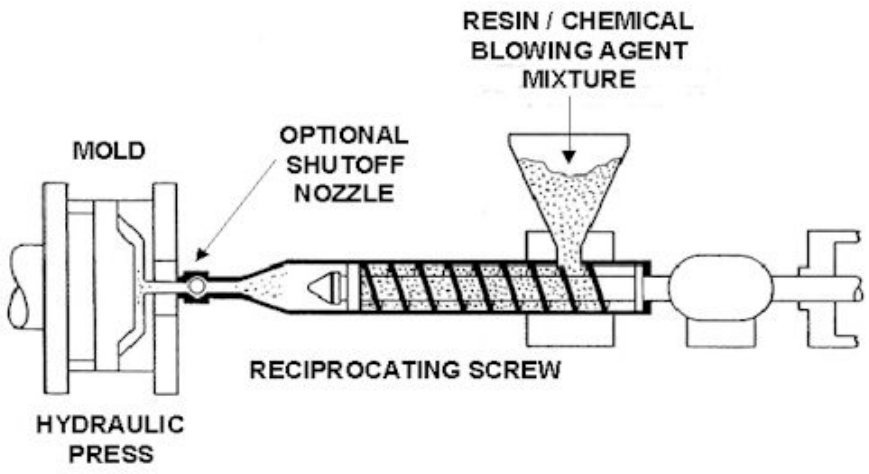

Figure 1-4. Schematic of the Chemical system for foaming

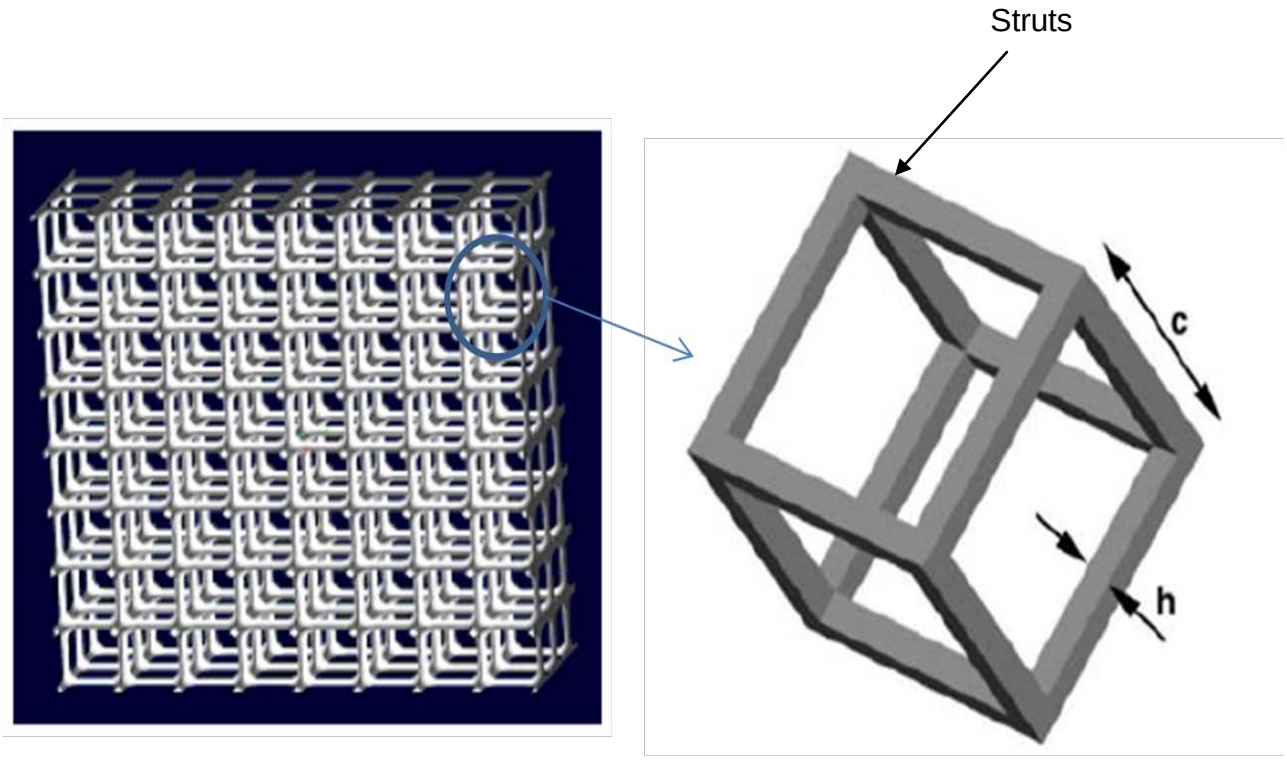

Figure 1-5. Repeating geometry made out of cubical unit cells

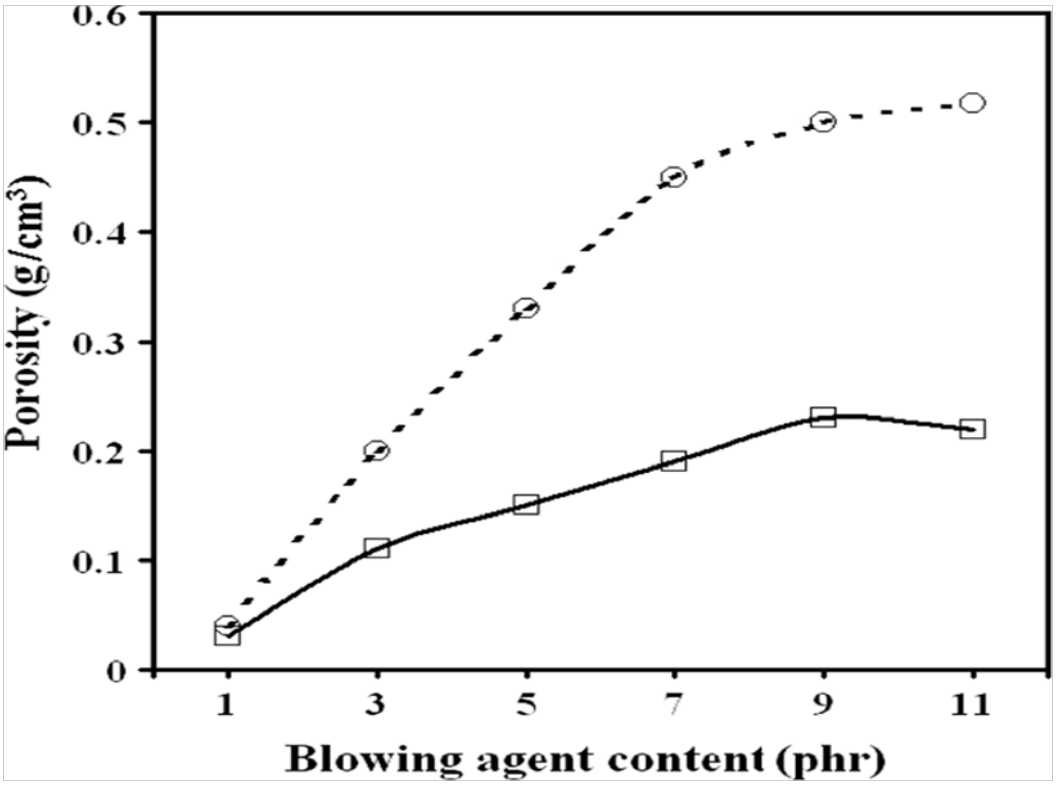

Figure 1-6. Variation of relative density with blowing agent content

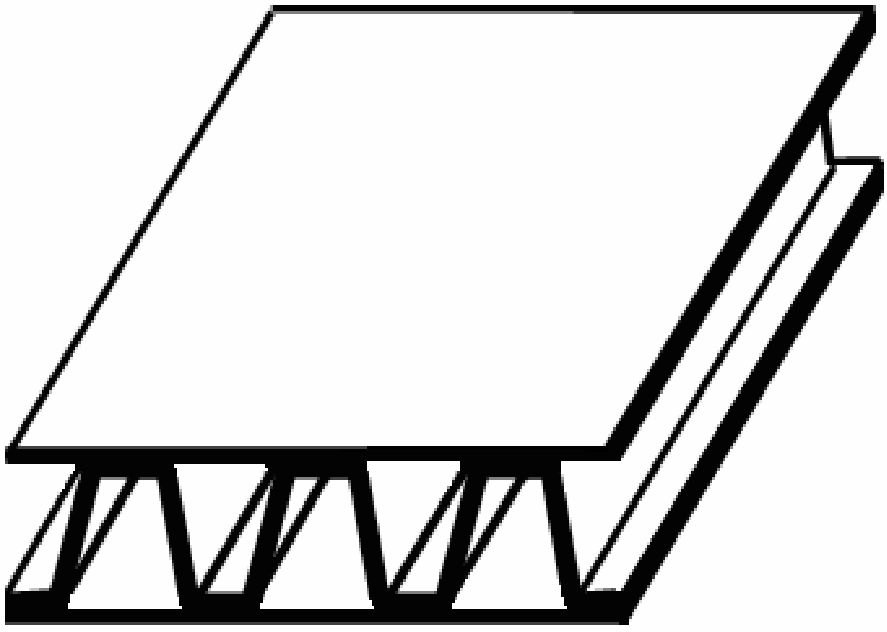

Figure 1-7. Corrugated Core Sandwich Panel (ITPS concept) (Martinez et al, 2007)

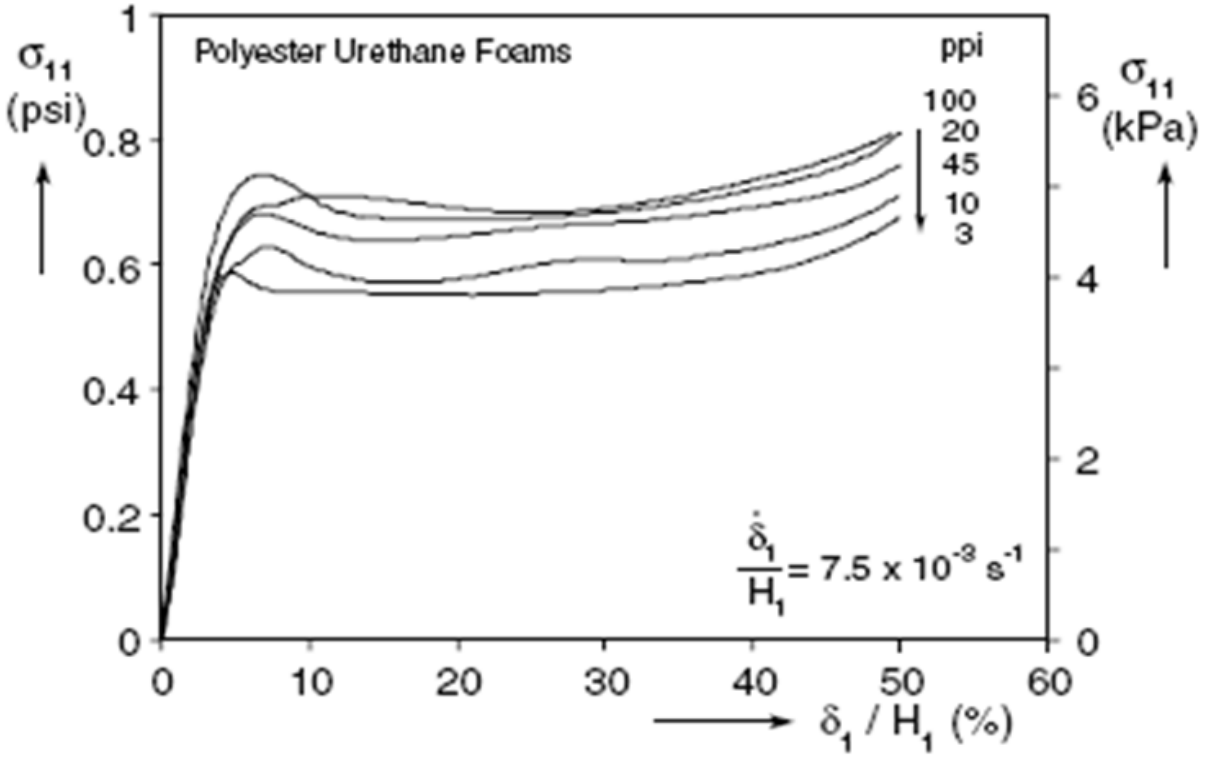

Figure 1-8 Compressive response of 5 different Polyurethane foams

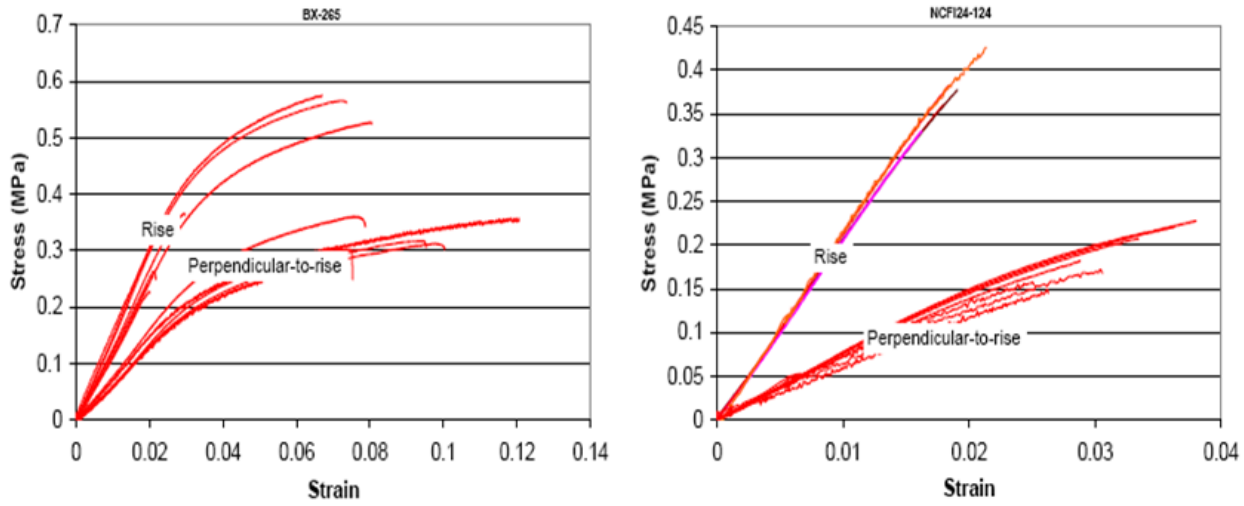

Figure 1-9. Mechanical response of polyurethane foams BX-265 and NCFI24-124 (Sullivan et al, 2008)

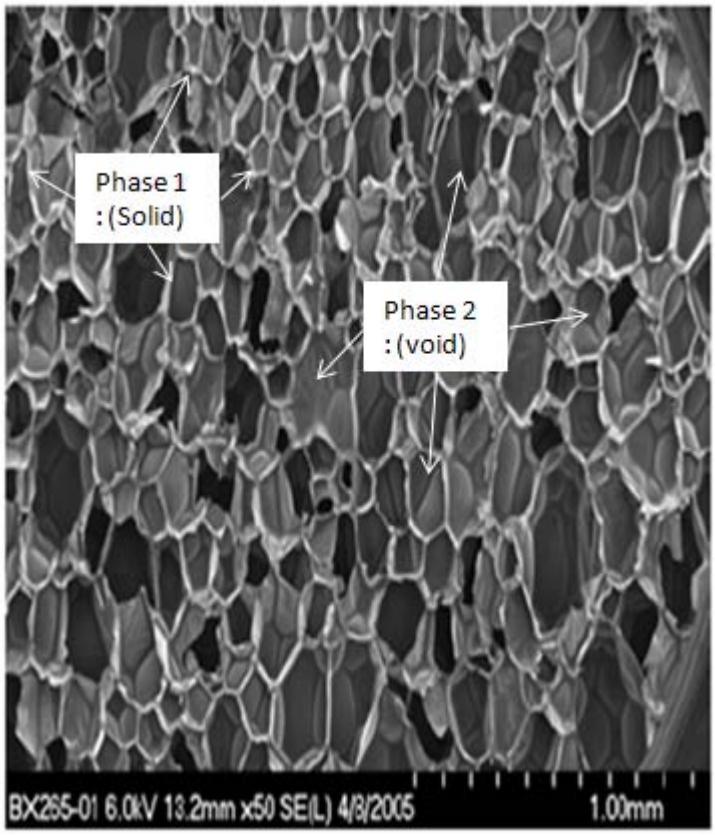

Figure 1-10. Micrograph of BX-265 foam to show that foam is a heterogeneous material

CHAPTER 2
ELASTIC PROPERTIES OF OPEN CELL FOAMS WITH TETRAKAIDECAHEDRAL UNIT CELLS USING FINITE ELEMENT ANALYSIS

A finite element (FE) method based micromechanics has been used for predicting the orthotropic properties of foams which have tetrakaidecahedral unit-cells. Foams with equisided and Kelvin-elongated tetrakaidecahedron as unit cells are studied. The results for elastic constants from the FE models agree well with that of available analytical models. The struts were modeled using both Euler-Bernoulli and Timoshenko beam elements. It is found that classical beam theory over predicts the elastic moduli when the struts have smaller length to thickness ratio. The effects of strut cross-section gradually decreasing from maximum value at support ends to minimum value at beam mid section over a uniform strut cross-section are also presented. It is found that for the same relative density, foams with varying cross section have much lower elastic moduli than foams with uniform cross-section.

Introduction

As mentioned earlier in Chapter 1, cellular solids are materials made out of solid strut or thin plate like structures bridged together. They occur in nature in the form of honeycombs, wood, bone, cork etc. These materials possess a unique combination of properties such as low thermal conductivity, low density and high energy-absorption. Foams are a class of cellular solids, generally made by dispersing gas into a liquid material and then cooling it to solidify. They are categorized as open-cell and closed-cell foams. Depending on the solid materials that are made into foams, they are also categorized as polymeric foams, metallic foams, and ceramic foams (Gibson and Ashby, 1997). Due to developments in material science and manufacturing techniques, advanced foams have found potential for use in automobile, aircraft, and space vehicle

structures. A special example is the use of foams in external fuel tanks and thermal protection system (TPS) of space vehicles. It has been accepted that packed in a BCC structure, a tetrakaidecahedron – a 14-faced polyhedron - satisfies the minimum surface energy condition for mono-dispersed bubbles (Thompson, 1887). Microcellular graphitic carbon foams were first developed at the US Air Force Research Laboratory in the 1990s (Hall and Hager, 1996). Clearly, it has been proven that the repeating unit cell of this foam can be approximated by a regular tetrakaidecahedron (Roy et al, 2003).

The catastrophic failure of Space Shuttle Columbia in February 2003 has given the necessary impetus to understand and reduce the likelihood and severity of foam shedding events that occur from the Shuttle's external fuel tanks. Currently, there is ongoing research focused on understanding the mechanisms that cause foam fracture and debris liberation (Arakere et al, 2008). This mandates a thorough understanding of the foam's mechanical response behavior, and characterization of its elastic properties is the first step in that direction.

In the same context, there is also ongoing research in the field of aero-structural composites focused on characterizing materials using principles of micromechanics, (Karkkainen and Sankar, 2006, Marrey and Sankar, 1997). These methods are based on simulating a characteristic representative part of the structure that periodically repeats itself, instead of simulating the entire model. Foams with simple representative unit cell structures such as cube (Choi and Sankar, 2005), to hexagonal cell structures, to a regular tetrakaidecahedron (Roy et al, 2003, Wang et al, 2007) as the unit cell, have been carefully studied and have been characterized for their mechanical behavior.

Currently, BX-265 and NCFI24-124 are the two foams used most exclusively in space shuttle external tanks. The photomicrographs (Sullivan et al, 2008) of these two foams are shown in Figure 2-1a and Figure 2-1b. Analysis of the foam structure from these micrographs has shown that due to forming and rising processes that takes place during fabrication, the unit cell of these foams is elongated in one of the three principal directions. Hence, this unit cell is called an elongated tetrakaidecahedron and the elongated direction is referred to as the rise direction. This makes the elongated foam strictly orthotropic.

Broadly, the available literature on foam mechanics can be classified into characterizing foams based on experimental studies (Sullivan et al, 2008, Wright et al, 2005, Huber et al, 1988) or characterizing foams based on analytical models (Sullivan et al, 2008b, zhu et al, 1997)

Analytical models that have been developed focus primarily on predicting the mechanical and strength properties. Assuming that the unit cell edges behave like a three dimensional beam, the mechanics of deformation of the tetrakaidecahedron unit cell leads to a set of equations for the effective Young's modulus, Poisson's ratio and tensile strength of the foam in the principal material directions (Sullivan et al, 2008). The equations for these elastic constants have been derived and written in terms of the cell edge length, and the axial, flexural and torsional rigidities of the strut cross section. Also the variation of these properties with relative density $\left(\frac{\rho^*}{\rho_s}\right)$ of the foam has been expressed.

The current chapter explores the possibility of using finite element based micromechanics procedures to calculate the elastic properties of foam materials. In

order to do this, periodic boundary conditions have been derived and applied to the unit cell model. The results obtained from this method have been compared with the results obtained from existing analytical models and they have been shown to match well for some of the elastic constants. Also, the advantages of using finite element based methods over analytical methods have been highlighted.

The analytical model by Zhu, Knott, Mills (Zhu et al, 1997) for predicting the elastic moduli, the poisson ratios and shear moduli has been used for comparison with the foam modeled with equi-sided tetrakaidecahedron as unit cell. The analytical model by Sullivan, Ghosn, Lerch, (Sullivan et al, 2008b) has been used for comparison with the foam modeled with elongated tetrakaidecahedron as unit cell. The requisite expressions from both these papers are reproduced in the Appendix at the end of this chapter, for completeness.

Setting up a Finite Element Model of a Tetrakaidecahedron Unit Cell

In general, a tetrakaidecahedron has 24 vertices and 36 edges comprising of 8 six-sided polygons and 6 four-sided polygons (Figure 2-2). It is more precisely called truncated octahedron, since it is created by truncating the corners of an octahedron (Weisstein, E.W, 1993). A regular tetrakaidecahedron is generated by truncating the corners of a cube. This is called an equisided tetrakaidecahedron. If it is generated by truncating the corners of a cuboid or hexahedron, it is called an elongated tetrakaidecahedron.

An equisided tetrakaidecahedron as the name indicates has all edges of equal length. The geometry of the equisided tetrakaidecahedron can be completely defined by defining just the length of one of its sides. It has 8 regular hexagons and 6 squares. An equisided tetrakaidecahedron has been shown in Figure 2-2a.

An elongated tetrakaidecahedron on the other hand has 8 irregular hexagons and 2 rhombuses (on the top and the bottom) and 4 squares (in the other 2 directions). The geometry of the elongated tetrakaidecahedron requires at least 3 dimensions (l, b, θ) as shown in Figure 2-2b.

In this study, the commercially available ABAQUS® finite element software is employed for developing the model. The principal directions X, Y, and Z are considered to be along the lines passing through the centers of the squares (Figure 2-2a , Figure 2-2b) on the front and back, the left and right and the top and the bottom, respectively. Al the struts in the unit cell are modeled as 3-D beam elements. Including the squares and the hexagons, the tetrakaidecahedron unit cell is made up of 24 beam elements. It should be noted that even though there are 36 edges in the geometry of the tetrakaidecahedron, only 24 beam elements have been modeled. This is due to periodicity of the unit cell, Out of the 6 squares (3 pairs of squares - the top and bottom pair, the left and the right pair and the front and the back pair) - only the top, front and right squares are modeled as shown in Figure 2-3.The lines shown in red-dotted lines in the figure are not modeled.

The geometry and the material properties of the constituent strut material used in the equisided tetrakaidecahedron model are listed in Table 2-1. The strut material is considered as isotropic. In the current example the beam cross sections are approximated to be an equilateral triangle. The dimensions required to completely describe an equisided tetrakaidecahedron unit cell, namely the length of the strut of the unit cell (L) and the side of the equilateral triangle (D) ,that are shown in Figure 2-2a have also been given in the table 2-1. The beam cross-sections are oriented such that

the bisector of one of the angles of the triangular cross section at the center of the strut passes through the unit-cell center (Figure 2-4). The cross section properties used in the model are also listed in Table 2-1.

Similar to an equisided tetrakaidecahedron, the geometry and the material properties of the constituent strut material used in the elongated tetrakaidecahedron model are listed in Table 2-2. The strut material is again considered to be isotropic. Actual micro-structural measurements (Sullivan et al, 2008) indicate that the strut cross section in polyurethane foams is actually a 3-cusp hypocycloid (Figure 2-2b). The dimensions required to completely describe the elongated tetrakaidecahedron unit cell, namely the length of the strut of the unit cell on the top and the bottom squares (l), the length of the struts in the other squares (b),the radius of the 3-cusp hypocycloid cross-section (r),and the orientation of the struts (θ) has been shown in Figure 2-2b. The cross section properties used in the model are listed in Table 2-2.

The use of beam elements to model the struts needs some explanation. Strictly the beam model will be valid only if the struts are slender and behave like a beam. This requires a slenderness ratio (L/r', where L is the length of the strut, r' is the radius of gyration defined by r'2=I/A) greater than about 10. If the slenderness ratio is less than 10 but greater than 6, one can use shear-deformable beam elements and hope to obtain good results. If L/r' is less than 6, one cannot use beam elements to model the deformation of the struts. One needs to resort to solid elements.

For both equi-sided and elongated tetrakaidecahedrons, two-node beam elements (classical Euler-Bernoulli beam element, B33 in the ABAQUS® material library) with cubic formulation were used to model the unit cell. Three-node quadratic elements

(shear deformable Timoshenko beam elements, B32 in the ABAQUS® material library) were used in some cases to study the effects of shear deformation on the overall properties of the foam.

Periodic Boundary Conditions

For computing the elastic constants using micromechanics, we need equations that relate the micro-strains to the corresponding macro-strains. Using these equations, the periodic boundary conditions (BCs) can be derived. From the periodicity of the cell structure (Figure 2-5), the representative volume element (RVE) is identified to be the smallest cuboid that completely encloses the tetrakaidecahedron such that 6 square sides of the tetrakaidecahedron are on the 6 faces of the cuboid.

In this section we derive the periodic boundary conditions that will be used to derive the elasticity matrix of the idealized foam. Consider the deformation gradient $\varepsilon_{ij} = u_{i,j}$. We would like to subject the RVE to a deformation such that the average of the above deformation gradient is equal to a given $\overline{\varepsilon}_{ij}$. Then this condition can be represented as

$$\overline{\varepsilon}_{ij} = \frac{1}{V}\int_V \frac{\partial u_i}{\partial x_j} dV \tag{2-1}$$

where *V* is the RVE volume. By applying divergence theorem to the right hand side of Eq.(2-1), the volume integral is converted into surface integral as

$$\overline{\varepsilon}_{ij} = \frac{1}{V}\int_S u_i n_j dS \tag{2-2}$$

where the integration is performed over the surface of the cuboid. Noting that n_j is non-zero only on two surfaces that are normal to the *j* direction, the above equation (2-2) can be written as

$$\overline{\varepsilon}_{ij} = \frac{1}{V}\left(u_i^{(+j)} - u_i^{(-j)}\right) A_j \tag{2-3}$$

where A_j is the area of the face normal to j-direction, $\left(u_i^{(+j)} - u_i^{(-j)}\right)$ represent the difference in the displacements u_i on the two surfaces normal to the j-direction. The superscripts $+j$ and $-j$ indicate, respectively, the two surfaces with positive and negative normals in the j-direction. From the above equation we obtain the periodic boundary condition as

$$\left(u_i^{(+j)} - u_i^{(-j)}\right) = \overline{\varepsilon}_{ij} \frac{V}{A_j} = \overline{\varepsilon}_{ij} a_j, \;\; i, j = 1,3 \tag{2-4}$$

Then the periodic BC for the three normal strains can be written as

$$\left(u_i^{(+j)} - u_i^{(-j)}\right) = \overline{\varepsilon}_{\mathrm{ii}} a_i \quad (i=1,2,3; \text{ no summation over } i) \tag{2-5}$$

For the case of shear strains the periodic BCs are not unique as the shear strain is given by the sum of two deformation gradients, $\gamma_{ij} = u_{i,j} + u_{j,i}$. Thus, one can apply either deformation gradient alone or both together. If, for example, one applies only $u_{i,j}$, then the BCs take the form

$$\left(u_i^{+j} - u_i^{-j}\right) = \overline{\gamma}_{\mathrm{ij}} a_j; \quad \left(u_j^{+i} - u_j^{-i}\right) = 0 \tag{2-6}$$

On the other hand if one chooses $u_{i,j} = u_{j,i} = \frac{\gamma_{ij}}{2}$, then two sets of BCs have to be applied as shown below:

$$\left(u_i^{+j} - u_i^{-j}\right) = \frac{\overline{\gamma}_{ij} a_j}{2}; \quad \left(u_j^{+i} - u_j^{-i}\right) = \frac{\overline{\gamma}_{ij} a_i}{2} \tag{2-7}$$

The above periodic BCs are explicitly presented in Table 2-3 through Table 2-8. These tables show the periodic boundary conditions in the form of difference in displacements between the set of nodes for the 3 unit strain load cases in the three principal directions. Figure 2-6, Figure 2-7 and Figure 2-8 show the pairs of node numbers that are subjected to these periodic boundary conditions. By using the reaction

forces that result after the unit normal strains are applied, the stiffness matrix for the foam can be computed. It should be noted that beam elements have rotational degrees of freedom, and we need to have periodic BCs for these DOFs also. Since, we do not have any curvature in the foam, the corresponding periodic BCs take the form

$$\left(\theta_i^{(+j)} - \theta_i^{(-j)}\right) = 0,\ i,\ j = 1,2,3 \tag{2-8}$$

Derivation of the Elastic Constants

In this section we derive the procedures for determining the equivalent elastic constants of the tetrakaidecahedral foam idealized as an orthotropic material. The representative volume element (RVE) of the foam is a cuboid. The equivalent orthotropic material has its principal material directions parallel to the edges of the cuboid. In this coordinate system the normal and shear deformations are uncoupled. First we will derive the equations to determine the Young's moduli and Poisson's ratios in the principal material coordinates, 1, 2 and 3 (which are shown as X, Y, Z in the figures). The (macro-scale) stress-strain relations of the foam are written as:

$$\begin{Bmatrix} \sigma_1 \\ \sigma_2 \\ \sigma_3 \end{Bmatrix} = \begin{bmatrix} C_{11} & C_{12} & C_{13} \\ C_{21} & C_{22} & C_{23} \\ C_{31} & C_{32} & C_{33} \end{bmatrix} \begin{Bmatrix} \varepsilon_1 \\ \varepsilon_2 \\ \varepsilon_3 \end{Bmatrix} \tag{2-9}$$

We subject the RVE to three independent deformations such that in each case only one normal strain is non-zero and other two normal strains are zero. For example, in the first case we apply periodic boundary conditions such that the cuboid expands only in the X-direction and the strains in the other two directions are equal to zero, i.e., the dimensions of the cuboid in those directions do not change. Then the macro-strains are given by:

$$\varepsilon_1 = 1, \varepsilon_2 = 0 \text{ and } \varepsilon_3 = 0 \tag{2-10}$$

Substituting Eq. (2-10) in (2-9), we get

$$\begin{Bmatrix}\sigma_1\\ \sigma_2\\ \sigma_3\end{Bmatrix}=\begin{bmatrix}C_{11} & C_{12} & C_{13}\\ C_{21} & C_{22} & C_{23}\\ C_{31} & C_{32} & C_{33}\end{bmatrix}\begin{Bmatrix}1\\ 0\\ 0\end{Bmatrix} \tag{2-11}$$

Let the corresponding force resultants (ABAQUS® output) in the three faces of the unit cell normal to the 1, 2 and 3 directions be, respectively, F_{11}, F_{21} and F_{31} (see Figure 2-9). Then the corresponding macro-stresses are obtained as:

$$\sigma_1=\frac{F_{11}}{A_1},\sigma_2=\frac{F_{21}}{A_2},\sigma_3=\frac{F_{31}}{A_3} \tag{2-12}$$

where A_1, A_2 and A_3 are areas normal to the 1,2 and 3 directions representing areas of the square surfaces in the 1, 2, and 3 directions of the RVE, in case of the equisided tetrakaidecahedron unit cell, and the areas of the rectangular surfaces in the 1, 2, 3 directions of the RVE, in case of the elongated tetrakaidecahedron unit cell.

Similarly we can deform the RVE in the other two directions and calculate second and third columns of [*C*].

For the case of shear, the calculations can be simplified, as there is no coupling between shear deformation and the normal deformation, and also between shear deformations in different planes. The periodic BCs for shear strains are given in Eqs. (2.7) and (2.8). The straightforward method of determining the shear modulus G_{ij} will be to relate the strain energy in the RVE to the strain energy density due to shear:

$$U=\frac{1}{2}G_{ij}\gamma_{ij}^2V \text{ or } G_{ij}=\frac{2U}{\gamma_{ij}^2V} \tag{2-13}$$

The deformation configurations when the unit cell is subjected to unit normal strain in Z direction and unit shear strain in the XY direction has been shown in Figure 2-10 and Figure 2-11.

Effect of Varying Cross-Section

It has been observed (Kyriakides et al, 2005) that in reality the cross-sectional area of the struts are not uniform but they gradually vary along the length of the beam with the cross-sectional area being maximum at the two ends of the beam and minimum at the center. For example, microstructural measurements (Kyriakides et al, 2005) indicate that the cross-sectional area varies according to the following function:

$$A(x) = A_0 f(x) = A_0 \left(86\frac{x^4}{l^4} + \frac{x^2}{l^2} + 1 \right) \tag{2-14}$$

where, A_0 is the Area at the mid-span of the strut, x is any point along the length of the strut $\left(-\frac{l}{2} \le x \le +\frac{l}{2} \right)$, l is the length of the strut.

The elastic constants of the foam with varying cross section could be determined by following the procedures similar to that of uniform cross section foam. In fact the struts can be modeled using one beam element as before but with equivalent cross sectional properties. Since the deformations (strains, curvatures, etc.) in a beam are inversely proportional to A, I and J the equivalent uniform cross sectional properties can be readily expressed as

$$\frac{1}{A_{eff}} = \frac{1}{l}\int_{-l/2}^{l/2} \frac{dx}{A(x)},$$

$$\frac{1}{I_{eff}} = \frac{1}{l}\int_{-l/2}^{l/2} \frac{dx}{I(x)}, \tag{2-15}$$

$$\frac{1}{J_{eff}} = \frac{1}{l}\int_{-l/2}^{l/2} \frac{dx}{J(x)}$$

where the suffix eff denotes effective properties. In order to determine the above effective properties, one has to assume the nature of the cross section. In this study we

assume the cross section of the strut is an equilateral triangle. Accordingly, the cross sectional dimension at midspan d0, corresponding area A0, and moments of inertia I0 and J0 are calculated as follows

$$A_0 = \frac{\sqrt{3}}{4} {d_0}^2$$
$$I_0 = \frac{\sqrt{3}}{96} {d_0}^4 \qquad (2\text{-}16)$$
$$J_0 = \frac{{A_0}^2}{5\sqrt{3}}$$

The variation of moments of inertia, using equation (16) along the length of the strut can then be written as

$$I(x) = I_0 \left[86 \frac{x^4}{l^4} + \frac{x^2}{l^2} + 1 \right]^2,$$
$$J(x) = J_0 \left[86 \frac{x^4}{l^4} + \frac{x^2}{l^2} + 1 \right]^2 \qquad (2\text{-}17)$$
$$\text{where,} \quad -\frac{l}{2} \le x \le +\frac{l}{2}$$

It is desirable to compare the properties of foam with struts having a varying cross-section to foam with struts having uniform cross-section. One approach to get a good comparison is by keeping the relative density same in both the cases. This can be achieved by keeping the volume of the strut same in both cases:

$$\int_{-l/2}^{+l/2} A(x)dx = \bar{A}l \qquad (2\text{-}18)$$

where, $\bar{A}$ is the area of the uniform cross-section, l is the length of the strut. Once $\bar{A}$ is calculated, one can determine the corresponding cross section dimension $\bar{d}$, and the moments of inertia $\bar{I}$ and $\bar{J}$.

Results and Discussion

Results obtained for the properties of equisided and elongated tetrakaidecahedron unit cells are shown in Table 2-9 and Table 2-10, respectively. The results for *E* and v match very well with the available analytical models – Model by Zhu, Knott, Mills for equisided tetrakaidecahedron unit cell and the model by Sullivan, Ghosn, Lerch for the elongated tetrakaidecahedron unit cell. The maximum error in the elastic constants was only 0.55% for the elastic moduli and 0.35% for the shear moduli, in case of the equisided tetrakaidecahedron unit cell. The maximum error in the elastic constants was 0.82% in the case of the elongated tetrakaidecahedron unit cell.

In addition, results from parametric studies have been shown as graphs in Figure 2-12 and Figure 2-13 for equisided and Figure 2-14 for elongated foam, respectively.

It is interesting to note that with the equisided tetrakaidecahedron as the unit cell, the results for the properties using either Euler-Bernoulli or shear deformable (Timoshenko) beam elements do not differ much (0.24% difference). This is because of the assumed beam aspect ratio (L/d = 17). With the beams being slender, the classical beam theory assumption holds good and the shear deformation is negligible. Hence the Euler-Bernoulli and the Timoshenko beams give comparable results.

However, in the case of the elongated tetrakaidecahedron wherein the beams are short and thick, especially on the squares on the top and the bottom faces the values for the properties have significant difference when a shear deformable element is assumed instead of a Euler-Bernoulli beam element. The elastic modulus assuming shear deformable beams is 9% lesser than the elastic modulus assuming Euler-Bernoulli beams as shown in the results.

Figure 2-12 and Figure 2-13 show the variation of elastic modulus and Poisson ratio with relative density. It is seen that the elastic modulus varies as square of the relative density. Figure 2-14 shows the variation of the elastic moduli in the rise direction and perpendicular to rise direction with relative density for the elongated tetrakaidecahedron unit cell. It is seen that as the relative density increases, the difference between the properties obtained from using Euler-Bernoulli elements and Timoshenko elements keeps increasing. Hence the existing analytical models assuming the unit cell edges completely made out of Euler-Bernoulli beams would not be accurate, and bringing in the effect of shear deformation in the analytical formulation would be important.

The results of elastic constants for the variable cross section foam along with that of idealized uniform cross section foam are presented in Table 2-11. The relative density is assumed to be 0.165% in both cases. It is seen that the Young's modulus and shear modulus of ideal foams with uniform cross section is about 2.4 times that of varying cross section foam. The reason for this is that most of the solid material being near the ends (Figure 2-15, Figure 2-16) of the strut, thus making majority of length (about 60%) in the middle slender. This reduces the moments of inertia considerably making the struts more flexible. The variation of the moment of inertia, area of cross-section and diameter across the length of the strut are compared with those of uniform cross section foam in Figure 2-15 and Figure 2-16 respectively. It is to be noted that our analysis is restricted for foams that have a relative density below 0.2% where in the classical beam theory assumptions would hold. This explains the trend dissimilarities between the current work and elsewhere (Kyriakides, 2005).

Conclusions

Finite element based micromechanics has been used to calculate the elastic properties of foams with tetrakaidecahedral unit cells. The results for elastic constants match well with the available analytical models. It is evident that using finite element methods gives a flexibility to choose between Euler-Bernoulli formulation or the shear-deformable formulation or a mix of both in the same unit cell over the existing analytical models. The biggest advantage of using finite element methods is that any kind of a unit cell with unequal sides that might be obtained from microstructural measurements could be modeled with ease and the technique for computing properties would still remain the same. It would also be easy to extend the same finite element methods to calculate inelastic behavior of the foam. The same finite element based micromechanics methods could also be easily used in the unit cell model to generate multi-axial failure envelopes for foams. Also the effect of varying cross-section on the elastic properties has been studied and has been shown that for the same relative density, foams with varying cross-sections are lesser stiffen compared to foams with uniform cross-section.

It is to be noted that in the current micromechanics based approach the assumption is that the foam is made out of exactly identical unit cells. However, in reality, as seen in the micrographs in figure 2-1, the cell sizes can vary considerably and there are many discontinuities in the real material. One way of getting an estimate of what varying cell sizes do to the properties is to do a sensitivity analysis of the stiffness properties obtained from these methods when different parameters such as geometry, strut properties etc are varied.

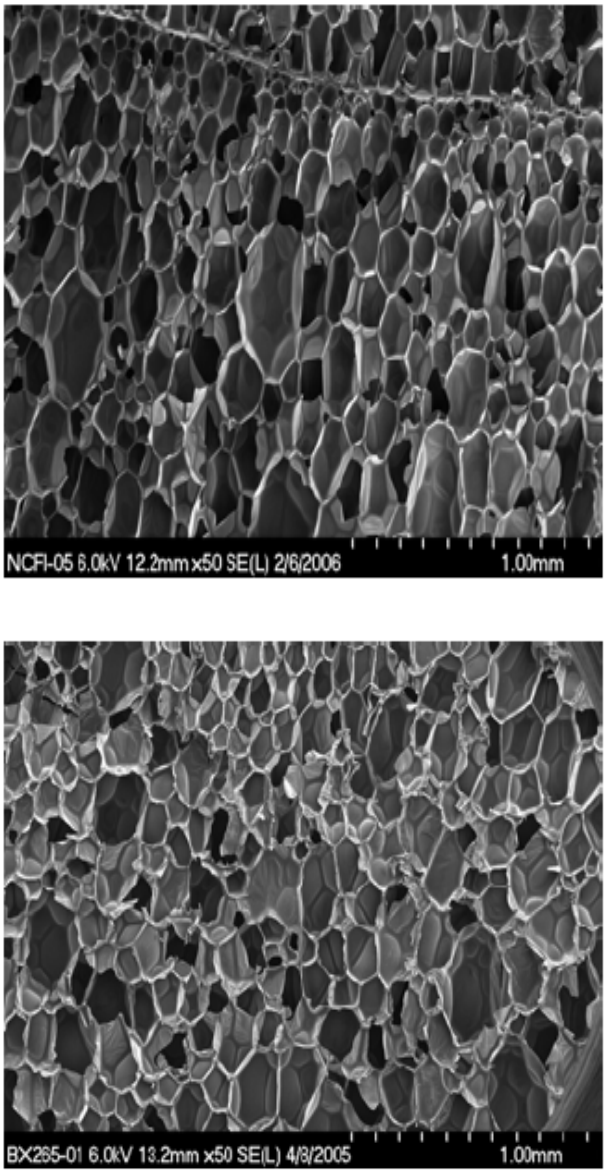

Figure 2-1. Photomicrographs of foams used for external fuel tanks A) NCFI24-124 B) BX-265

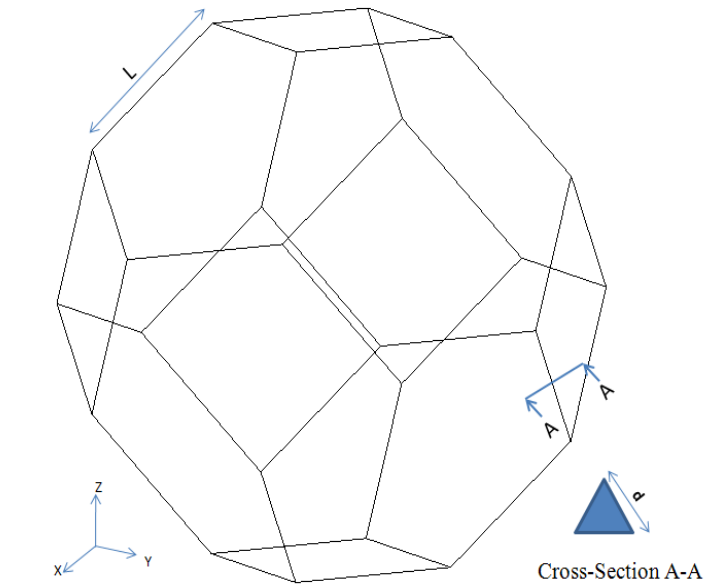

A

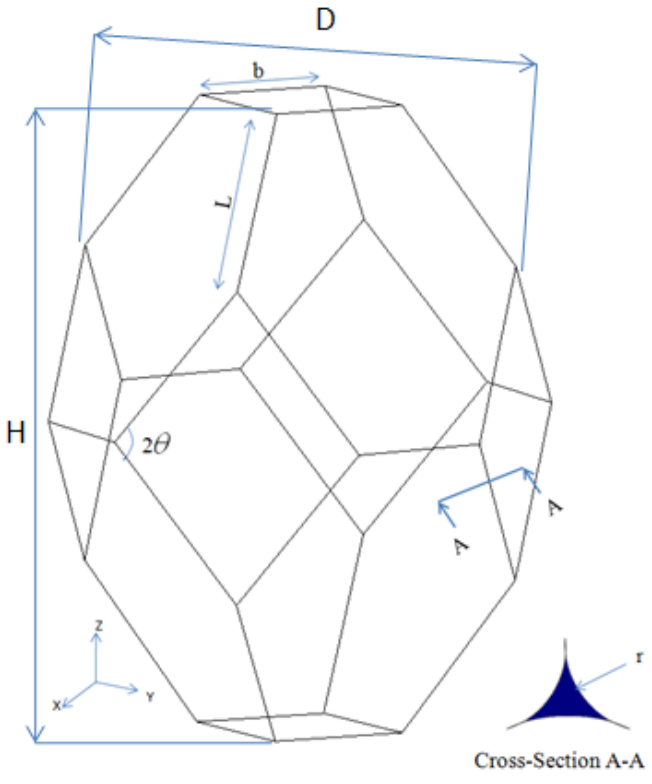

B

Figure 2-2. Geometry definition of a tetrakaidecahedron unit cell A) Equisided tetrakaidecahedron B) Elongated tetrakaidecahedron

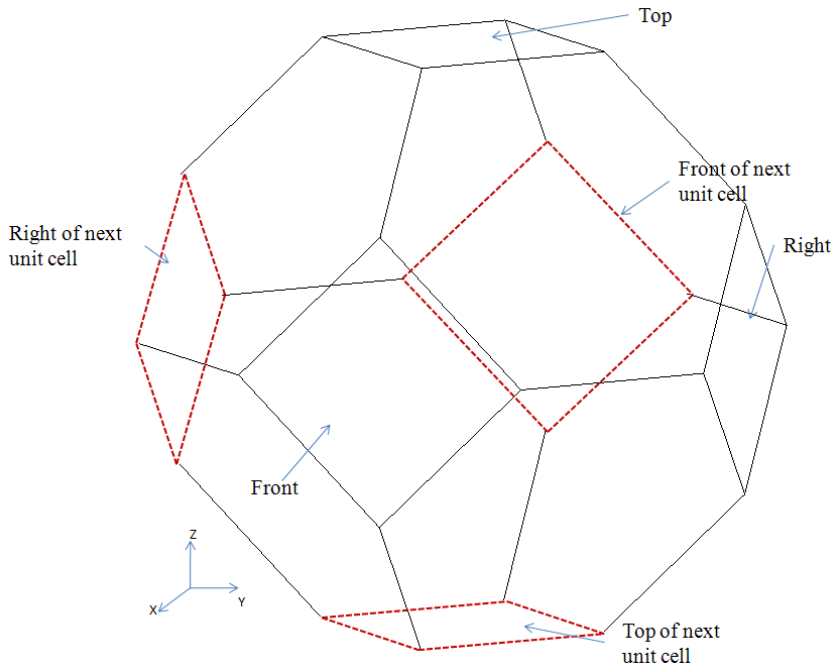

Figure 2-3. Beam elements that are modeled in the unit cell

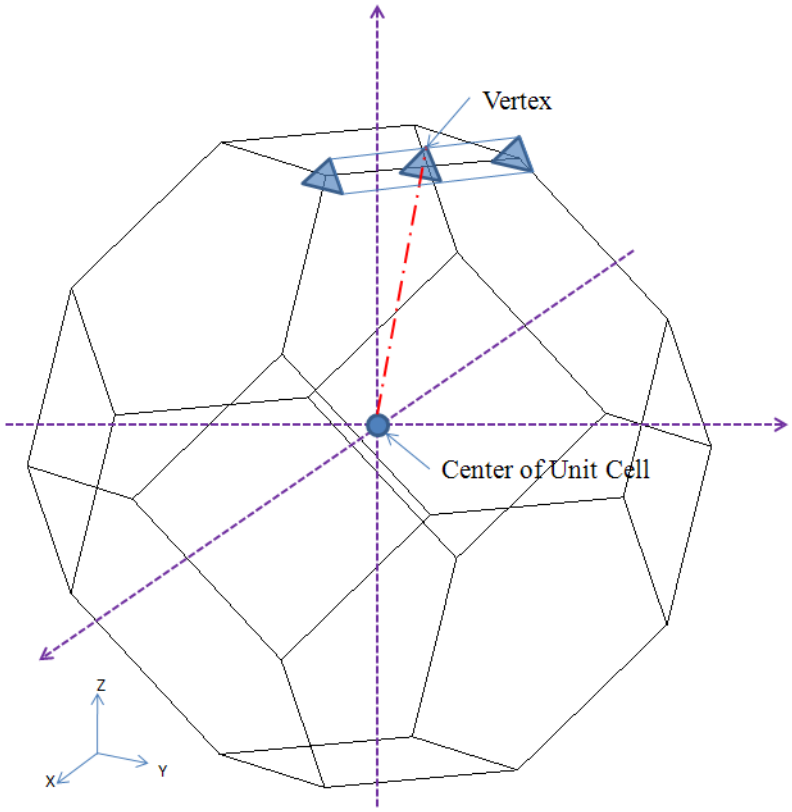

Figure 2-4. Defining the orientation of the beams of the tetrakaidecahedron unit cell

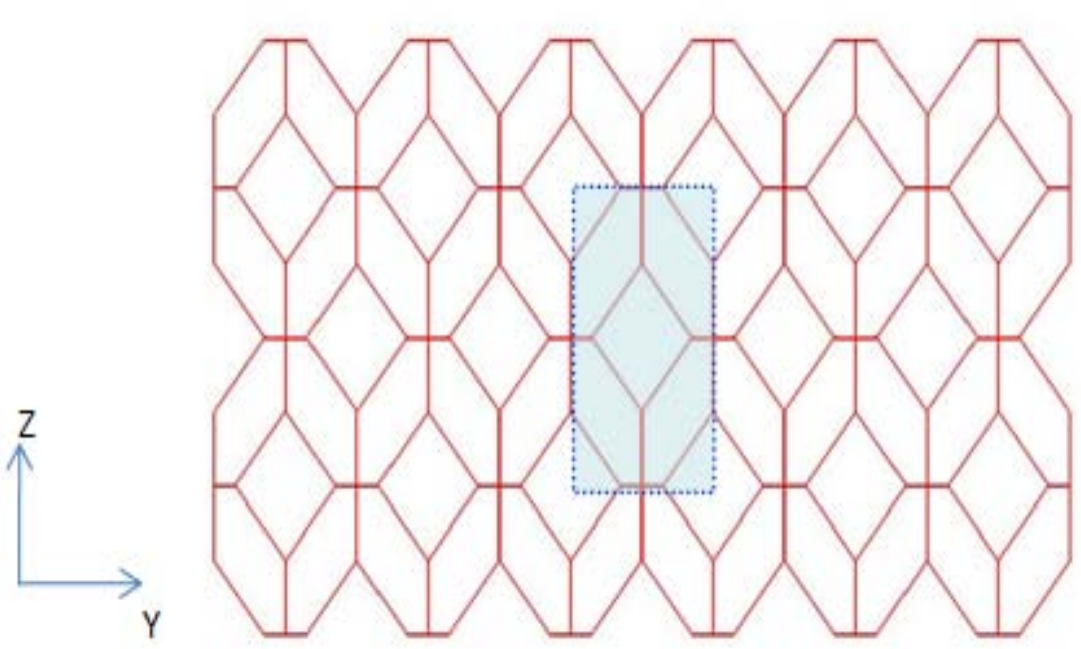

Figure 2-5. Identifying the Representative Volume Element (RVE)

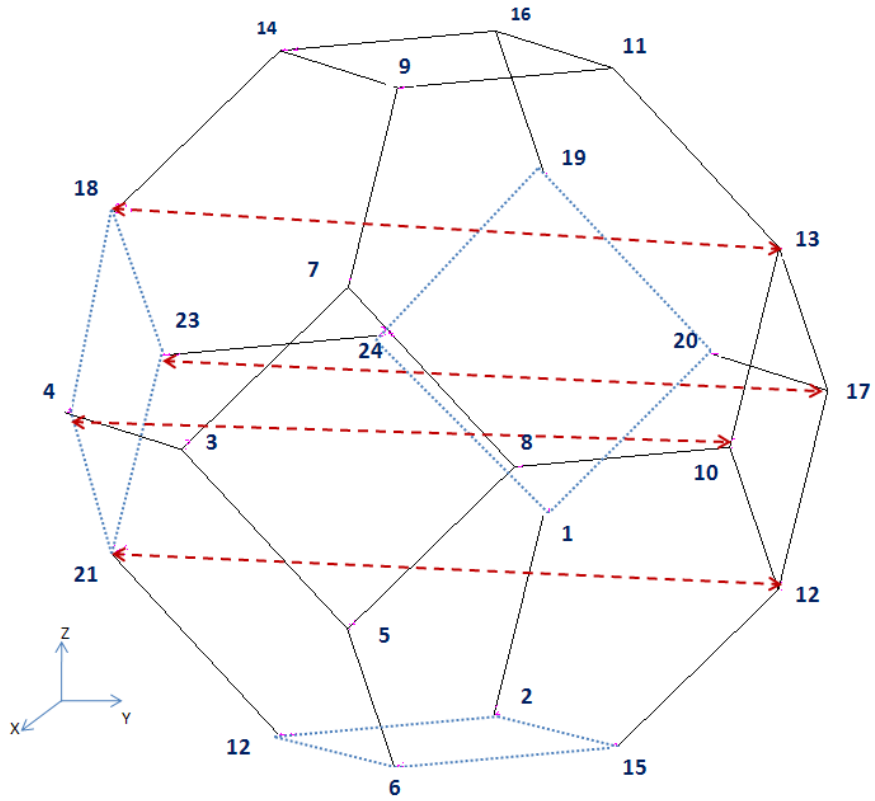

Figure 2-6. Nodal pairs subjected to PBCs (Left-Right)

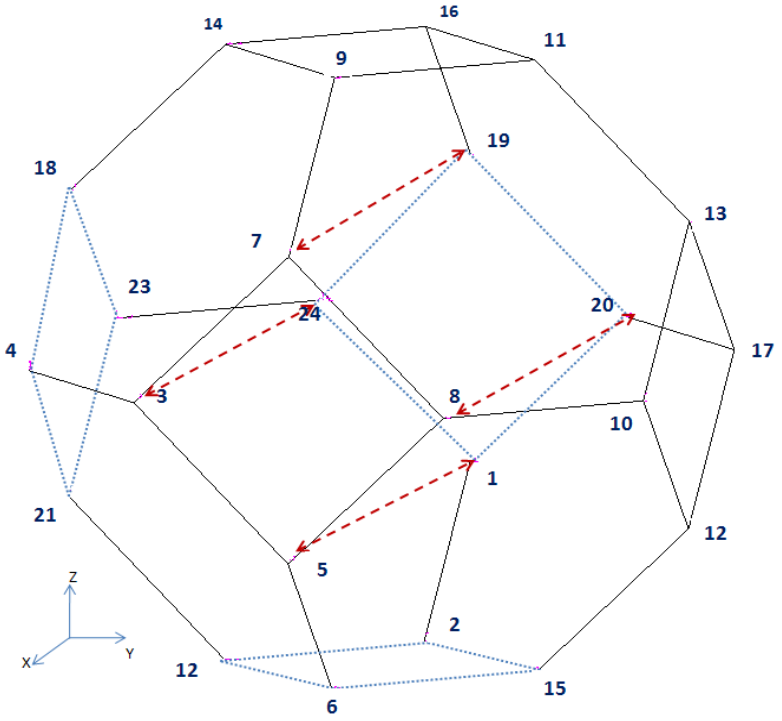

Figure 2-7. Nodal pairs subjected to PBCs (Front-Back)

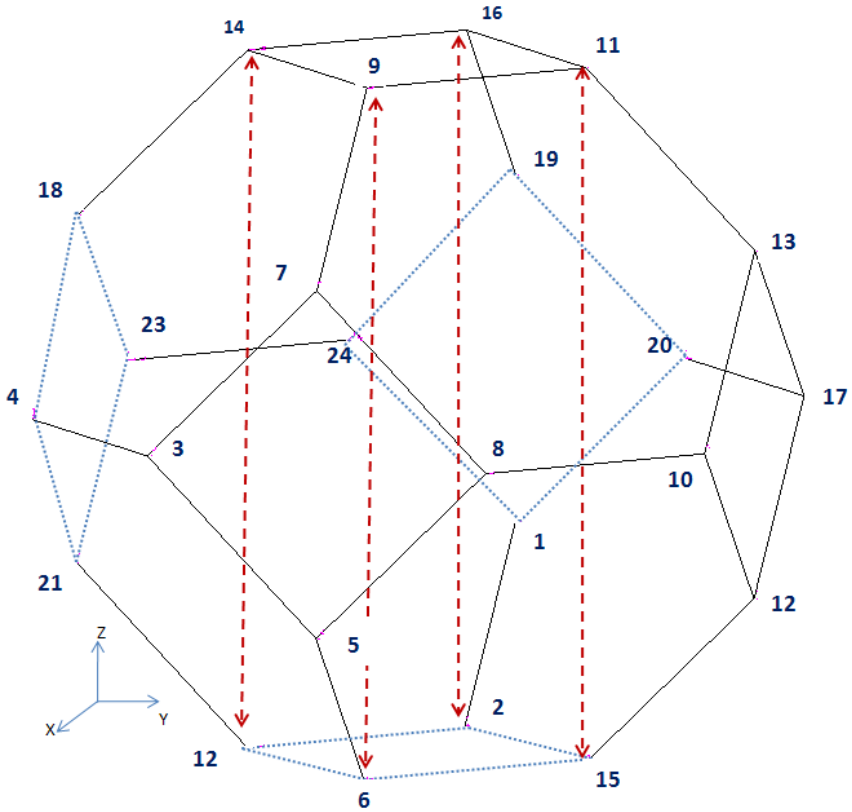

Figure 2-8. Nodal pairs subjected to PBCs (Top-Bottom)

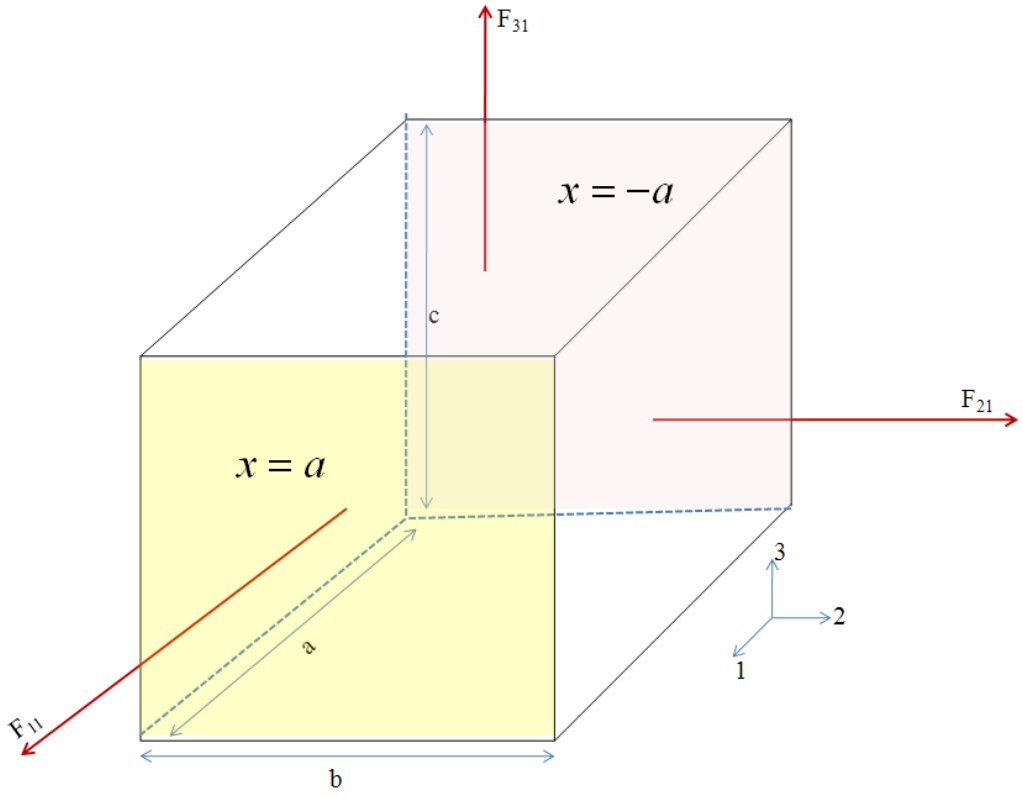

Figure 2-9. Representative Volume Element (RVE) showing force resultants in the 3 directions

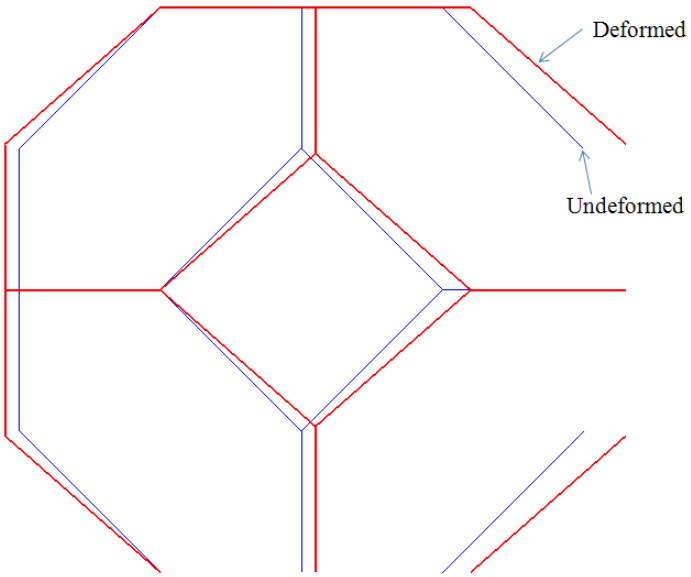

Figure 2-10. Deformed configuration resulting from unit normal strain applied in the X-direction

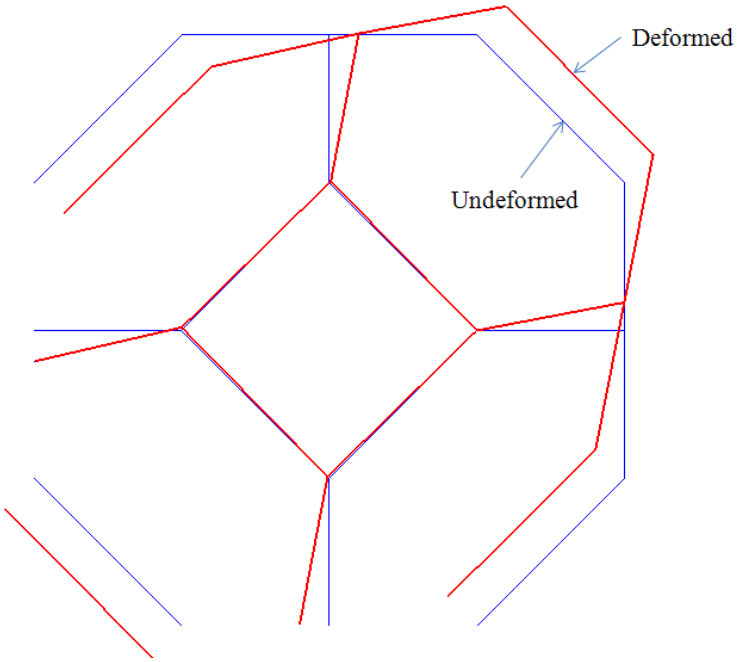

Figure 2-11. Deformed configuration resulting from unit shear strain applied in the XY-direction

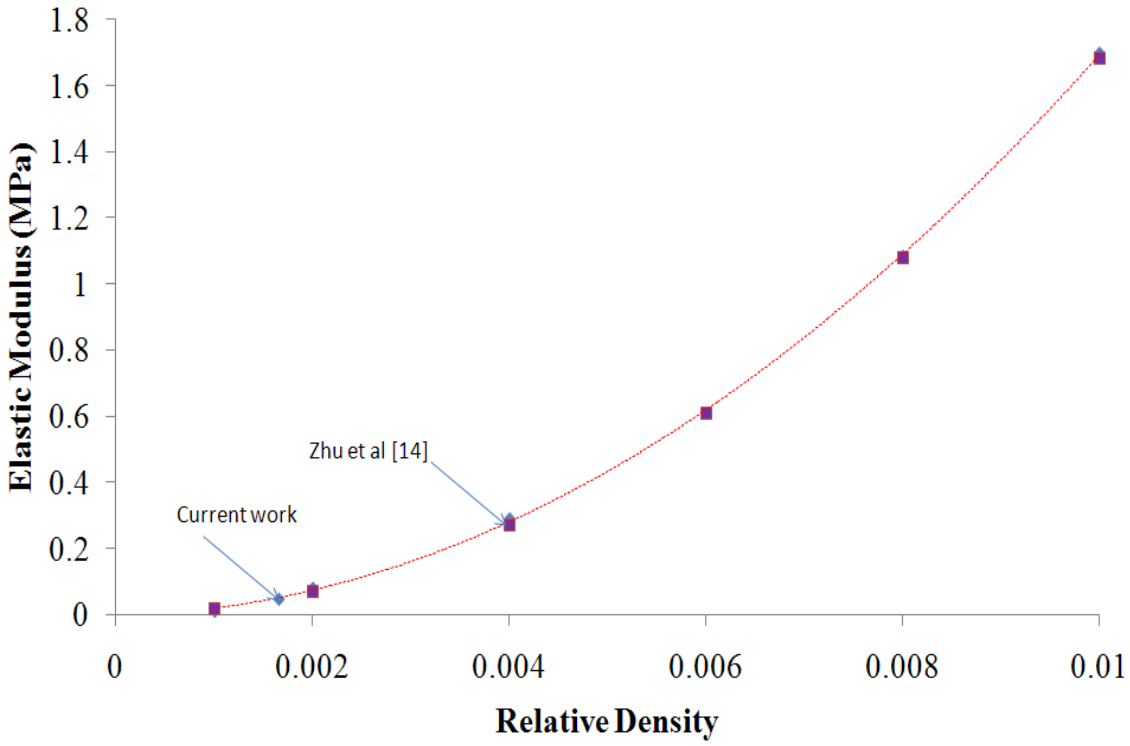

Figure 2-12. Variation of elastic modulus with relative density for equisided tetrakaidecahedron unit cell

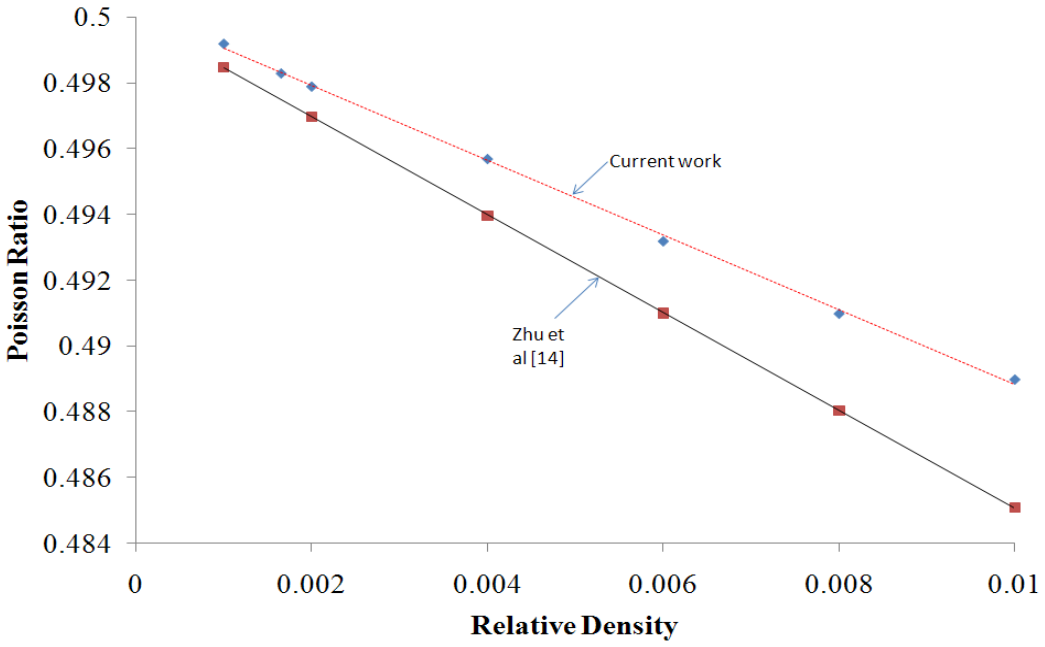

Figure 2-13. Variation of poisson ratio with relative density for equisided tetrakaidecahedron unit cell

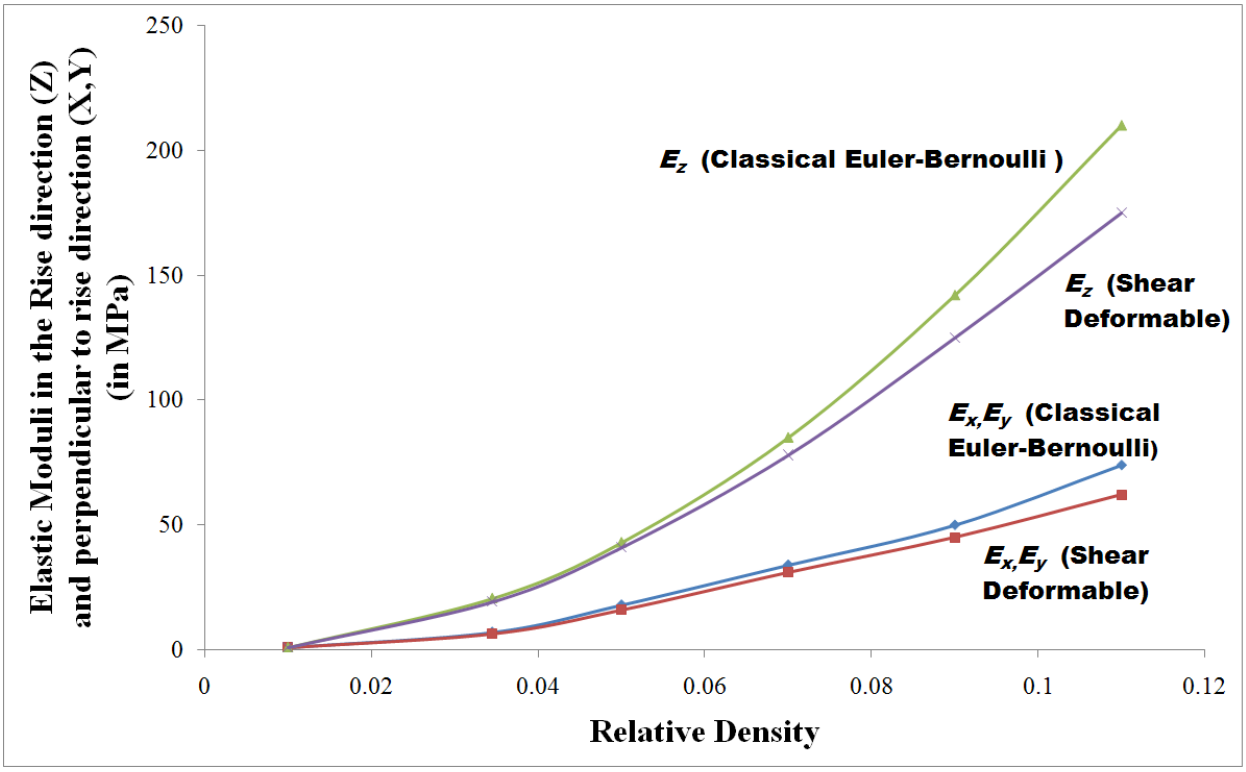

Figure 2-14. Variation of moduli in the rise and the perpendicular to rise direction for elongated tetrakaidecahedron unit cell

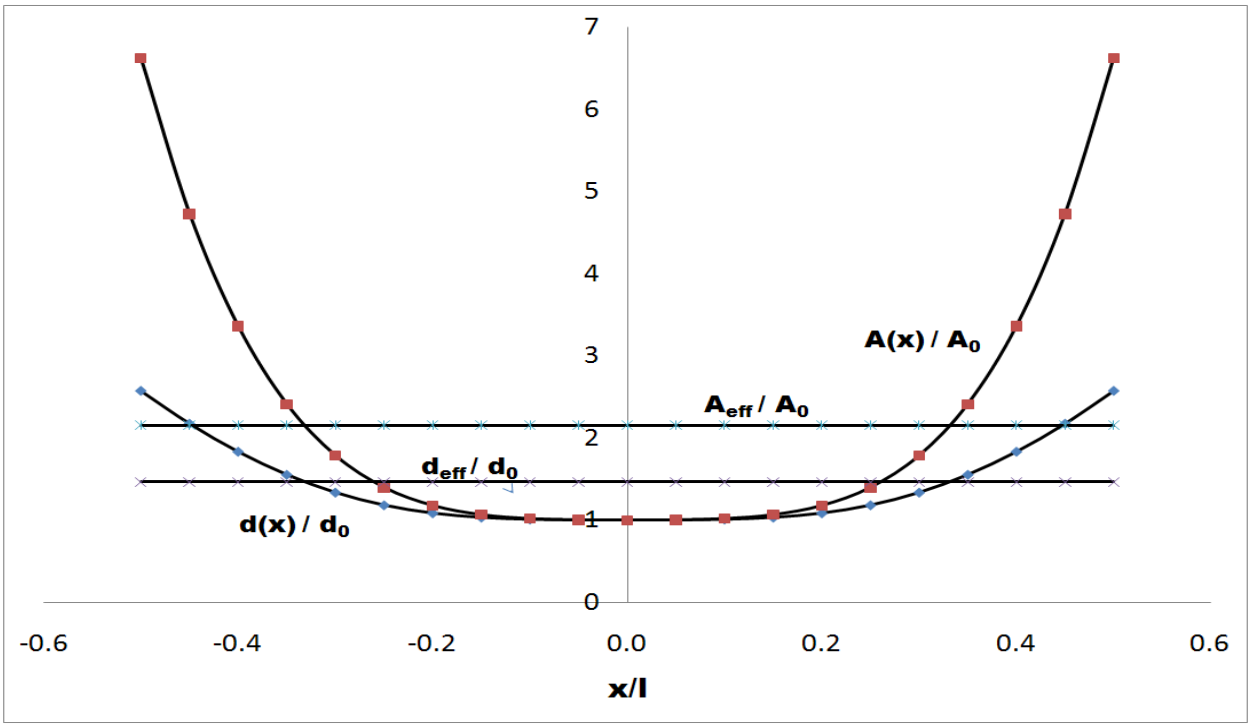

Figure 2-15. Variation of area of cross section, diameter along the length of the strut

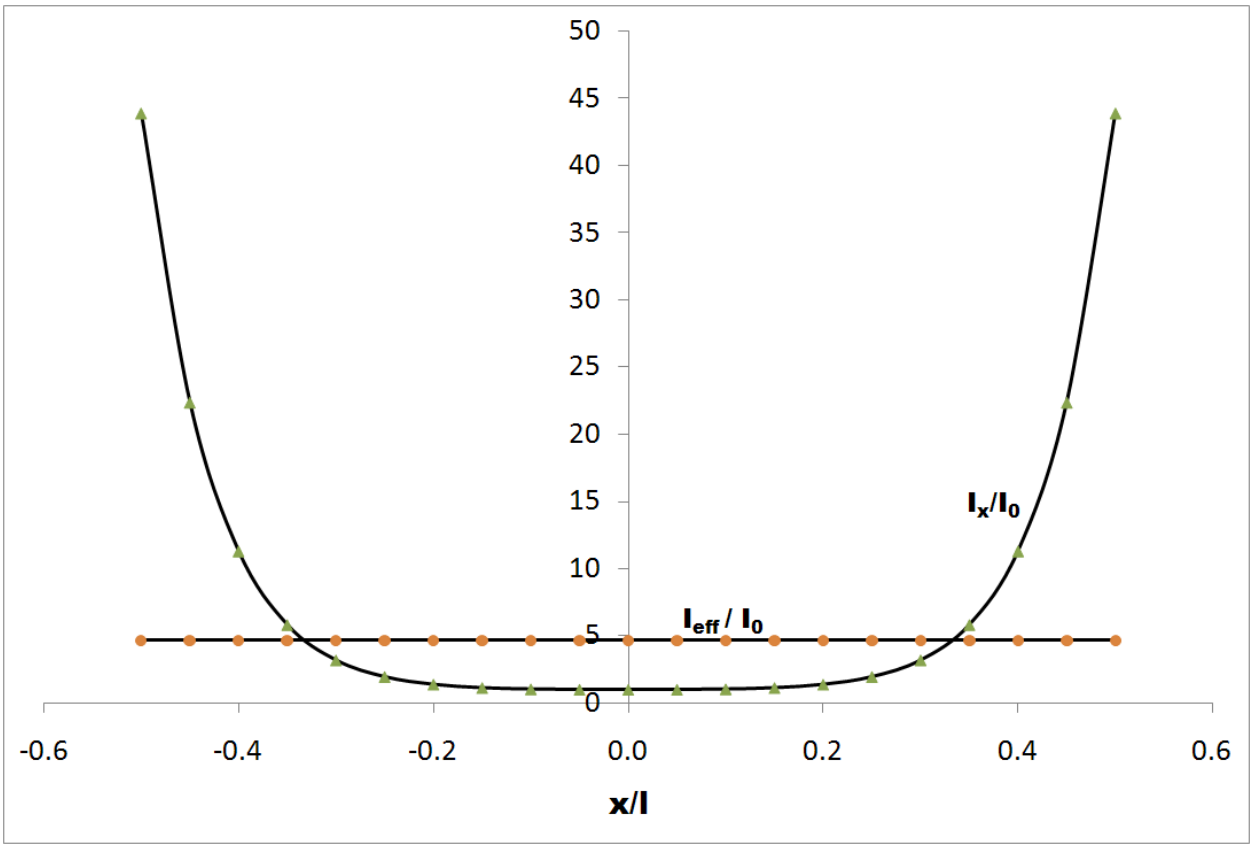

Figure 2-16. Variation of moment of inertia along the length of the strut

Table 2-1. Material properties of the strut, cross sectional properties of equisided tetrakaidecahedron unit cell

	Property	Value
Material Properties of the strut	Density, ρ_s (Kg/m^3)	1650
	Elastic modulus, E_s (GPa)	23.42
	Poisson ratio, ν_s	0.33
Geometry of the equisided tetrakaidecahedron unit cell	L (mm)	1
	d (mm)	0.06
	Relative density	0.001653
Cross-section properties (Equilateral Triangle)	Cross sectional area, A (m^2)	1.5588×10^{-9}
	Moment of Inertia, I_x ,I_y (m^4)	2.3382×10^{-19}
	Torsion constant, J (m^4)	4.6765×10^{-19}

Table 2-2. Material properties of strut, geometric properties and cross sectional properties of elongated tetrakaidecahedron unit cell

	Property	Value
Material Properties of the strut	Density, ρ_s (Kg/m^3)	1650
	Elastic modulus, E_s (GPa)	17
	Poisson ratio, v_s	0.33
Geometry of the elongated tetrakaidecahedron unit cell	L (μm)	77.2
	b (μm)	35.6
	r (μm)	26
	H (μm)	248.85
	D (μm)	142.04
	Relative density	0.03481
Cross-section properties (3-cusp hypocycloid)	Cross sectional area, A (m^2)	1.024×10^{-10}
	Moment of Inertia, I_x ,I_y (m^4)	1.403×10^{-21}
	Torsion constant, J (m^4)	2.806×10^{-21}

Table 2-3. PBCs for unit normal strain in X-direction

		Difference in displacements		
Faces	Pair of node numbers	U_x	U_y	U_z
Top–Bottom (Faces normal to the principal *Z*-axis)	16-2	0	0	0
	14-22	0	0	0
	6-9	0	0	0
	15-11	0	0	0
Front–Back (Faces normal to the principal *X*-axis)	9-7	a_1	0	0
	24-3	a_1	0	0
	5-1	a_1	0	0
	20-8	a_1	0	0
Left–Right (Faces normal to the principal *Y*-axis)	18-13	0	0	0
	10-4	0	0	0
	21-12	0	0	0
	23-17	0	0	0

Table 2-4. PBCs for unit normal strain in Y-direction

		Difference in displacements		
Faces	Pair of node numbers	U_x	U_y	U_z
Top – Bottom (Faces normal to the principal *Z*-axis)	16-2	0	0	0
	14-22	0	0	0
	6-9	0	0	0
	15-11	0	0	0
Front – Back (Faces normal to the principal *X*-axis)	9-7	0	0	0
	24-3	0	0	0
	5-1	0	0	0
	20-8	0	0	0
Left – Right (Faces normal to the principal *Y*-axis)	18-13	0	a_2	0
	10-4	0	a_2	0
	21-12	0	a_2	0
	23-17	0	a_2	0

Table 2-5. PBCs for unit normal strain in Z-direction

Faces	Pair of node numbers	Difference in displacements		
		U_x	U_y	U_z
Top – Bottom (Faces normal to the principal *Z*-axis)	16-2	0	0	a_3
	14-22	0	0	a_3
	6-9	0	0	a_3
	15-11	0	0	a_3
Front – Back (Faces normal to the principal *X*-axis)	9-7	0	0	0
	24-3	0	0	0
	1-5	0	0	0
	20-8	0	0	0
Left – Right (Faces normal to the principal *Y*-axis)	18-13	0	0	0
	10-4	0	0	0
	21-12	0	0	0
	23-17	0	0	0

Table 2-6. PBCs for unit shear strain in XY-direction

Faces	Pair of node numbers	Difference in displacements		
		U_x	U_y	U_z
Top – Bottom (Faces normal to the principal *Z*-axis)	16 - 2	0	0	0
	14 - 22	0	0	0
	6-9	0	0	0
	15-11	0	0	0
Front – Back (Faces normal to the principal *X*-axis)	9-7	0	$a_1/2$	0
	24-3	0	$a_1/2$	0
	5-1	0	$a_1/2$	0
	20-8	0	$a_1/2$	0
Left – Right (Faces normal to the principal *Y*-axis)	18-13	$a_2/2$	0	0
	10-4	$a_2/2$	0	0
	21-12	$a_2/2$	0	0
	23-17	$a_2/2$	0	0

Table 2-7. PBCs for unit shear strain in YZ-direction

		Difference in displacements		
Faces	Pair of node numbers	U_x	U_y	U_z
Top – Bottom (Faces normal to the principal *Z*-axis)	16-2	0	$a_2/2$	0
	14-22	0	$a_2/2$	0
	6-9	0	$a_2/2$	0
	15-11	0	$a_2/2$	0
Front – Back (Faces normal to the principal *X*-axis)	9-7	0	0	0
	24-3	0	0	0
	5-1	0	0	0
	20-8	0	0	0
Left – Right (Faces normal to the principal *Y*-axis)	18-13	0	0	$a_3/2$
	10-4	0	0	$a_3/2$
	21-12	0	0	$a_3/2$
	23-17	0	0	$a_3/2$

Table 2-8. PBCs for unit shear strain in XZ-direction

		Difference in displacements		
Faces	Pair of node numbers	U_x	U_y	U_z
Top – Bottom (Faces normal to the principal *Z*-axis)	16-2	$a_1/2$	0	0
	14-22	$a_1/2$	0	0
	6-9	$a_1/2$	0	0
	15-11	$a_1/2$	0	0
Front – Back (Faces normal to the principal *X*-axis)	9-7	0	0	$a_3/2$
	24-3	0	0	$a_3/2$
	5-1	0	0	$a_3/2$
	20-8	0	0	$a_3/2$
Left – Right (Faces normal to the principal *Y*-axis)	18-13	0	0	0
	10-4	0	0	0
	21-12	0	0	0
	23-17	0	0	0

Table 2-9. Results for foam with equisided tetrakaidecahedron unit cell with relative density 0.01653%

Property	Finite Element Model			Analytical Model (Zhu et al, 1997)	% difference between analytical and Finite Element Model
	Euler-Bernoulli (2-node cubic)	Shear deformable (3-node quadratic)	% difference between Euler-Bernoulli model and Shear-deformable model		
$E_x = E_x = E_z$ (GPa)	46.7×10^{-6}	46.6×10^{-6}	0.24	46.4×10^{-6}	0.55
$v_{xy} = v_{yz} = v_{xz}$	0.498	0.498	0.11	0.497	0.14
$G_{xy} = G_{yz} = G_{xz}$ (GPa)	14.9×10^{-6}	14.8×10^{-6}	0.43	14.9×10^{-6}	0.35

Table 2-10. Results for foam with elongated tetrakaidecahedron unit cell with relative density 3.45%

Property	Finite Element Model			Analytical Model (Sullivan et al, 2008)	% difference between analytical and Finite Element Model
	Euler-Bernoulli (2-node cubic)	Shear deformable (3-node quadratic)	% difference between Euler-Bernoulli model and Shear-deformable model		
$E_x = E_y$ (Mpa)	7.09	6.5	-9.04	7.07	0.29
E_z (Mpa)	20.63	19.28	-6.99	20.8	-0.82
$v_{xy} = v_{yx}$	0.0588	0.0757	22.28	0.0598	-1.84
$v_{xz} = v_{yz}$	0.3745	0.3694	-1.39	0.373	0.47
$v_{zx} = v_{zy}$	1.0934	1.0991	0.52	1.09	-0.31
G_{xy} (Mpa)	2.07	1.95	-6.03	2.06	0.39
$G_{yz} = G_{xz}$ (Mpa)	6.74	6.25	-7.88	6.66	1.17

Table 2-11. Results for comparison of properties of foam with equisided tetrakaidecahedron

	Uniform Cross-section	Varying Cross-Section	Ratio
Elastic Modulus *(E)* (Pa)	46,402	19172	2.42
Shear Modulus *(G)* (Pa)	14920	6183	2.41
Moment of Inertia *(I)* (m^4)	2.34×10^{-19}	0.965×10^{-19}	2.42
Poisson Ratio (*v*)	0.4975	0.4989	1.00

CHAPTER 3
FAILURE ENVELOPES OF OPEN CELL FOAMS WITH TETRAKAIDECAHEDRAL UNIT CELLS USING MICROMECHANICS BASED METHODS

In this chapter, finite element method based micromechanics methods have been used for predicting the multi-axial failure strengths of low density open cell foams with a microstructure made out of tetrakaidecahedral unit cells. For this, it is a pre-requisite to have calculated the elastic properties of the foam beforehand. Hence this is a logical extension to calculating the properties of the foam, the procedure for which was explained in chapter 2. Here, foams with both equisided tetrakaidecahedron and Kelvin-elongated tetrakaidecahedron unit cells have been studied. The struts of the unit cell are modeled using three-dimensional beam elements. Failure strengths in different material directions are computed using Direct Micromechanics based Methods (DMM). The effect of varying cross section on the failure strengths is presented. Failure envelopes for two-dimensional and three-dimensional stress states are plotted for foams with equisided and elongated tetrakaidecahedron unit cells. Bi-axial failure envelope for foams with equisided tetrakaidecahedron unit cells has been shown to be a regular hexagon in the hydrostatic plane. The tri-axial failure envelope for foams with equisided tetrakaidecahedron unit cells is shown to be a double hexagonal pyramid in the hydrostatic plane. The bi-axial and tri-axial failure envelopes of foams with elongated tetrakaidecahedron unit cells are plotted and the effect of anisotropy in foams with these unit cells on the failure envelopes is also discussed.

Introduction

As seen from Chapter 2, with the recognition of a repeating geometric pattern which is typical in cellular materials (which is a tetrakaidecahedron), the principles of micromechanics have been the choice for material characterization of foams. The

analytical models for the elastic properties and failure strengths of open cell foams typically assume that the unit cell edges or struts of these materials behave like a three dimensional beam. Beam equations are used to model the struts in the identified repeating unit of the foam structure (Figure 3-1, Figure 3-2) subjected to external loads and a set of equations for the effective Young's modulus, Poisson's ratio and tensile strength are written in the principal material directions (Zhu et al, 1997, Sullivan et al, 2008). The elastic constants for foams have been derived in terms of the cell edge length, and the axial, flexural and torsional rigidities of the strut cross section.

Direct Micromechanics Method (DMM) to Compute Multi-Axial Failure Strengths

Analytical models in literature (Sullivan et al, 2008) typically estimate the failure strength of foams to be the stress level where the constituent element strut undergoes brittle failure. This is represented as an expression for failure strength in a particular material direction. In practice, foam structures experience multiaxial states of stress. Analytical models fail to show the effect of multi-axial state of stress on the failure strength in a particular direction. The Direct Micromechanics Methods (DMM) can address this limitation very efficiently.

The DMM was originally proposed by Sankar et al and its effectiveness has been demonstrated in several of his papers (Leong et al, 2008, Rao et al, 2009, Stamblewski et al, 2008, Marrey et al, 1997). These methods have been successfully implemented for material characterization of textile composites. The failure envelopes obtained from DMM for these materials are also compared with available phenomenological failure criteria which have been derived for plane stress states (Marrey et al,1997). Also failure envelopes from DMM have also been shown to agree well with experimental results (Daniel and Ishai, 2004).

Approach

DMM can be considered as a computational tool to estimate failure strengths. The broader objective of predicting failure strength of foams using DMM is computing a load factor when it is subjected for a generalized state of loading. The procedure to calculate the load factor is as follows.

Consider the foam being subject to a state of macro-stress given by $\{\sigma\} = \{\sigma_x \quad \sigma_y \quad \sigma_z \quad \tau_{xy} \quad \tau_{yz} \quad \tau_{xz}\}^T$. The macro-strains due to the above stress state can be calculated as:

$$\{\varepsilon\} = [C]^{-1}\{\sigma\} \tag{3-1}$$

where, $[C]$ is the stiffness matrix of the foam. This matrix can be calculated using the elastic properties that were calculated from Chapter 2. The above macro-strain $\{\varepsilon\}$ can be represented as, $\{\varepsilon\} = \{\varepsilon_{xx} \quad \varepsilon_{yy} \quad \varepsilon_{zz} \quad \gamma_{xy} \quad \gamma_{yz} \quad \gamma_{xz}\}^T$

This macro-strain manifests as micro-stresses in each constituent strut of the unit cell. In order maintain continuity, we apply PBCs on the unit cell surfaces corresponding to the above macro strains. Then the detailed stress field (micro-stresses) at specific locations on all the 36 struts is calculated. These micro-stresses are calculated using the principle of superposition. Principle of superposition involves scaling the micro-stresses obtained from the unit macro strain cases (considered earlier for calculating the elastic properties) to get micro-stresses for the applied macro-strains.

Thus, from the 6 unit strain cases, detailed stress field (micro-stresses) can be computed on multiple points chosen on the 36 struts is calculated. Stress field for unit strain cases can be computed from ABAQUS® output of Shear forces (SF1) and Bending moments (BM, BM2) on each of the beams using beam theory.

Using the micro stresses for unit strains, micro stresses for any given generalized strain field can be calculated using the principle of superposition. From the calculated micro-stresses, principal stresses at all the points considered in the unit cell can be calculated. From the principal stresses, an appropriate failure theory is used for calculating load factor. As mentioned earlier we assume that the failure strength for the strut material is known. For example, if the maximum stress theory is used for calculating the load factor, then the load factor is calculated as:

$$\lambda = \frac{\sigma_*}{\max\left(|\sigma_1|, |\sigma_2|, |\sigma_3|\right)} \tag{3-2}$$

Where σ_* the strength of the solid is strut material and $\sigma_1, \sigma_2, \sigma_3$ are the 3 principal stresses. Thus load factor can be calculated across all points considered in the 36 struts and the lowest load factor would be the critical load factor for the given state of loading $\{\sigma\}$. If that lowest load factor is λ_L then $\lambda_L \times \{\sigma\}$ would be the critical load that can be applied before the failure onset in the foam.

When the load factor is unity, the input loads correspond to the strength of the foam in that direction. Hence depending upon how we define the input stress $\{\sigma\}$ we could obtain a bi-axial failure envelope or a tri-axial failure envelope using DMM.

The algorithm for calculating the load factor with an example for the approach given has been explained below:

Step 1: Use the procedures given in Chapter 2 and calculate the properties and compliance matrix $[s]$ for the foam considered with a particular geometry of unit cell.

Example: Consider foam with the following unit cell geometry and strut properties:

These are tables from Chapter 2 and have been shown here once again just for illustration purposes.

Using those properties the compliance matrix *[S]* is calculated as:

$$[S]=[C]^{-1}=\begin{bmatrix} 2.155e-5 & -1.073e-5 & -1.073e-5 & 0 & 0 & 0 \\ -1.073e-5 & 2.155e-5 & -1.073e-5 & 0 & 0 & 0 \\ -1.073e-5 & -1.073e-5 & 2.155e-5 & 0 & 0 & 0 \\ 0 & 0 & 0 & 6.679e-5 & 0 & 0 \\ 0 & 0 & 0 & 0 & 6.679e-5 & 0 \\ 0 & 0 & 0 & 0 & 0 & 6.679e-5 \end{bmatrix} \quad (3\text{-}3)$$

Step 2: A generalized state of macro stress is assumed and the macro strain is calculated from this macro stress using the compliance matrix.

Example:

$$\{\sigma\}=\begin{Bmatrix} 2200 \\ 0 \\ 0 \\ 0 \\ 0 \\ 0 \end{Bmatrix} \text{(Pa)} \quad (3\text{-}4)$$

A uniaxial state of stress has been assumed just for convenience. The macro strain is calculated as:

$$\{\varepsilon\}=[C]^{-1}\{\sigma\}=\begin{Bmatrix} 0.0474 \\ -0.0236 \\ -0.0236 \\ 0 \\ 0 \\ 0 \end{Bmatrix} \quad (3\text{-}5)$$

Step 3: Assume a set of points on which we want to calculate micro stresses on the entire unit cell. Calculate micro stresses due to the 6 unit macro strains that were used for calculating properties in Chapter 2 on all the points that are considered.

Example:

Consider the unit cell given in Figure 3-3. In each of the 24 struts, 5 cross sections have been chosen as shown in Figure 3-3. In each cross section 12 points are considered. Hence a total of $24\times5\times12=1440$ points would be chosen in the unit cell. This has also been shown in Figure 3-3.

Step 4: Find the shear forces and bending moments for the unit strain cases as ABAQUS ® outputs. These have been shown in Figure 3-4. Each strut has been modeled as a 2 Node cubic element. Hence in each of the 2 nodes 6 values are to be output from ABAQUS ®. These are 'field output variables', $SF_1^{(1)}, SF_2^{(1)}, SF_3^{(1)}, BM_1^{(1)}, BM_2^{(1)}, BM_3^{(1)}$ at node 1 and $SF_1^{(2)}, SF_2^{(2)}, SF_3^{(2)}, BM_1^{(2)}, BM_2^{(2)}, BM_3^{(2)}$ at node 2 respectively as shown in Figure 3-4.

Step 5: These 12 values are to be computed at each of the 1440 points for all the 6 unit strain cases. Now by using the 'principal of superposition' these Section forces and bending moments can be converted to the given macro strain.

By using the new section forces and bending moments that have been obtained for the given macro strain value, we can find the stresses using Euler-Bernoulli beam theory. In general the stresses are calculated as:

$$\sigma_x = \frac{F}{A} + \frac{Mc}{I} \tag{3-6}$$

Where, *F* is the section force, *M* is the bending moment

Similarly using torsion equations for a triangular cross section, shear stresses (τ_{xy}) can be calculated.

Using the normal stress and shear stress, principal stresses $(\sigma_1, \sigma_2, \sigma_3)$ can be calculated.

Step 6: Once the principal stresses are calculated, any failure theory can be used to calculate the loading factor at each of the 1440 points. The smallest of the 1440 loading factors is the loading factor for the given load.

Example: For the case for which a load of $\{\sigma\} = \begin{Bmatrix} 2200 \\ 0 \\ 0 \\ 0 \\ 0 \\ 0 \end{Bmatrix}$ was applied, the loading factor was obtained to be 1.0068 $\approx$1. As the factor of safety is obtained is close to unity, this load 2200Pa can be considered to its failure strength in the *X*-direction.

Results and Discussion

Based upon the procedure discussed above a total of nine loading cases are considered and failure envelopes are presented for each case. Four of these cases are for foams made out of equisided tetrakaidecahedron unit cells and the remaining five are for foams made out of elongated tetrakaidecahedron unit cells. The details of the cases are listed in Table 3-3. The geometric and material properties used in the examples here are the same used earlier as shown in Chapter 2.

Case (a): Figure 3-5 shows the failure envelope for foam with equisided tetrakaidecahedral unit cells with constant strut cross section subjected to different states of biaxial stresses. The limiting values along the axes (2,190Pa) correspond to the uniaxial failure strengths along that direction. Interestingly, the failure envelope obtained resembles the Tresca (Maximum shear stress) failure theory even though brittle (maximum stress theory) failure was assumed in the strut level. Thus brittle

failure in the strut level manifests as a pseudo-ductile failure at macrolevel as shown in Figure 3-6.

An explanation of the hexagonal shape of the failure envelope is as follows. The maximum stress in each of the 36 struts due to the applied macro stress can be represented as follows:

$$\sigma_{beam}^{(i)} = \alpha_i \sigma_x + \beta_i \sigma_y, 1 \le i \le 36 \tag{3-7}$$

And for the stress to be in the failure envelope,

$$\begin{aligned} \sigma_{beam}^{(i)} &= \sigma_f \text{ (Tensile) or} \\ \sigma_{beam}^{(i)} &= -\sigma_f \text{ (Compressive)} \end{aligned} \tag{3-8}$$

Hence for each beam there would be 2 facets in the envelope and hence 72 facets (36×2) would be expected to be there in the failure envelope. However, from envelope, it is seen that there are only 6 facets (3 pairs of lines) in the biaxial failure envelope. This is due to the symmetry in the geometry of the unit cell due to which more than one beam fails at the same time.

Case (b): Figure 3-7 shows failure envelopes obtained for foam with equisided tetrakaidecahedral unit cells with constant strut cross section subjected to biaxial stresses and an in-plane shear stress. This type of loading is common when foam structures form thin plates. As the magnitude of the in-plane shear stress increases, struts experience greater effective stresses and hence the failure envelope shrinks in area. If the in-plane shear stress is sufficiently high, the failure envelope will collapse to a point and that will correspond to the shear strength of the foam.

Case (c): Failure envelopes obtained for foam with equisided tetrakaidecahedral unit cells with constant strut cross section subjected to triaxial stresses is shown in Figure 3-8. It should be noted that the stresses are plotted on a new coordinate axis

aligned along the hydrostatic stress axis with direction cosines $\left(1/\sqrt{3}, 1/\sqrt{3}, 1/\sqrt{3}\right)$ in the $\sigma_1, \sigma_2, \sigma_3$ space (shown in Figure 3-9). As seen in Figure 3-8, the failure envelopes have been plotted for various S_1 values, where $S_1 = \frac{\left(\sigma_x + \sigma_y + \sigma_z\right)}{3}$. They are a set of irregular hexagons. As S_1 is increased, the hexagons contract in area.

A 3-dimensional representation in the form of failure surfaces for triaxial loading case has been shown in Figure 3-10. The shape resembles a double hexagonal pyramid converging to a point on both the ends meaning that there would be a hydrostatic failure stress level, contrasting a ductile material which does fail in any hydrostatic state of stress.

Case (d): Figure 3-11 shows the contrast in the failure envelopes for foam with equisided tetrakaidecahedral unit cells with constant strut cross section and varying cross section subjected to biaxial stresses. The failure strength in the principal directions with varying cross section is reduced to a third of the strength for constant cross section because of the reduction in the cross sectional area at the centre of the strut.

There are multiple facets (ten facets) in the failure envelope in the case of varying cross section compared to the six-sided hexagon for the constant cross section. This is because: (a) The symmetry in case of varying cross section is different than that of the constant cross section. (b) There is truncation near the edges.

One can note that for a given density, the strength of foam with struts of varying cross-section is much lower than that with uniform cross section. The reason is that for

the varying cross section, the section modulus at the center of the strut is much smaller than the average making it to fail at a much lower load.

Case (e): Figure 3-12 shows the failure envelope for foam with elongated tetrakaidecahedral unit cells with constant strut cross section subjected to biaxial stress state applied in the rise-direction and perpendicular to rise-direction. Because of anisotropy, the failure envelope is very different from that of equisided tetrakaidecahedral unit cells. The tensile failure strength of the strut is assumed to be 0.17 GPa and the failure strength of the foam is obtained to be 0.177 MPa in the rise direction and 0.88 MPa in the perpendicular to rise directions.

Case (f): Failure envelope for foam with elongated unit cells subjected to different states of biaxial stresses applied on both of the perpendicular to rise-directions is shown in Figure 3-13. Failure strength in both the principal directions are obtained to be the same value (0.088MPa)

Case (g): Figure 3-14 shows failure envelopes obtained for foam with elongated tetrakaidecahedral unit cells with constant strut cross section subjected to biaxial stress states in the rise direction and the perpendicular-to-rise direction along with an in-plane shear stress. As the magnitude of the in-plane shear stress increases, struts experience greater stresses and hence the failure envelope shrinks in area. If the in-plane value is sufficiently high, the failure envelope will collapse to a point and will correspond to the shear strength of the foam.

Case (h): Figure 3-15 shows failure envelopes obtained for foam with elongated tetrakaidecahedral unit cells subjected to triaxial stresses. Again as in the case of the equisided tetrakaidecahedral unit cell case, the failure envelopes are plotted in the

hydrostatic plane. However, unlike that of the equisided foam, the hexagons don't appear to contract towards the centre to a point, but rather to a line. It is quite possible the hexagon would converge to a point if sufficient numbers of stress states are considered. This is due to the anisotropic nature of the foam and warrants further investigation. A 3-dimensional plot of the same is shown in Figure 3-16.

Conclusions

A finite element based micromechanics that was earlier used to calculate the elastic properties of foams has been extended to calculate multi-axial failure strengths. Both equisided and elongated tetrakaidecahedral unit cells are considered. Using the Direct Micromechanics Method (DMM), biaxial and triaxial failure envelopes for foams with both these kind of unit cells have been plotted. It is shown that the biaxial failure envelope closely resembles the maximum shear stress (Tresca) failure envelope in the macro level. The effect of inplane shear stress on biaxial normal stress has illustrated and increasing inplane shear stress has been shown to contract the failure envelope. Triaxial failure envelopes for foams with equisided tetrakaidecahedron unit cells have been shown to take a shape of a double hexagonal pyramid in the hydrostatic plane. The effect of varying cross-section on the failure envelope has been studied and the varying cross sections have been shown to cause failure strength knock downs. Uniaxial failure strengths in the rise and perpendicular to rise directions for foams with elongated tetrakaidecahedron unit cells have been shown to be different thereby showing that such foams are anisotropic. Also, both biaxial and triaxial failure envelopes are plotted to demonstrate the anisotropy in these foams due to non-symmetric geometry.

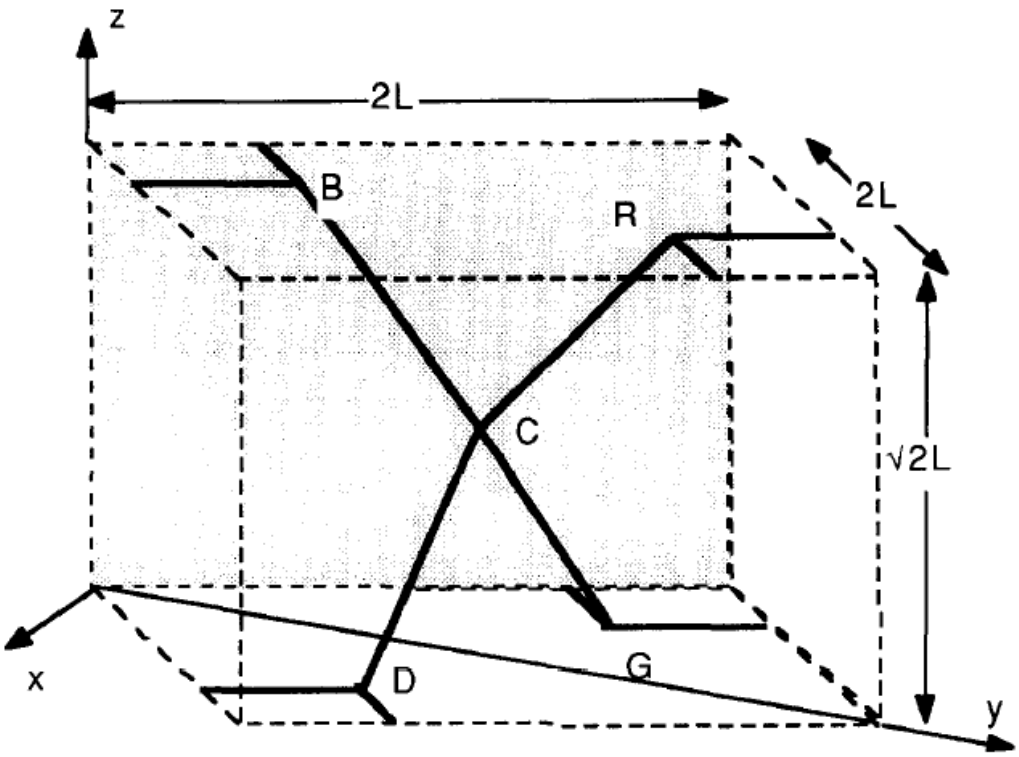

Figure 3-1. Identifying repeating unit in deriving analytical model for elastic modulus for open cell foams

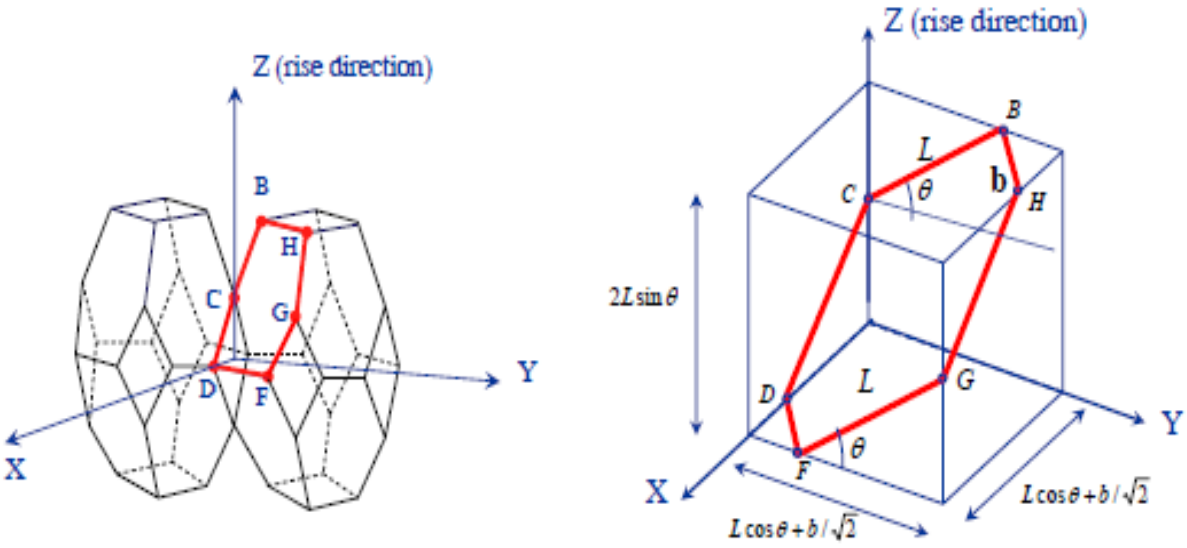

Figure 3-2. Repeating unit cell for loading in Y-direction

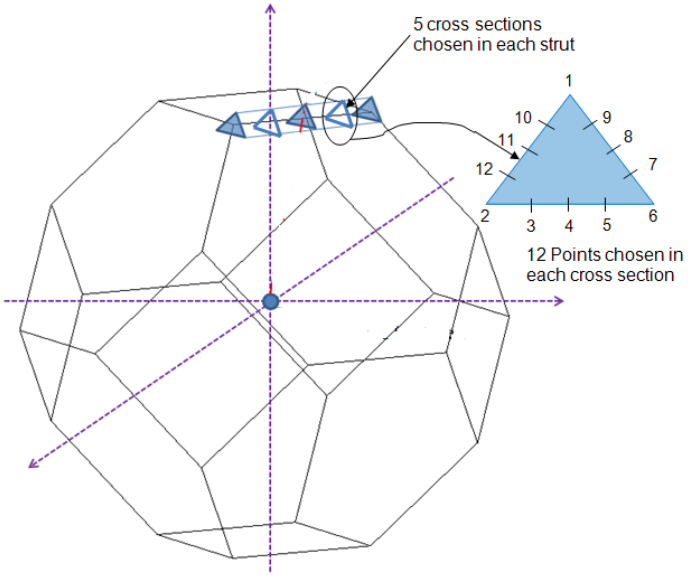

Figure 3-3. Points considered in the unit cell for calculating Micro stresses

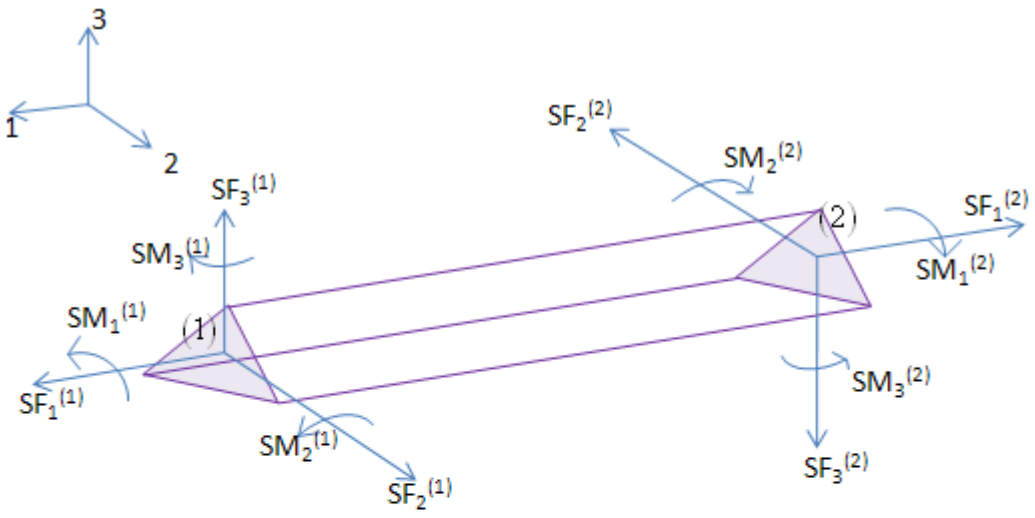

$SF_1^{(1)}$	Force in local '1' direction at Node (1)	$SF_1^{(2)}$	Force in local '1' direction at Node (2)
$SF_2^{(1)}$	Shear Force in local '2' direction at Node (1)	$SF_2^{(2)}$	Shear Force in local '2' direction at Node (2)
$SF_3^{(1)}$	Shear Force in local '3' direction at Node (1)	$SF_3^{(2)}$	Shear Force in local '3' direction at Node (2)
$SM_1^{(1)}$	Twisting Moment about '1' at Node (1)	$SM_1^{(2)}$	Twisting Moment about '1' at Node (2)
$SM_2^{(1)}$	Bending Moment about '2' at Node (1)	$SM_2^{(2)}$	Bending Moment about '2' at Node (2)
$SM_3^{(1)}$	Bending Moment about '3' at Node (1)	$SM_3^{(2)}$	Bending Moment about '3' at Node (2)

Figure 3-4. Section forces and bending moments used for calculating load factor

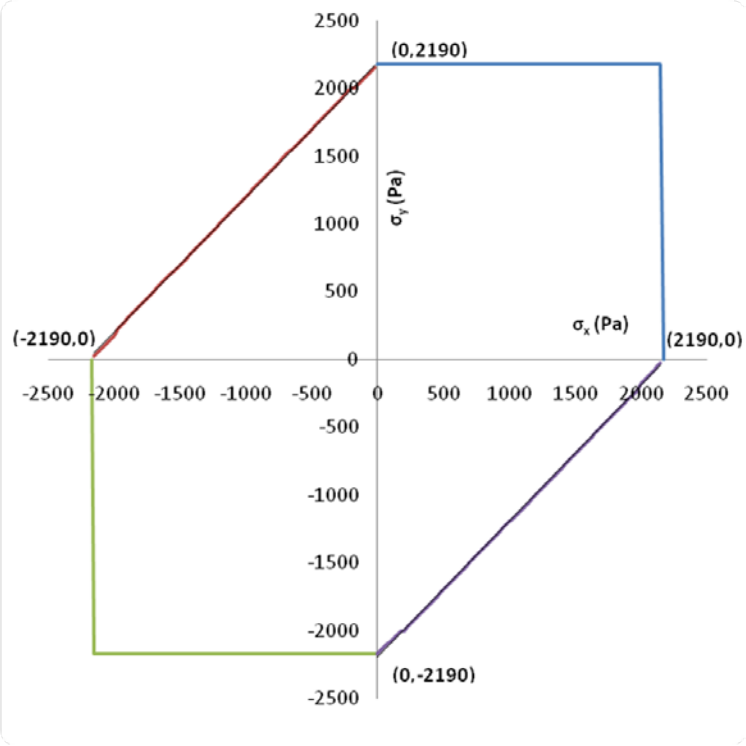

Figure 3-5. Failure envelope plot for Case (a) (Table 3-3)

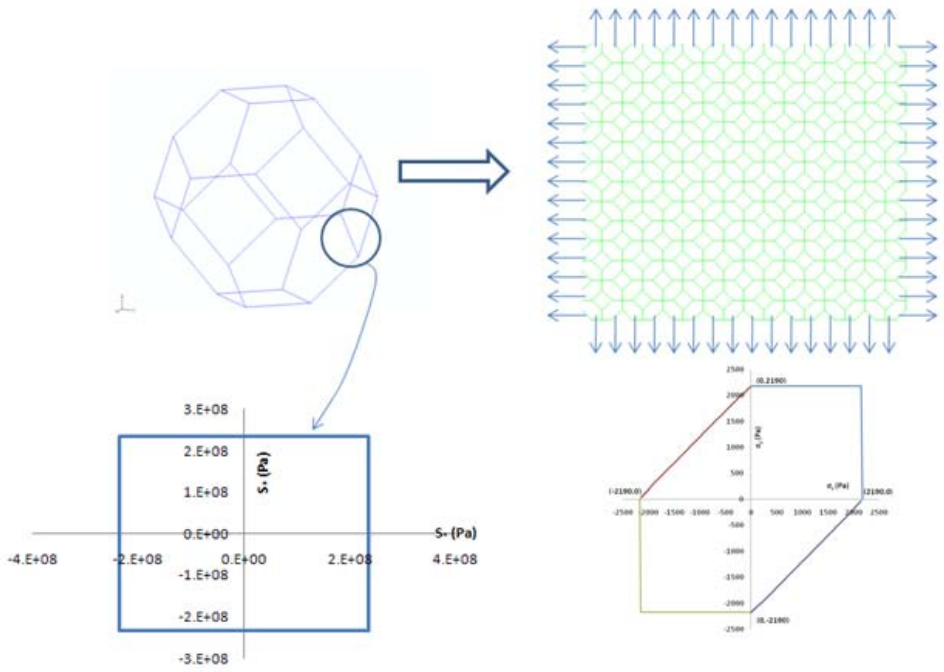

Figure 3-6. Brittle failure in micro level manifesting into ductile failure in the macro level

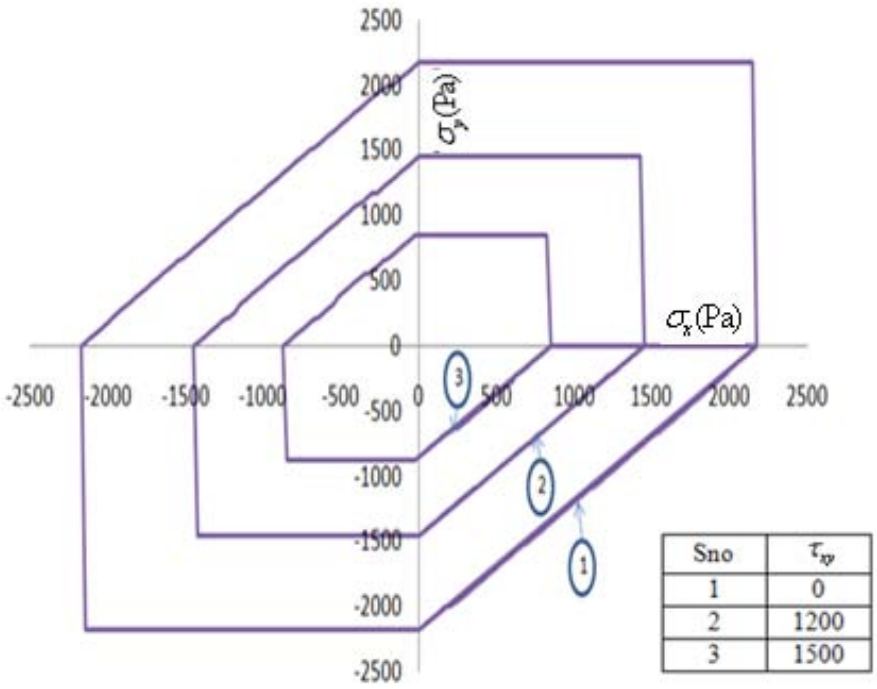

Sno	τ_{xy}
1	0
2	1200
3	1500

Figure 3-7. Failure envelope plot Case (b) Table 3-3

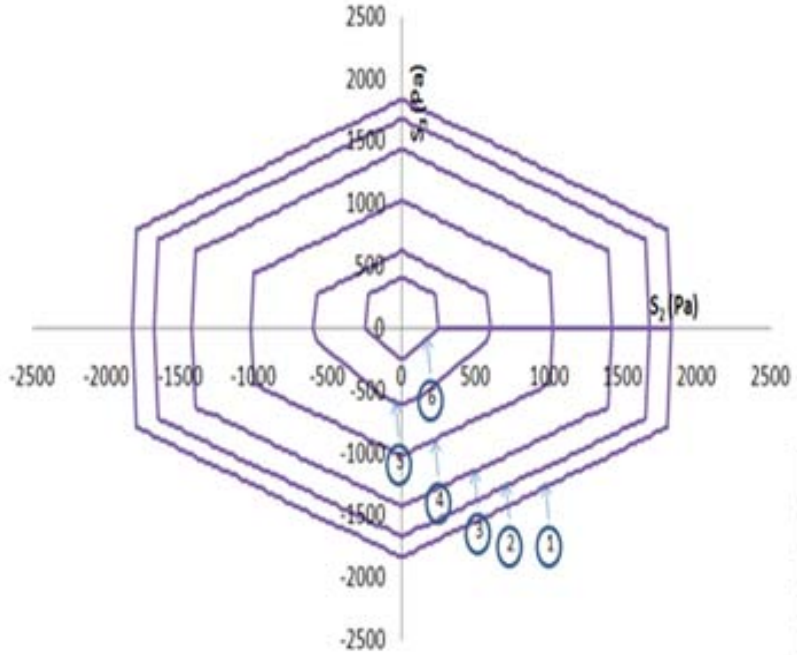

Sno	S_1
1	0
2	20000
3	50000
4	100000
5	150000
6	175000

Figure 3-8. Failure envelope Case (C) Table 3-3

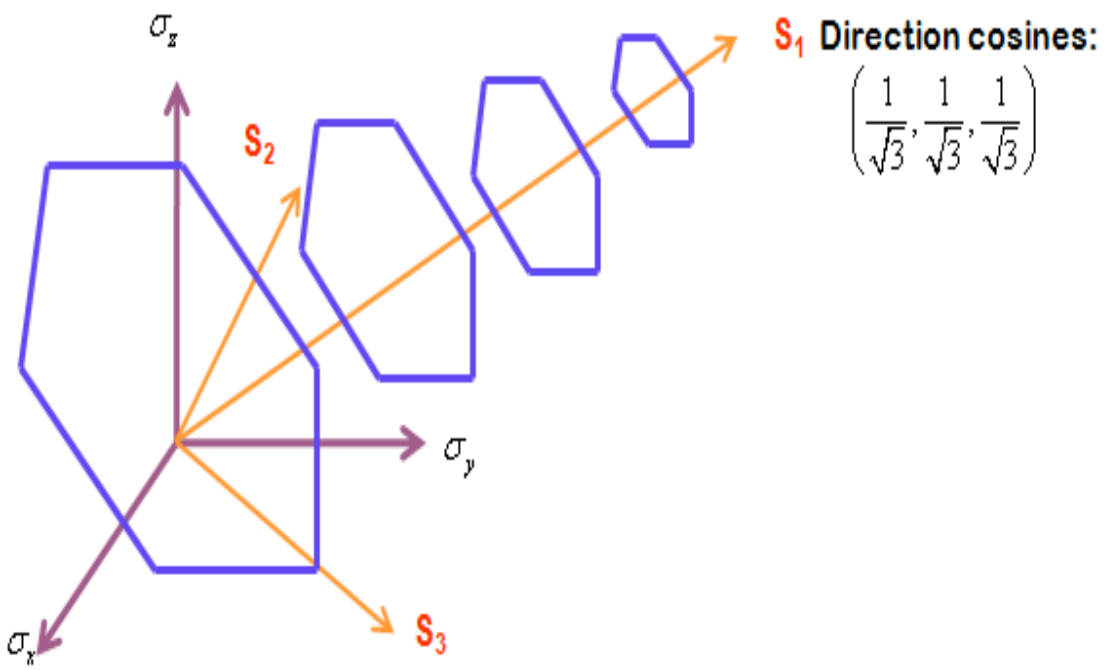

Figure 3-9. Coordinate system having the hydrostatic line as one of its axes

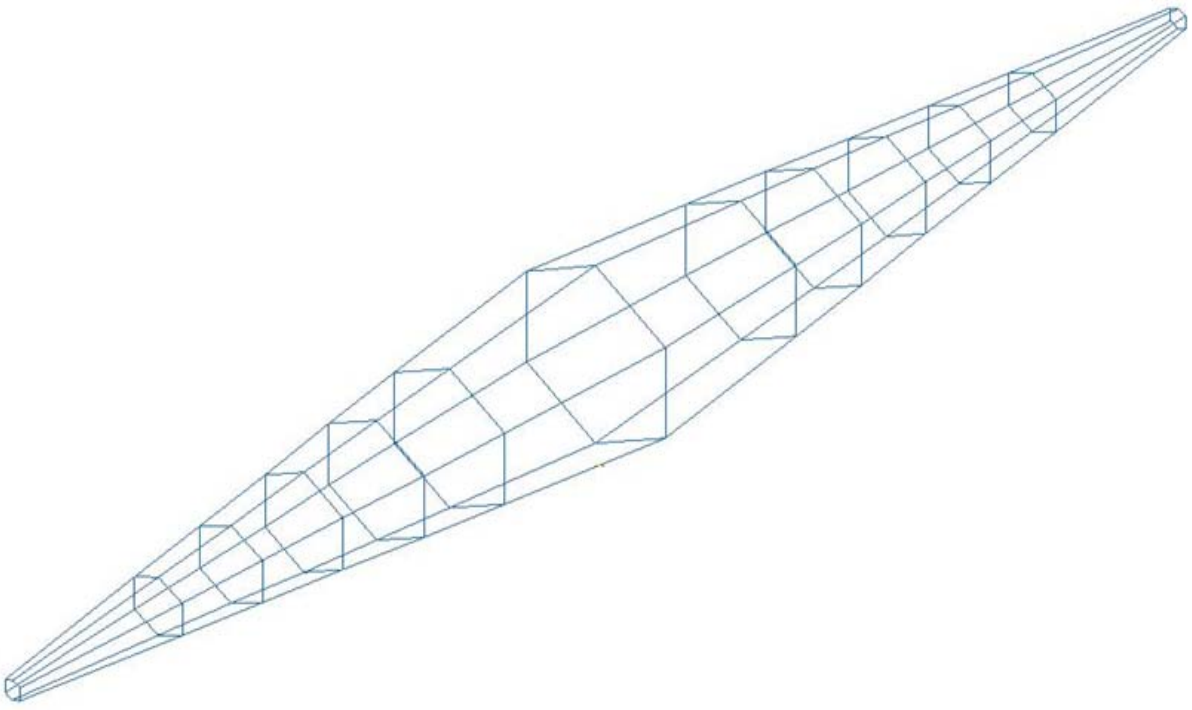

Figure 3-10. Failure surface for Case (C) Table 3-3

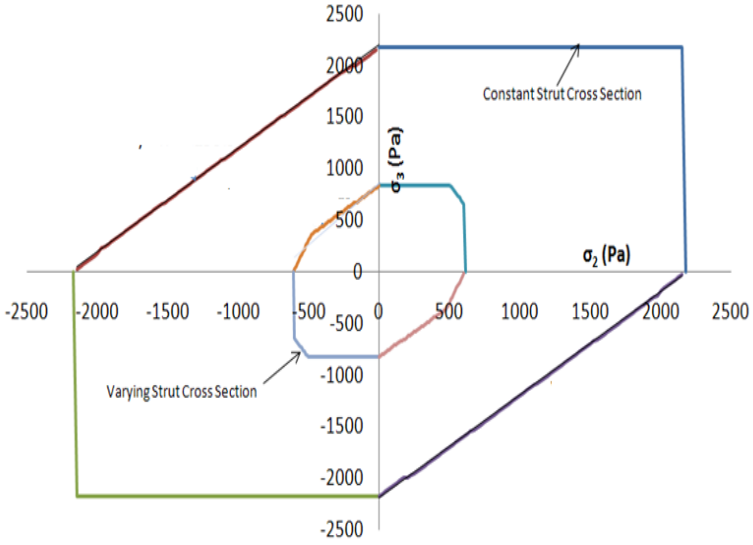

Figure 3-11. Failure envelope for case (d) Table 3-3

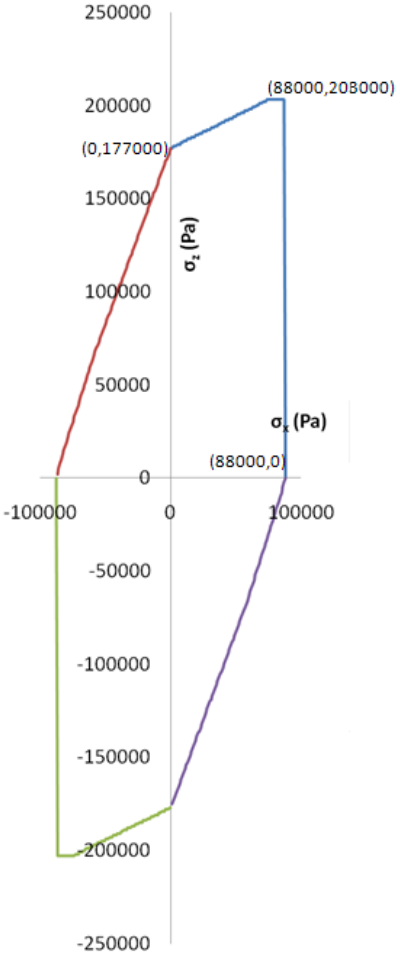

Figure 3-12. Failure envelope for Case (e) Table 3-3

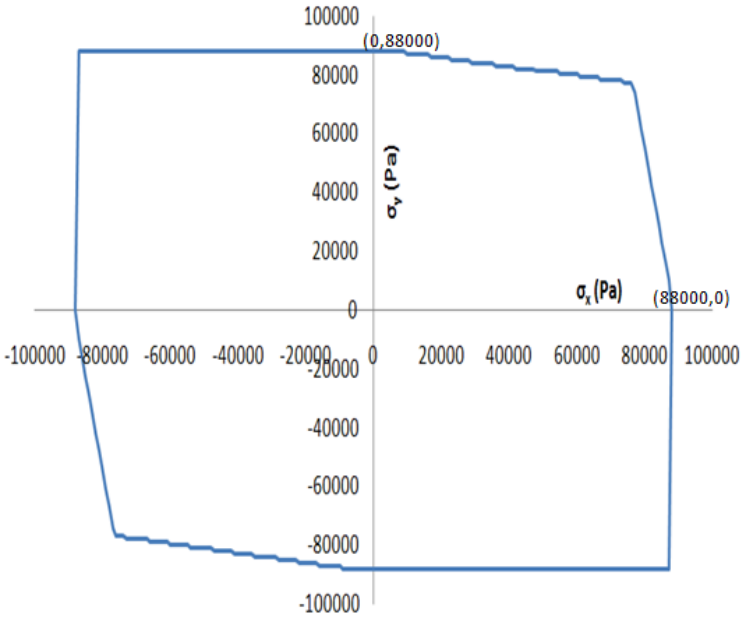

Figure 3-13. Failure envelope for Case (f) Table 3-3

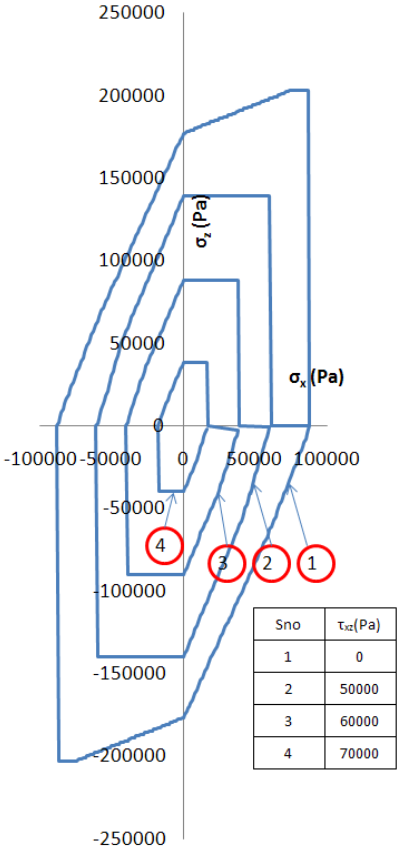

Figure 3-14. Failure envelope for Case (g) Table 3-3

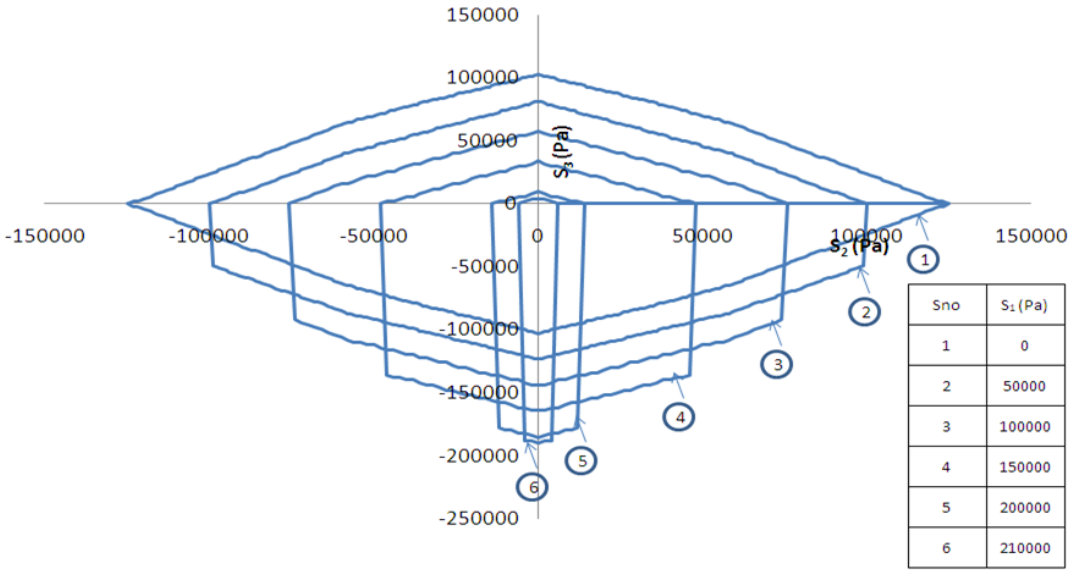

Sno	S_1 (Pa)
1	0
2	50000
3	100000
4	150000
5	200000
6	210000

Figure 3-15. Failure envelope for Case (h) Table 3-3

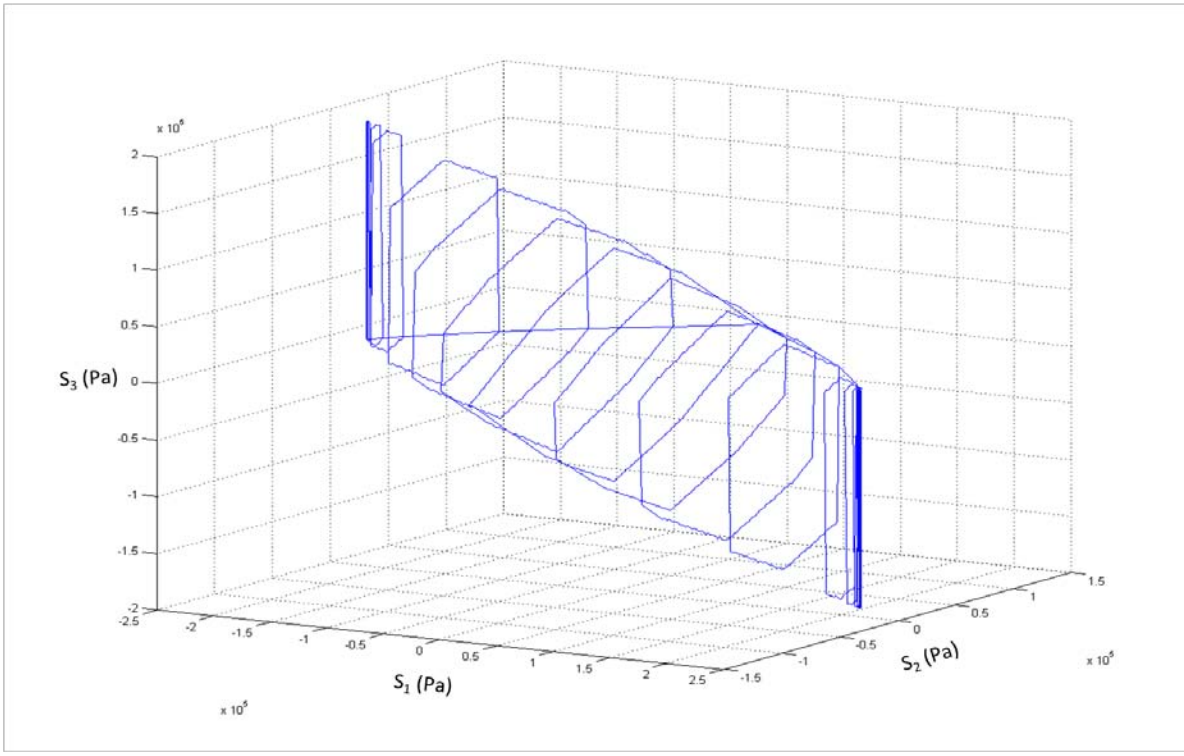

Figure 3-16. Failure envelope surfaces for Case (h) Table 3-3

Table 3-1. Unit cell geometry and strut properties used for example to calculate load factor

	Property	Value
Material Properties of the strut	Density, ρ_s (Kg/m^3)	1650
	Elastic modulus, E_s (GPa)	23.42
	Poisson ratio, ν_s	0.33
Geometry of the equisided tetrakaidecahedron unit cell	L (mm)	1
	d (mm)	0.06
	Relative density	0.001653
Cross-section properties (Equilateral Triangle)	Cross sectional area, A (m^2)	1.5588×10^{-9}
	Moment of Inertia, I_x , I_y (m^4)	2.3382×10^{-19}
	Torsion constant, J (m^4)	4.6765×10^{-19}

Table 3-2. Elastic properties used for example to calculate load factor

Property	Value
$E_x = E_x = E_z$ (GPa)	46.7×10^{-6}
$v_{xy} = v_{yz} = v_{xz}$	0.498
$G_{xy} = G_{yz} = G_{xz}$ (GPa)	14.9×10^{-6}

Table 3-3. Cases considered for plotting failure envelopes

Case	Unit cell	Cross section	Applied macro-stress	Failure envelope type
a	Equisided	Constant	$\begin{Bmatrix} \sigma_x \\ \sigma_y \\ 0 \\ 0 \\ 0 \\ 0 \end{Bmatrix}$	Biaxial
b	Equisided	Constant	$\begin{Bmatrix} \sigma_x \\ \sigma_y \\ 0 \\ \tau_{xy} \\ 0 \\ 0 \end{Bmatrix}$	Biaxial + Shear
c	Equisided	Constant	$\begin{Bmatrix} \sigma_x \\ \sigma_y \\ \sigma_z \\ 0 \\ 0 \\ 0 \end{Bmatrix}$	Triaxial
d	Equisided	Varying	$\begin{Bmatrix} \sigma_x \\ \sigma_y \\ 0 \\ 0 \\ 0 \\ 0 \end{Bmatrix}$	Biaxial
e	Elongated	Constant	$\begin{Bmatrix} \sigma_x \\ \sigma_y \\ 0 \\ 0 \\ 0 \\ 0 \end{Bmatrix}$	Biaxial

Table 3-3. Continued

Case	Unit cell	Cross section	Applied macro-stress	Failure envelope type
f	Elongated	Constant	$\begin{Bmatrix} 0 \\ \sigma_y \\ \sigma_z \\ 0 \\ 0 \\ 0 \end{Bmatrix}$	Biaxial
g	Elongated	Constant	$\begin{Bmatrix} \sigma_x \\ \sigma_y \\ 0 \\ \tau_{xy} \\ 0 \\ 0 \end{Bmatrix}$	Biaxial + Shear
h	Elongated	Constant	$\begin{Bmatrix} \sigma_x \\ \sigma_y \\ \sigma_z \\ 0 \\ 0 \\ 0 \end{Bmatrix}$	Triaxial

CHAPTER 4
FRACTURE TOUGHNESS OF OPEN CELL FOAMS USING FINITE ELEMENT BASED METHODS

Fracture toughness of open cell foams consisting of tetrakaidecahedral unit cells is predicted by simulating crack opening using a FE based micromechanical model. The inputs to the model are the geometric parameters required to model the repeating unit cell and tensile strength of the foam ligament or strut. Cracks are created by removing certain number of cells pertaining to a crack length. The FE model consists of a local micro-scale region surrounding the crack-tip. For an assumed stress intensity factor, the displacements along the boundary of an assumed K-field are calculated and applied. The stresses in the ligaments ahead of the crack tip calculated from this micro-model are used to predict fracture toughness. A parametric study with different micro model sizes and different crack lengths is performed to check for convergence of the predicted mode-I, mode-II and mixed mode fracture toughness values. The effect of applying rotations as additional boundary conditions along with the translational displacement boundary conditions on the predicted fracture toughness values is also studied.

Introduction

Literatures available on predicting fracture toughness of foams include analytical models using relatively simple unit cell structures such as a cuboid (Maiti et al, 1984). It has been shown that Mode I and Mode II fracture toughness vary either as a cube or as a square of its relative density.ie K_{Ic} is proportional to $(\rho^*/\rho_s)^3$ for open cell and to $(\rho^*/\rho_s)^2$ for closed cell foams (Maiti et al., 1984). This model has been further confirmed by experimental studies of several open-cell foams with short cracks (Huang and Gibson, 1991, Brezny and Green, 1990). A comprehensive summary of mechanical

properties of foams including fracture toughness could be found in Gibson and Ashby's book (Gibson and Ashby, 1997).

FEM based micromechanics is one of the methods to investigate the fracture toughness of cellular materials. In this method, displacement boundary conditions corresponding to a given stress intensity factor are applied to the micro-model. This approach was first used to study the fracture toughness of carbon foam (Choi and Sankar, 2003) where cubical unit cells were used to model the foam. The results obtained from these simulations were further verified by experiments (Choi and Sankar, 2005). Next, the same technique was further used to derive analytical models for foams made up of cubical unit cells (Wang and Sankar, 2008). These analytical models relate the fracture toughness of the foam to the relative density, to the length of the ligament of the foam, and to the cross-sectional properties of the foam. Furthermore, these methods have also been used to study the damage tolerance of elastic-brittle, 2-D isotropic lattices (Fleck and Qiu, 2007). After modeling cubical cells of carbon foams, Wang and Sankar have further extended the same methodology to foams made out of equisided tetrakaidecahedral unit cells and have done further parametric studies to study the effects of the dimensions of the struts on the predicted values of fracture toughness.

In the current work, the same approach is used to determine the fracture toughness of foams made out of tetrakaidecahedral unit cells. The specific objective of the current work is to evaluate the effect of applying rotations in addition to prescribed translational displacement boundary conditions on the predicted fracture toughness.

Approach

The approach for the Finite Element (FE) model is to model only a region near the crack tip in detail. This is done by choosing a small region near the crack tip and creating the detailed geometry using tetrakaidecahedral cells for the chosen model size surrounding the crack tip instead of modeling the entire foam as one single homogenous continuum material. This has been shown in Figure 4-3. This model could be imagined as a truss structure made out of a number of struts (beams) joined together. The properties and dimensions of the strut material used in the model have been shown in Table 4-1. The geometry description of a single equisided tetrakaidecahedron used in the model is shown in Figure 4-1.

The next step is calculating the homogenous elastic properties of the foam made out of these equisided tetrakaidecahedral unit cells. The details for the methodology for calculating all the elastic properties have already been explained in the previous work by the same authors (Thiyagasundaram et al, 2010). The same approach has been used here to calculate the elastic properties. The compliance matrix of the calculated elastic properties would be used in the calculation of the boundary displacements to be applied in the FE model as would be explained in the next section. The homogenized material properties used for the calculation of the constants in the displacement fields has been shown Table 4-2.

Next, an appropriate size is to be chosen for the micromechanical model. In order for principles of linear elastic fracture mechanics to be applicable to the current problem, the size of the model is chosen such that it is much larger than the size of a strut or ligament of the unit cell. By merging multiple *instances* in ABAQUS®, the geometric model with required number of cells (Figure 4-3) is created from one unit cell for the

assumed size of the micromechanical model. It should be noted that a plain-strain condition has been assumed in the model and hence in all the FE models there is only one unit cell in the thickness direction, i.e., in the z-direction in the Figure 4-3. Next a crack size is chosen for the given size of the model. In this study the crack size is typically chosen to be half of the width that has been chosen for the model as this could minimize the edge effects coming from the boundary conditions applied on the edges. The crack is created by removing required number of unit cells according to the crack size chosen in the model (Figure 4-2).

Next a stress intensity factor (K_I for mode I or K_{II} for mode II) is assumed. Using this stress intensity factor, displacements on the points in the outer edges in the chosen micro mechanical model is calculated (Sih and Liebowitz, 1968). It is to be noted that these formulae have been derived by Sih and Liebowitz for an orthotropic homogenous continuum material. These calculated displacements can be directly applied on the micromechanical model that is, on the nodes in the boundary of the FE model.

The displacement fields near the crack tip for Mode I:

$$u = K_I \sqrt{\frac{2r}{\pi}} \operatorname{Re}\left\{ \frac{1}{s_1 - s_2} \left[s_1 p_2 \left(\cos\theta + s_2 \sin\theta \right)^{1/2} - s_2 p_1 \left(\cos\theta + s_1 \sin\theta \right)^{1/2} \right] \right\}$$
$$v = K_I \sqrt{\frac{2r}{\pi}} \operatorname{Re}\left\{ \frac{1}{s_1 - s_2} \left[s_1 q_2 \left(\cos\theta + s_2 \sin\theta \right)^{1/2} - s_2 q_1 \left(\cos\theta + s_1 \sin\theta \right)^{1/2} \right] \right\} \quad (4\text{-}1)$$

The displacement fields near the crack tip for Mode II:

$$u = K_{II} \sqrt{\frac{2r}{\pi}} \operatorname{Re}\left\{ \frac{1}{s_1 - s_2} \left[p_2 \left(\cos\theta + s_2 \sin\theta \right)^{1/2} - p_1 \left(\cos\theta + s_1 \sin\theta \right)^{1/2} \right] \right\}$$
$$v = K_{II} \sqrt{\frac{2r}{\pi}} \operatorname{Re}\left\{ \frac{1}{s_1 - s_2} \left[q_2 \left(\cos\theta + s_2 \sin\theta \right)^{1/2} - q_1 \left(\cos\theta + s_1 \sin\theta \right)^{1/2} \right] \right\} \quad (4\text{-}2)$$

The parameters p_1, p_2, q_1, q_2, s_1 and s_2 in the above equations are dependent on the compliance properties that are obtained from material elastic constants

(Thiyagasundaram et al, 2010, Table 4-2). The details about obtaining the stiffness matrix has also been given in Appendix. Using the values of u and v from the above equations, rotations can be calculated using,

$$\omega_{xy} = \frac{1}{2}\left[\frac{\partial v}{\partial x} - \frac{\partial u}{\partial y}\right] \tag{4-3}$$

The details for obtaining the deformation gradients ($\frac{\partial v}{\partial x}, \frac{\partial u}{\partial y}$) in the above equation is given Appendix.

For brittle foams, once the stress intensity factor at macroscale is known, the corresponding maximum microscale tensile stresses in the struts ahead of the crack can be calculated from the FE simulation. The methodology for calculating stresses in each beam is to choose a number of struts close to the crack tip and calculate stresses in each strut. For this, in each of the strut a number of points are chosen and standard principles that are used for calculating stresses in an Euler-Bernoulli beam from the axial forces and bending moments resulting from the applied loads is used to calculate the stresses in the struts. The procedure for calculating stresses has been explained elaborately with example in Chapter 3. The maximum stress value among all the stresses calculated in the different beams (struts) is the required stress (σ_{tip}). Using this stresses (σ_{tip}), the fracture toughness of the foam by the following equation (Choi and Sankar, 2005):

$$\text{Mode I}: \frac{K_I}{K_{Ic}} = \frac{\sigma_{tip}}{\sigma_u} \quad \text{or}$$

$$\text{Mode II}: \frac{K_{II}}{K_{IIc}} = \frac{\sigma_{tip}}{\sigma_u}$$

$$K_{Ic} = \frac{K_I}{\sigma_{tip}} \sigma_u$$
$$K_{IIc} = \frac{K_{II}}{\sigma_{tip}} \sigma_u \quad (4\text{-}4)$$

where K_I is Mode I stress intensity factor, K_{II} is Mode II stress intensity factor K_{Ic} is Mode I fracture toughness, K_{IIc} is Mode II fracture toughness σ_u is the tensile strength of struts or the foam ligaments, and σ_{tip} is the maximum tensile stress in the first unbroken strut ahead of the crack tip.

Results – Mode I Fracture Toughness

A convergence study is conducted by calculating the fracture toughness choosing different micromechanical model sizes. The size of the model is varied by increasing the number of unit cells chosen along the x and the y directions.

In the current study, two sets of cases have been chosen, one which does not include rotations as a boundary condition and the other which includes rotations. The question of including rotation arises because of the fact that beam elements are used in the local region in the vicinity of the crack tip and the nodes have rotation as a degree of freedom. In some previous work Choi and Sankar (Choi et al, 2003) ignored the rotations basically setting the corresponding couple to be equal to zero. On the other hand Fleck et al. (Fleck et al, 1999) included the rotation as a boundary condition. In the present study we considered both cases – with and without rotation boundary condition.

Thirteen different models were considered to check convergence for mode I. Four models out of the thirteen models are shown in Figure 4-4. The crack size is 50% of the width in all the cases chosen. The results obtained have been shown in Table 4-3. The total number of nodes in the models varies from 1,800 to almost 20,000 nodes

respectively as shown in the Table 4-3. It is seen that as the size of the model is increased, there is convergence (Figure 4-5).

The results show that for foam with relative density 0.16% (Table 4-3, Figure 4-5), the mode I fracture toughness converges to 622 $\mathrm{Pa}\sqrt{\mathrm{m}}$ when rotational boundary conditions are not applied and to 622.5 $\mathrm{Pa}\sqrt{\mathrm{m}}$ when the rotations are applied. The highest and the lowest fracture toughness values are 622.2 $\mathrm{Pa}\sqrt{\mathrm{m}}$ and 615.4 $\mathrm{Pa}\sqrt{\mathrm{m}}$ respectively which makes the maximum variation to be only about 1.1 %. This would mean that calculated value can be used as a material property. Also since the variation in the converged fracture toughness values between fracture toughness with and without rotational BC is only 0.1 %, it can be concluded that there is no significant change in fracture toughness values when rotations are applied. One of the reasons could be that the boundaries of the local model are sufficiently away from t he crack tip.

Results - Mode II Fracture Toughness

Similar to the procedure for Mode I, by imposing the displacements of K_{II} field on the boundary to micromechanical model, we can obtain the maximum tensile stress near the crack tip from the ABAQUS results and hence calculate the Mode II fracture toughness. Again a convergence study is conducted by calculating the fracture toughness choosing different micromechanical model sizes. Like before, the size of the model is varied by increasing the number of unit cells chosen along the *X* and the *Y* directions. Similar to what was done for Mode I, 2 sets of cases have been chosen, one which does not include rotations as boundary conditions and the other which includes rotations. Deformed configurations of a few models chosen for this study have been shown in Figure 4-6. The results obtained have been shown in Table 4-4.

The results show that the mode II fracture toughness converges to about 522 $\mathrm{Pa}\sqrt{\mathrm{m}}$ when rotational displacements are not applied and to 521.5 $\mathrm{Pa}\sqrt{\mathrm{m}}$ when the rotations are applied. The highest and the lowest fracture toughness values are 551.6 $\mathrm{Pa}\sqrt{\mathrm{m}}$ and 521.7 $\mathrm{Pa}\sqrt{\mathrm{m}}$ respectively which makes the maximum variation in to be only about 5.3 %. Also since the variation in the converged fracture toughness values between fracture toughness with and without rotational BCs is only 0.1 %, there is no significant change in fracture toughness values when rotations are applied.

Mixed Mode Fracture Toughness

In calculating mixed mode fracture toughness, two stress intensity factors are required as input for calculation of boundary displacements. In the current case, in order to understand the combined effect of the stress intensity factors, the mode II stress intensity factor has been assumed as a function of mode I stress intensity factor. That is:

$$K_{II} = K_I \tan\psi \ (0 \le \psi \le 90) \tag{4-5}$$

All the other equations for calculating displacements and rotations remain the same and have been given in Appendix.

Results obtained from simulations for predicting mixed mode fracture toughness have been shown in Table 4-5. This is also shown in the graph in Figure 4-9. Some deformed configurations for different combinations of K_I and K_{II} have been shown in Figure 8. The size of the local region is assumed to be 30×31 cells.

Conclusions

A finite element based method developed by Choi and Sankar (2005) has been used to calculate the fracture toughness of foams. This procedure has been used to calculate Mode I, Mode II and Mixed mode fracture toughness of foams with

tetrakaidecahedral unit cells by developing micromechanical models. Fracture toughness has been shown to converge as the size of micromechanical model is increased. As the difference obtained for fracture toughness varies very less as the model size is increased, the calculated value can be used as a material property. It has also been shown that applying rotation boundary conditions does not influence the calculated fracture toughness and can be neglected.

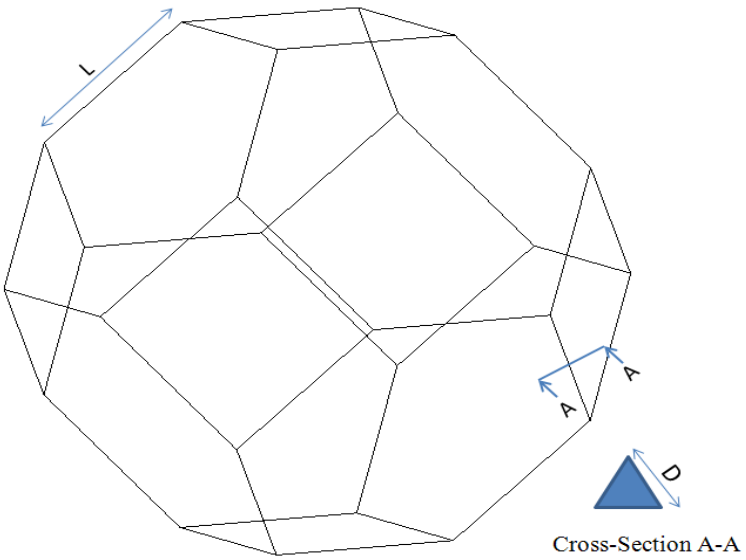

Figure 4-1. Geometry of unit cell chosen for fracture toughness prediction

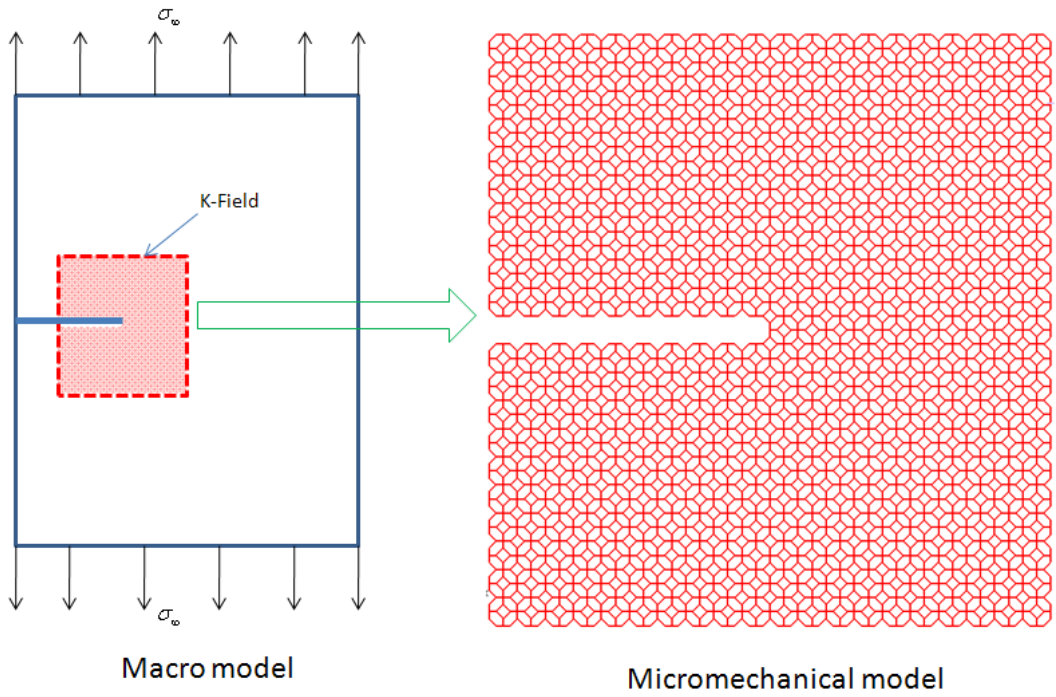

Figure 4-2. Micromechanical model to predict fracture toughness

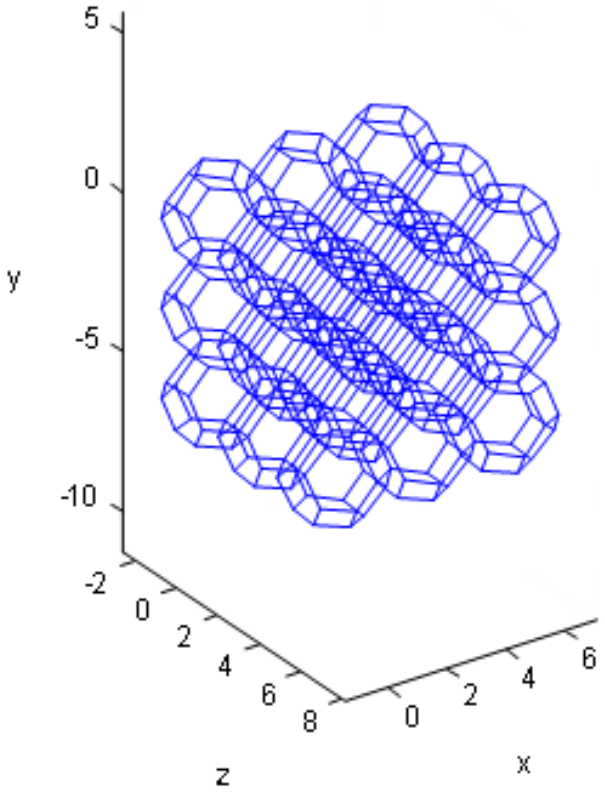

Figure 4-3. Foam with 27 unit cells (3x3x3)

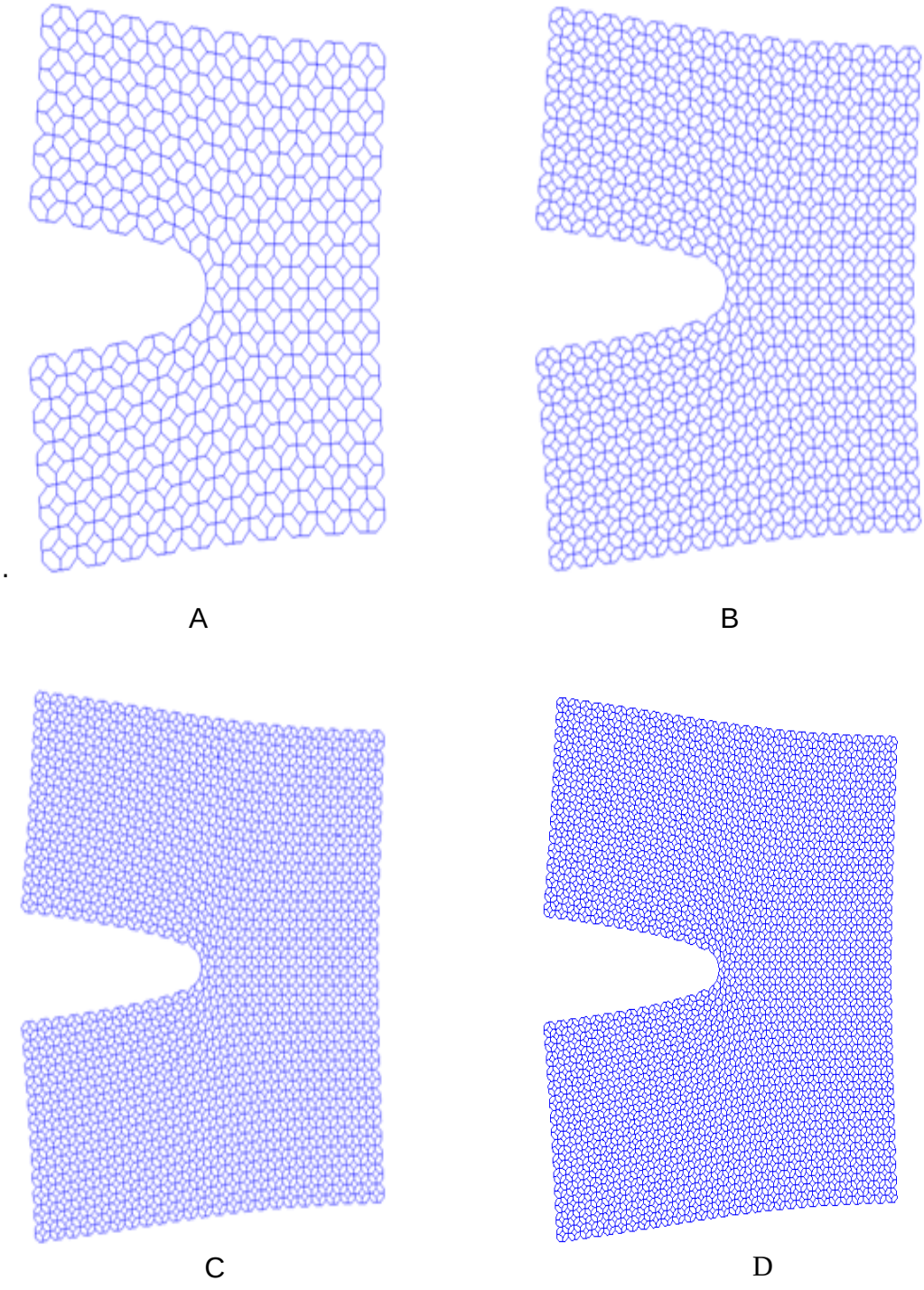

Figure 4-4. Mode I fracture toughness (Deformed configurations) (A) 10(w)x11(h) (B) 16(w)x15(h) (C) 24(w)x25(h) (D) 30(w)x31(h)

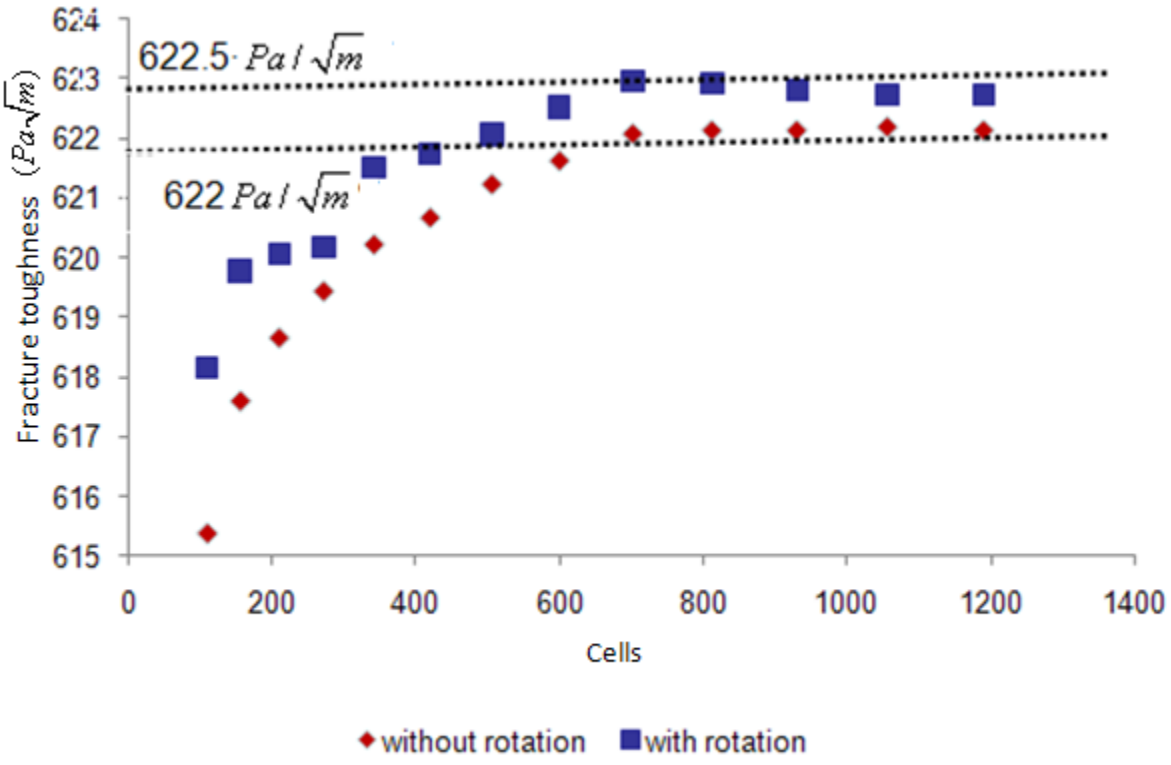

Figure 4-5. Mode I fracture toughness convergence

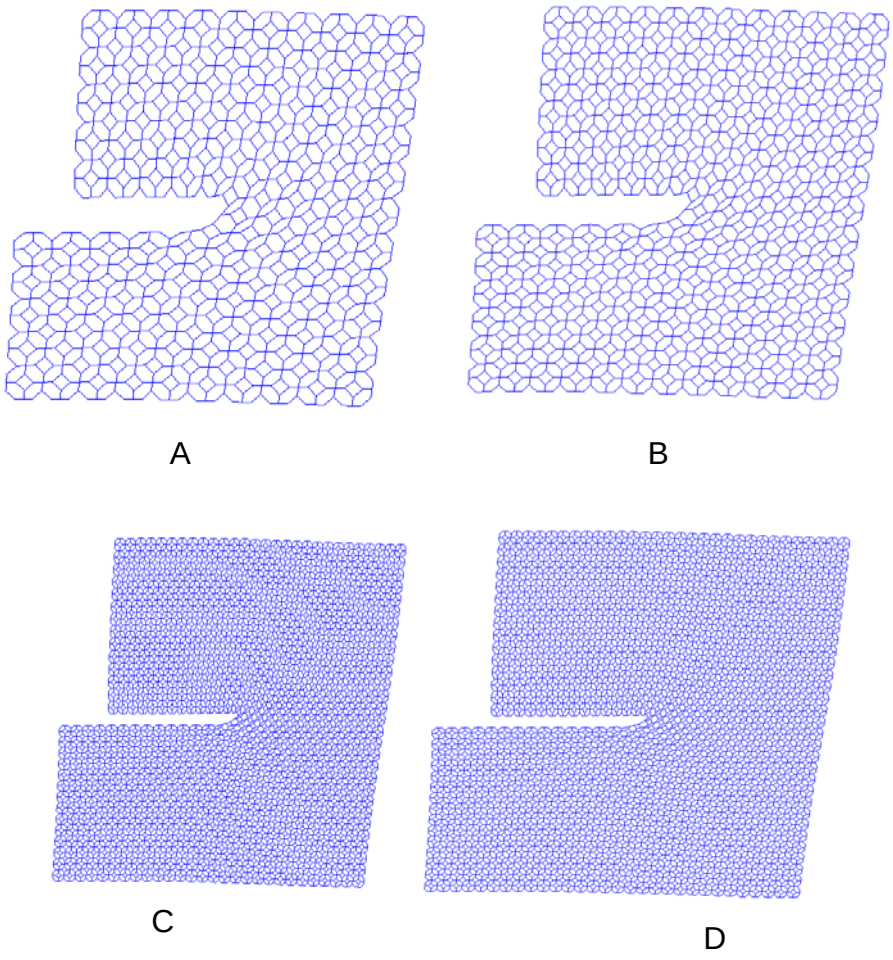

Figure 4-6. Mode II fracture - deformed configurations (A) 10(w)x11(h) (B) 12(w)x13(h) (C) 28(w)x29(h) (D) 30(w)x31(h)

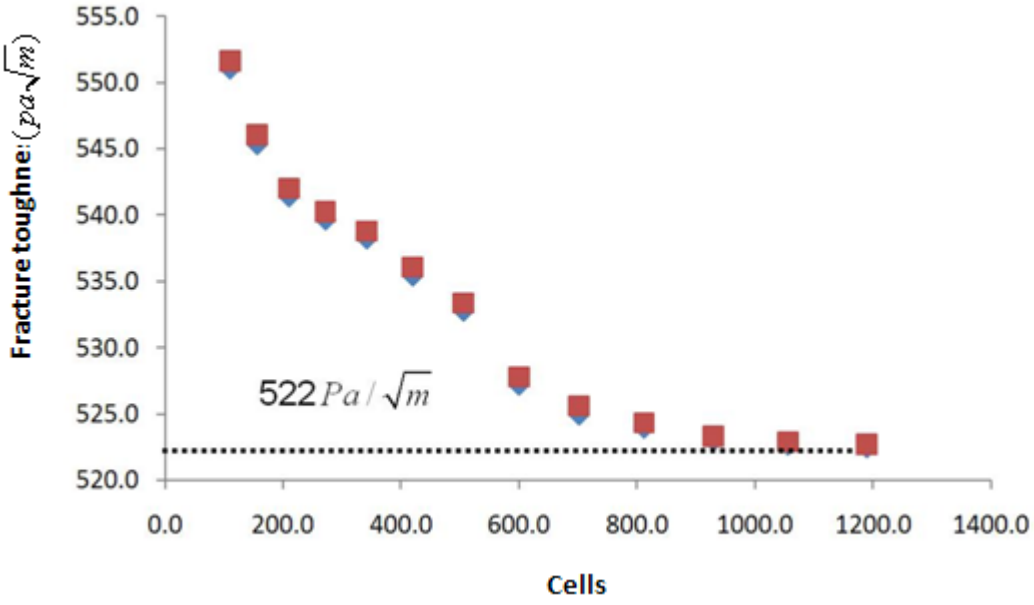

Figure 4-7. Mode II fracture toughness convergence

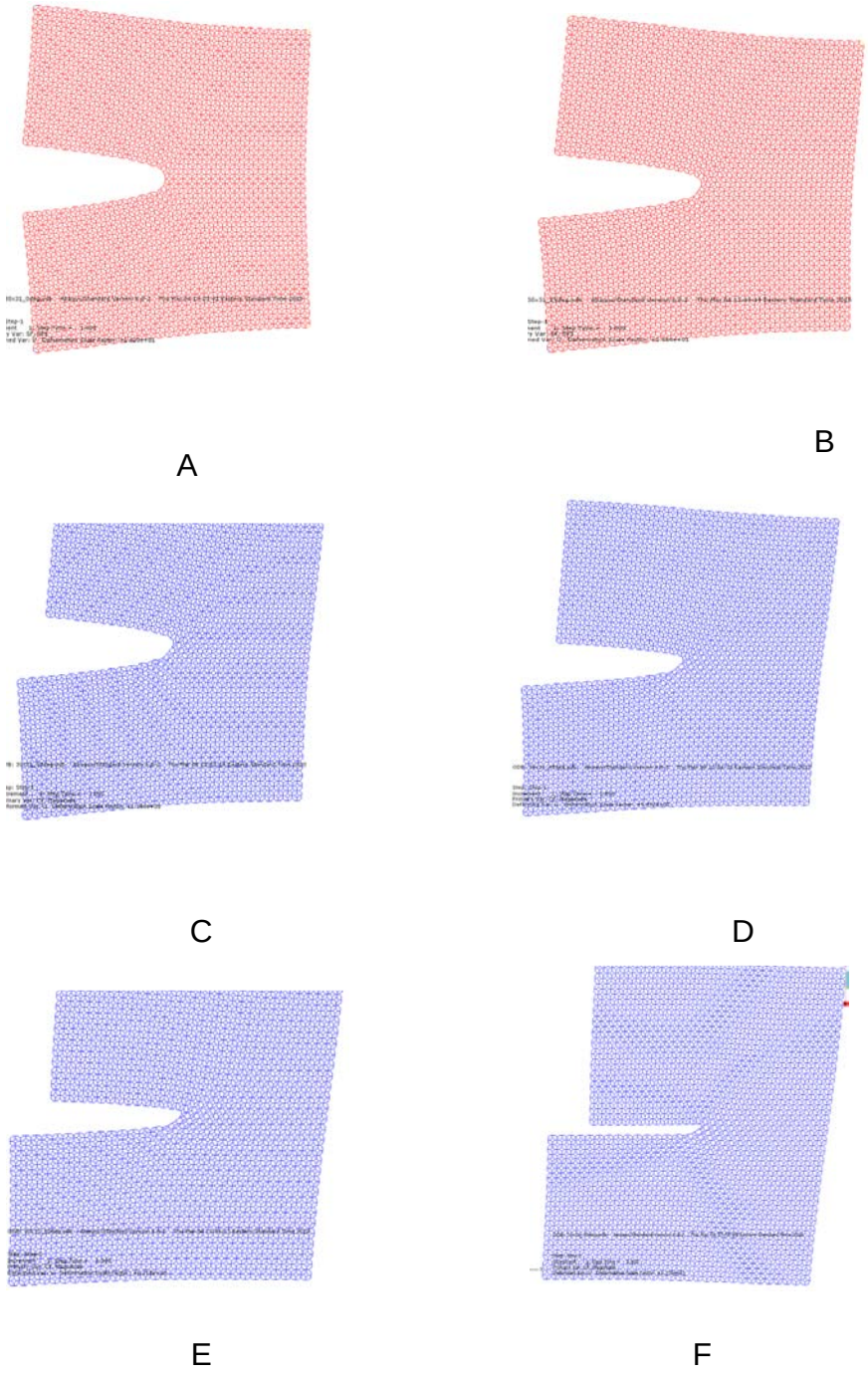

Figure 4-8. Mixed mode fracture toughness - Deformed configurations (30x31) (A) $\psi = 0$ (B) $\psi = 15$ (C) $\psi = 30$ (D) $\psi = 45$ (E) $\psi = 60$ (F) $\psi = 90$

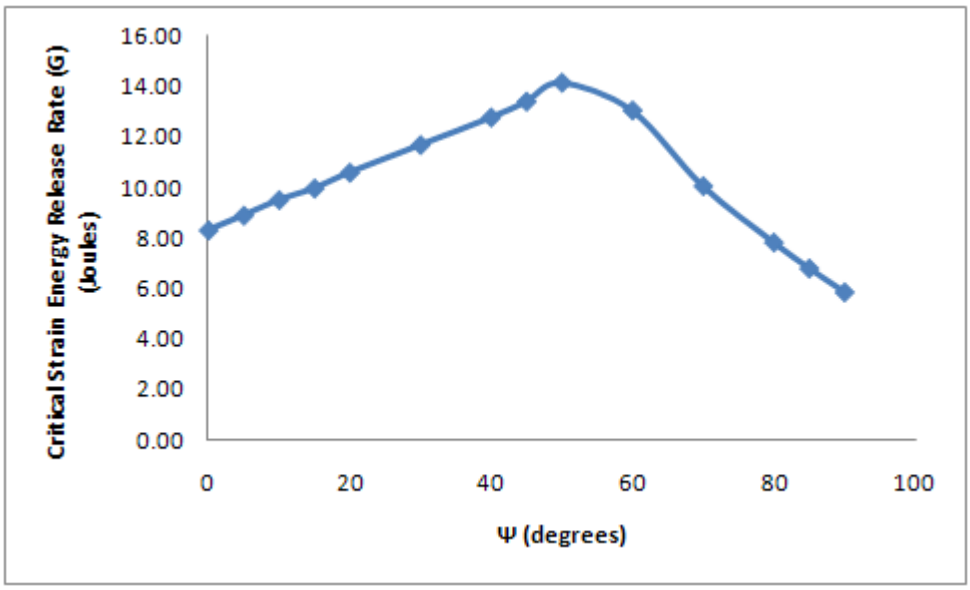

Figure 4-9. Mixed mode fracture toughness results (30x31 configuration)

Table 4-1. Properties of the strut chosen for Fracture toughness calculation

	Property	Value
Material Properties of the strut	Density, ρ_s (Kg/m^3)	1650
	Elastic modulus, E_s (GPa)	23.42
	Poisson ratio, ν_s	0.33
Geometry (Fig. 4-1)	L (mm)	1
	D (mm)	0.06
	Relative density	0.001653
Cross-section properties (Equilateral Triangle)	Cross sectional area, A (m^2)	1.5588×10^{-9}
	Moment of Inertia, I_x ,I_y (m^4)	2.3382×10^{-19}
	Polar moment of Inertia, J (m^4)	4.6765×10^{-19}

Table 4-2. Elastic properties of the foam to predict fracture toughness

	Property	Value
Elastic moduli	$E_x = E_x = E_z$ (GPa)	46.7×10^{-6}
Poisson ratios	$v_{xy} = v_{yz} = v_{xz}$	0.498
Shear moduli	$G_{xy} = G_{yz} = G_{xz}$ (GPa)	14.9×10^{-6}

Table 4-3. Mode I fracture toughness results with Input K_1=100

Sno	Width (Cells)	Height (Cells)	Crack (Cells)	Total nodes	Strut tip stress (*Mpa*)		Fracture toughness (*Pa.sqrt(m)*)		% difference between with and without rotation
					W/O rotation	With rotation	W/O rotation	With rotation	
1	10	11	5	1844	112	111.5	615.4	618.2	0.45
2	12	13	6	2596	111.6	111.3	617.6	619.8	0.35
3	14	15	7	3476	111.5	111.2	618.7	620.1	0.22
4	16	17	8	4484	111.3	111.2	619.4	620.2	0.12
5	18	19	9	5620	111.2	110.9	620.2	621.5	0.21
6	20	21	10	6884	111.1	110.9	620.7	621.7	0.17
7	22	23	11	8276	111	110.8	621.2	622.1	0.14
8	24	25	12	9796	110.9	110.8	621.6	622.5	0.14
9	26	27	13	11444	110.8	110.7	622.1	623	0.14
10	28	29	14	13220	110.8	110.7	622.1	622.9	0.13
11	30	31	15	15124	110.8	110.7	622.1	622.8	0.11
12	32	33	16	17156	110.8	110.7	622.2	622.7	0.09
13	34	35	17	19316	110.8	110.7	622.1	622.7	0.10

Table 4-4. Mode II fracture toughness results with Input KII = 100

Sno	Width (Cells)	Height (Cells)	Crack (Cells)	Total nodes	Strut tip stress (*Mpa*)		Fracture toughness (*Pa.sqrt(m)*)		% difference between with and without rotation
					W/O rotation	With rotation	W/O rotation	With rotation	
1	10	11	5	1844	125.1	125	551	551.6	0.11
2	12	13	6	2596	126.4	126.3	545.3	546.1	0.13
3	14	15	7	3476	127.4	127.2	541.4	542	0.11
4	16	17	8	4484	127.8	127.6	539.6	540.2	0.11
5	18	19	9	5620	128.1	128	538.2	538.8	0.10
6	20	21	10	6884	128.8	128.6	535.4	536.1	0.12
7	22	23	11	8276	129.4	129.3	532.8	533.4	0.11
8	24	25	12	9796	130.8	130.6	527.2	527.8	0.11
9	26	27	13	11444	131.4	131.2	524.9	525.6	0.13
10	28	29	14	13220	131.6	131.5	523.9	524.3	0.07
11	30	31	15	15124	131.8	131.8	523	523.3	0.06
12	32	33	16	17156	131.9	131.9	522.7	522.9	0.04
13	34	35	17	19316	132	131.9	522.5	522.7	0.04

Table 4-5. Results obtained for Mixed mode fracture toughness (30x31 configuration)

Sno	ψ (deg)	Max. strut stress (MPa)	Fracture toughness $(Pa\sqrt{m})$	Critical Strain Energy Release Rate (G) *(Joules)*
1	0	110.7	622.8	8.31
2	5	116.4	644.3	8.89
3	10	121.7	666.3	9.51
4	15	128.2	682.1	9.96
5	20	133.7	703.2	10.59
6	30	147.3	738.6	11.68
7	40	164.2	772.3	12.77
8	45	174.3	791	13.40
9	50	185.9	812.8	14.15
10	60	241.3	780.6	13.05
11	70	377	685.4	10.06
12	80	760.8	604.6	7.83
13	85	1520.8	563.6	6.80
14	90	131.8	523	5.86

CHAPTER 5
CONCLUSIONS AND FUTURE WORK

Conclusions

The main objective of this research has been to develop alternative approaches that can be used for fundamental material characterization of cellular materials, specifically foams. From the literature review on existing methodologies for doing this, it has been shown that the currently available experimental methods and analytical models to characterize foams have certain shortcomings due to which alternative approaches are sought after. These deficiencies have been elaborately explained in the introduction chapter and have also been mentioned in different appropriate places in the subsequent chapters. This work is primarily about using finite element based micromechanics approaches to successfully address all these deficiencies.

Chapter 1 explains the special attributes of the foam microstructure such as its repeating geometry pattern and its associated periodicity. Through an example considering a chemical system, the general principle of the fabrication processes of foams - phenomenon such as bubble nucleation have been explained. Also the reason for a tetrakaidecahedron to be the best choice for the repeating geometry for open cell foams has also been explained. Chapter 1 also explains the currently available experimental and analytical techniques for characterization of foams. Finally as mentioned earlier, the deficiencies in the currently available models for material characterization have been explained.

In Chapter 2, methods based on finite element based micromechanics have been used to calculate the elastic properties of foams with tetrakaidecahedral unit cells. It has been shown that the results for elastic constants match well with the available analytical

models. Also the advantages of using these finite element methods over analytical models such as a flexibility to choose between Euler-Bernoulli formulation or the shear-deformable formulation or a mix of both in the same unit cell model have been explained. As shown, the biggest advantage of using finite element methods is the generality in modeling any kind of a unit cell and using the same technique. Also the effect of varying cross-section on the elastic properties has been studied and it has been shown that for the same relative density, foams with varying cross-sections are lesser stiff compared to foams with uniform cross-section.

In Chapter 3, the finite element based micromechanics that was used in Chapter 2 to calculate the elastic properties have been extended to calculate multi-axial failure strengths for foams with both equisided and elongated tetrakaidecahedral unit cells. Consequently biaxial and triaxial failure envelopes for foams with both equisided and elongated unit cells have been plotted. The effect of inplane shear stress on biaxial normal stress has also been shown. Triaxial failure envelopes for foams with equisided tetrakaidecahedron as unit cell have been shown to be in the shape of a double hexagonal pyramid in the hydrostatic plane. Again, the effect of varying cross-section on the failure envelope has been studied.

In Chapter 4, the finite element based method developed by Choi and Sankar (2005) has been used to study the fracture toughness of foams with tetrakaidecahedral unit cells. Mode I, Mode II and Mixed mode fracture toughness of foams is predicted by developing micromechanical models. Fracture toughness has been shown to converge as the size of micromechanical model is increased. It has also been shown that

applying rotation boundary conditions does not influence the calculated fracture toughness.

Future Work

When calculating the elastic properties and failure strengths, the foam material has been assumed to be ideal without any imperfections, that is, it is assumed to be made out of perfectly packed regular tetrakaidecahedral unit cells. However, in reality there are many imperfections in foams. These imperfections include dislocations, random cell sizes, voids, dislocation of a vertex which connects several struts, non-uniform strut thickness or non-uniform material properties. In order to understand the effect of varying geometry of the strut dimensions and cell size, a sensitivity analysis can be done as future work and a range can be assigned to the calculated properties. This would be a very useful and important exercise, as this would help pin point to what parameter in the geometry is most important to control in the fabrication process. To bring in the effect of varying cell sizes in the foam structure, micromechanics based methods cannot be used and a full scale model has to be developed. This model would be similar to a tensile test specimen which could be used for predicting the properties with random cell sizes. Another area of interest in characterizing the properties of foams would be to predict its thermal properties. Foams are used primarily for thermal insulation and predicting thermo-mechanical property such as coefficient of thermal expansion, and thermal property such as thermal conductivity would be a significant area to contribute.

Also, even in the current work by doing more parametric studies using the methodology for predicting elastic properties, mathematical models relating the relative

density of the foams to the properties could be derived. These models could give a good comparison with the existing analytical models.

When predicting failure strengths, it would be important to understand how foams behave when subjected to compressive load. This area has been left as potential future work. Foam struts are subjected to bending and also buckle during compression. It would be interesting to understand the dominating failure mechanism that leads to failure during compression. Also even in the current study, the anisotropy of foams modeled using elongated tetrakaidecahedron unit cells has not been covered completely and could be studied further. Also, more parametric studies to calculate failure strengths and plot failure envelopes with different relative densities could be carried out and mathematical models could be derived to predict failure strengths.

The fracture toughness prediction methodology that has been presented in the current work is calculated based on the maximum stress in one strut near the crack tip. Not stopping here, a progressive fracture can be studied to trace the path of the crack growth by continuously loading the plate and failing a series of struts. This can be done by progressively removing the failing struts and studying the strut that gets subjected to maximum stress after the failing strut has been removed.

APPENDIX A
SUMMARY OF EQUATIONS FROM ZHU ET AL

Summary of Equations from Zhu et al, (Zhu, Knott, Mills, 1997):

Young's Modulus **(** E_{100} **):**

$$\frac{1}{E_{100}} = \frac{1}{6\sqrt{2}}\left(\frac{12L^2}{EA} + \frac{L^4}{EI}\right) \tag{A-1}$$

Poisson ratio (ν_{12}):

$$\nu_{12} = 0.5\left(\frac{AL^2 - 12I}{AL^2 + 12I}\right) \tag{A-2}$$

Shear modulus (G_{12}):

$$\frac{1}{G_{12}} = \frac{2\sqrt{2}L^2}{EA} + \frac{2\sqrt{2}L^4}{6EI}\left(\frac{8EI + GJ}{5EI + GJ}\right) \tag{A-3}$$

APPENDIX B
SUMMARY OF EQUATIONS FROM SULLIVAN ET AL

Summary of Equations from Sullivan et al, (Sullivan, Ghosn, Lerch, 2008):

Young's Moduli (E_x, E_y):

$$E_x = E_y = \frac{12EI}{L\sin\theta\left[2L^3\sin^2\theta + b^3 + \frac{12I}{A}\left(2L\cos^2\theta + b\right)\right]} \tag{B-1}$$

Young's modulus (E_z):

$$E_z = \frac{24EI\sin\theta}{L^2\left(\cos^2\theta + \frac{12I}{AL^2}\sin^2\theta\right)\left(\sqrt{2}L\cos\theta + b\right)^2} \tag{B-2}$$

Poisson ratios:

$$\begin{aligned}
\nu_{xy} = \nu_{yx} &= \frac{b\left(Ab^2 - 12I\right)}{12I\left(2L\cos^2\theta + b\right) + A\left(2L^3\sin^2\theta + b^3\right)} \\
\nu_{zx} = \nu_{zy} &= \frac{\sqrt{2}L\left(AL^2 - 12I\right)\cos\theta\sin^2\theta}{\left(12I\sin^2\theta + AL^2\cos^2\theta\right)\left(\sqrt{2}L\cos\theta + b\right)} \\
\nu_{xz} = \nu_{yz} &= \frac{\left(AL^2 - 12I\right)\left(2L\cos\theta + \sqrt{2}b\right)\cos\theta}{2\left[12I\left(2L\cos^2\theta + b\right) + A\left(2L^3\sin^2\theta + b^3\right)\right]}
\end{aligned} \tag{B-3}$$

Shear modulus (G_{xy}):

$$G_{xy} = \frac{1}{\left(4l\sin\theta\left\{\frac{b}{EA} + \frac{l^3\left[(2+4\frac{b}{l}\cos^2\theta)EI + \left(\frac{b}{l}\sin^2\theta\right)GJ\right]}{12EI\left[(2+\frac{b}{l}\cos^2\theta)EI + \left(\frac{b}{l}\sin^2\theta\right)GJ\right]}\right\}\right)} \tag{B-4}$$

Shear modulus (G_{yz}):

$$G_{yz} = \frac{1}{\left(\frac{l}{4\sin\theta} \left\{ \frac{L\left[\frac{b}{l}\cos\theta + \sqrt{2}\left(1+\sin^2\theta\right) \right]^2}{EA} + \frac{L^3\left[\lambda_1 \left(EI\right)^2 + \lambda_2 \left(EIGJ\right) + \lambda_3 \left(GJ\right)^2 \right]}{12EI\left[\left(1+\sin^2\theta + 2\frac{b}{l}\sin^2\theta\right)\left(EI\right)^2 + \left(2+2\frac{b}{l}\cos^2\theta\right)EIGJ + \left(\cos^2\theta\right)\left(GJ\right)^2 \right]} \right\} \right)} \quad \text{(B-5)}$$

Please note that $\lambda_1, \lambda_2, \lambda_3$ expressions have not been listed here and can be found in (Sullivan et al, 2008)

Failure Strength in the *Y*-direction (σ_{yy}^{ult}):

$$\sigma_{yy}^{ult} = \frac{\sigma^{ult}}{\left[\frac{L\cos\theta\sin\theta}{A} + \frac{L^2\sin^2\theta}{2S_x^L}\right]\left[2L\cos\theta + \sqrt{2}b\right]} \tag{B-6}$$

Failure Strength in the *Z*-direction (σ_{zz}^{ult}):

$$\sigma_{zz}^{ult} = \frac{\sigma^{ult}}{\left[\frac{\sin\theta}{2A} + \frac{L\cos\theta}{4S_x^L}\right]\left[\sqrt{2}L\cos\theta + b\right]^2} \tag{B-7}$$

APPENDIX C
CRACK TIP DISPLACEMENT FIELDS FOR ORTHOTROPIC MATERIALS

The displacement fields near the crack tip for Mode I:

$$u = K_I \sqrt{\frac{2r}{\pi}} \operatorname{Re}\left\{ \frac{1}{s_1 - s_2} \left[s_1 p_2 \left(\cos\theta + s_2 \sin\theta \right)^{1/2} - s_2 p_1 \left(\cos\theta + s_1 \sin\theta \right)^{1/2} \right] \right\}$$
$$v = K_I \sqrt{\frac{2r}{\pi}} \operatorname{Re}\left\{ \frac{1}{s_1 - s_2} \left[s_1 q_2 \left(\cos\theta + s_2 \sin\theta \right)^{1/2} - s_2 q_1 \left(\cos\theta + s_1 \sin\theta \right)^{1/2} \right] \right\} \quad \text{(C-1)}$$

The displacement fields near the crack tip for Mode II:

$$u = K_{II} \sqrt{\frac{2r}{\pi}} \operatorname{Re}\left\{ \frac{1}{s_1 - s_2} \left[p_2 \left(\cos\theta + s_2 \sin\theta \right)^{1/2} - p_1 \left(\cos\theta + s_1 \sin\theta \right)^{1/2} \right] \right\}$$
$$v = K_{II} \sqrt{\frac{2r}{\pi}} \operatorname{Re}\left\{ \frac{1}{s_1 - s_2} \left[q_2 \left(\cos\theta + s_2 \sin\theta \right)^{1/2} - q_1 \left(\cos\theta + s_1 \sin\theta \right)^{1/2} \right] \right\} \quad \text{(C-2)}$$

The parameters p_1, p_2, q_1, q_2, s_1 and s_2 in the above equations are dependent on the compliance properties that are obtained from material elastic constants. The details about the same can be obtained from Wang et al, 2003

LIST OF REFERENCES

Arakere, N.K., Knudsen, E., Wells, D., McGill, P., Swanson, G., 2008, Determination of mixed-mode stress intensity factors, fracture toughness, and crack turning angle for anisotropic foam material, International Journal of Solids and Structures, 45 pp. 4936–4951

Ashby, M., 2008. Materials-a brief history. Philosophical Magazine Letters 88: 9, 749–755

Brezny, R., D.J. Green, 1990, The Effect of Cell-Size on the Mechanical-Behavior of Cellular Materials, Acta Metallurgica Et Materialia 38: 2517–2526

Brezny, R., D.J. Green, C.Q. Dam, 1989, Evaluation of Strut Strength in Open-Cell Ceramics, Journal of the American Ceramic Society 72: 885–889

Choi, S.,B.V. Sankar, 2003, Fracture toughness of carbon foam. Journal of Composite Materials 37:2101–2116

Choi, S. and B.V. Sankar, 2005, A micromechanical method to predict the fracture toughness of cellular materials. International Journal of Solids and Structures 42:1797–1817

Daniel, I.M., Ishai, O, 1994, Engineering Mechanics of Composite Materials, Oxford University Press, New York, USA

Demir H, Sipahioglu M, Balköse D, Ülkü S., 2008, Effect of additives on flexible PVC foam formation, Journal of Materials Processing Technology 195:144–153

Ernest C. Holdredge, Jr., 1987, Very Low Density Structural Foam with a new, simple process – Web resource: http://www.techfoam.com/paper_page.htm

Fleck, N. A., and Qiu, X., 2007, the damage tolerance of elastic-brittle, two dimensional isotropic lattices. Journal of the Mechanics and Physics of Solids 55:562–588

Gibson, L.J., Ashby, M.F., 1997, Cellular solids: structure and properties, Second ed. Cambridge University Press, Cambridge, UK

Gong, L., Kyriakides, S., Jang, W.Y., 2005, Compressive response of open-cell foams. Part I: Morphology and elastic properties, International Journal of Solids and Structures 42:1355–1379

Hall, R. B., Hager, J. W., 1996, Performance limits for stiffness-critical graphitic foam structures, Comparisons with high-modulus foams, refractory alloys and graphite-epoxy composites, Journal of Composite Materials 30:1922–1937

Hibbit, Karlsson, Sorensen, 2003, Abaqus ® User's Manual, Version 6.7, Pawtucket, RI

Hooke, R., 1664. Micrographia. The Royal Society, London,

Huang, J.S. and L.J. Gibson, 1991, Fracture-Toughness of Brittle Honeycombs, Acta Metallurgica Et Materialia, 39:1617–1626

Huber A.T., Gibson, L.J., 1988, Anisotropy of foams, Journal of Material Science 23:3031–3040

Jang, W.Y., Kraynik, A.M., Kyriakides, S., 2008, On the microstructure of open-cell foams and its effect on elastic properties, International Journal of Solids and Structures 45:1845–1875

Karkkainen, R., Sankar, B.V., 2006, A direct micromechanics method for analysis of failure initiation of plain weave textile composites, Composite Science and Technology 66:137–150

Lee, S., J. Wang, and B.V. Sankar, 2007, A micromechanical model for predicting the fracture toughness of functionally graded foams. International Journal of Solids and Structures 44:4053–4067

Leong, M., B.V. Sankar, 2008, Effect of Thermal Stresses on the Failure Criteria of Fiber Composites, Mechanics of Advanced Materials & Structures (in press)

Li, K., Gao, X. L., Roy, A. K., 2003, Micromechanics model for three-dimensional open-cell foams using a tetrakaidecahedral unit cell and Castigliano's second theorem, Composites Science and Technology 63:1769–1781

Maiti, S.K., M.F. Ashby, and L.J. Gibson, 1984, Fracture-Toughness of Brittle Cellular Solids, Scripta Metallurgica 18(3): 213–217

Oscar A. Martinez, Bhavani V. Sankar, Raphael T. Haftka, Satish K. Bapanapalli, Max L. Blosser, 2007, Micromechanical Analysis of Composite Corrugated-Core Sandwich Panels for Integral Thermal Protection Systems, AIAA Journal 45: 2323–2336

Plateau, J. A. F., 1873, Statique Experimentale et Theorique des Liquides Soumis aux Seules Force Moleculaires

Rao, M.P., B.V. Sankar, G.Subhash, 2009, Effect of Z-Yarns on the Stiffness and Strength of Three-Dimensional Woven Composites, Composites Part B 40: 540–551

Ridha, M., Shim, V. P. W., and Yang, L. M., 2006, An elongated tetrakaidecahedral cell model for fracture in rigid polyurethane foam, Fracture and Strength of Solids 306:43–48

Sankar, B.V., Marrey, RV., 1997, Analytical Method for Micromechanics of Textile Composites, Composites Science and Technology 57:703 – 713.

Sihna, S., Roy, A.K., 2004, Modeling and prediction of bulk properties of open-cell carbon foam, Journal of the Mechanics and Physics of Solids 52:167–191

Stamblewski, C., B.V. Sankar, D.Zenkert, 2008,Analysis of Three-Dimensional Quadratic Failure Criteria for Thick Composites using the Direct Micromechanics Method, Journal of Composite Materials 42:635–654

Sullivan, R.M., Ghosn, L.J., Lerch, B.J, 2008, A general tetrakaidecahedron model for open-celled foams, International Journal of Solids and Structures 45:1754–1765

Sullivan, R.M., Ghosn, L.J., Lerch, B.J, 2008, Application of an Elongated Kelvin Model to Space Shuttle Foams, Journal of Spacecraft and Rockets 46:111–118

Sullivan, R.M., Ghosn, L.J., Lerch, B.J, 2009, Shear moduli for non-isotropic, open-cell foams using a general elongated Kelvin foam model, International Journal of Engineering Science 47: 990–1001

Thiyagasundaram, P., Sankar, B.V., Arakere, N.K., 2010, Elastic Properties of Open-Cell Foams with Tetrakaidecahedral Cells Using Finite Element Analysis, AIAA Journal 48: 818–828

Thomas NL, Eastup RP, Quirk JP., 1997, Aspects of formulation technology of rigid poly(vinyl chloride) foam. Plastic Rubber Composite Processes and Applications 26:47–54

Thomson, W., 1887, On the division of space with minimum partitional area Philosophical Magazine 24: 503–505.

Wang, J., B.V. Sankar, 2008, Fracture Toughness of Cellular Solids using Finite Element Based Micromechanics, Proceedings of the American Society for Composites, Twenty-Third Technical Conference, Memphis, TN,September 9–11, 2008

Weaire, D., 1997, The Kelvin Problem: Foam structures of minimum surface area. 1st edition, London, Taylor and Francis

Weiser. S.E., Nemeth. P.M., 2004, Assessment of Technologies for the Space Shuttle External Tank Thermal Protection System and Recommendations for Technology Improvement Part 1: Materials Characterization and Analysis, NASA Contractor Report NASA/TM-2004-213238

Weisstein, E. W., Truncated Octahedron, MathWorld-A Wolfram Web Resource: http://mathworld.wolfram.com/TruncatedOctahedron.html

Wright L.S. and Lerch B.A., 2005, Characterization of space shuttle insulative materials, NASA/TM-2005-213596

Yamsaengsung, W., Sombatsompop, N., 2009, Effect of chemical blowing agent on cell structure and mechanical properties of EPDM foam, and peel strength and thermal conductivity of wood/NR composite–EPDM foam laminates, Composites Part B: Engineering 40: 594–600

Zhu, H., B.V. Sankar, Marrey, R.V., 1998, Evaluation of Failure Criteria for Fiber Composites Using Finite Element Micromechanics, Journal of Composite Materials 32: 766–782

Zhu, H.X., Knott, J.F., Mills, N.J., 1997, Analysis of the Elastic Properties of Open-Cell Foams with Tetrakaidecahedral Cells, Journal of Mechanics and Physics of Solids, 45:319–343

BIOGRAPHICAL SKETCH

Prasanna Thiyagasundaram received his Bachelor of Technology degree in production and industrial engineering at Motilal Nehru National Institute of Technology (MNNIT), Allahabad, Uttar Pradesh (U.P.), India in 2003. Between 2003 and 2006, he worked for an automotive company by name of Tata Motors Limited as a Design Engineer in India. In August 2006, he was admitted to the graduate program in the Department of Mechanical and Aerospace Engineering at the University of Florida where he just completed his work towards a Doctor of Philosophy degree in the general research area of computational mechanics.